NEW CONDUCTING AND ELECTRICALLY SWITCHING MOLECULAR MATERIALS BASED ON MAIN GROUP AND TRANSITION METAL IONS BRIDGED BY TCNQ DERIVATIVES

A Dissertation

by

ZHONGYUE ZHANG

Submitted to the Office of Graduate Studies of
Texas A&M University
in partial fulfillment of the requirements for the degree of

DOCTOR OF PHILOSOPHY

Chair of Committee,	Kim R. Dunbar
Committee Members,	Hongcai Zhou
	François P. Gabbaï
	Joseph Ross
Head of Department,	David H. Russell

August 2013

Major Subject: Chemistry

Copyright 2013 Zhongyue Zhang

ABSTRACT

The field of molecular electronics has been under investigation by materials scientists for the last two decades, activity that has increased in recent years as their potential to be components in modern quantum computing devices began to be discussed in a more sophisticated manner. In this field, the challenge is to obtain stable highly conducting materials and to manipulate their properties with external stimuli. As one of the most stable organic radicals, the singly reduced form of TCNQ (7,7,8,8-tetracyanoquinodimethane) has played a central role in the design of many unprecedented conducting materials including the first purely organic conductor (TTF)(TCNQ) (TTF = tetrathiafulvalene) which is nearly metallic and the electrically bistable switching material Cu(TCNQ). The research in this dissertation focused on the application of TCNQ and its derivatives in order to tune the structure and conductivity of these materials, with the overarching goal being to understand the mechanism of conductivity. This dissertation reports the details of the first main-group TCNQ binary compound, Tl(TCNQ). Two distinct polymorphs have been discovered and a remarkable water-induced phase transition from one to the other was observed. With different modes of TCNQ stacking (alternating or homogenous distances), the two polymorphs exhibit very different conductivities, namely 2.4×10^{-4}S/cm and 5.4×10^{-1}S/cm. With this inspiration, a series of semiconductors, $Tl(TCNQX_2)$ (X =Cl, Br, I) was prepared and structurally characterized. The steric effect of the halogen substituents leads to a variety of structures and a band structure simulation has suggested a clear structure-property relationship that involves perturbation of the Tl 6s orbital into the conduction band.

Inspired by the switching material Ag(TCNQ), semiconducting frameworks $Ag(TCNQCl_2)$ and $Ag(TCNQBr_2)$ were prepared by electrocrystallization methods. Importantly, the former material exhibits a high room temperature conductivity of 0.25 S/cm and an unusual room temperature negative differential resistance (NDR) which is the source of intrinsic switching behaviors. The effect of solvent on the structure of these binary phases was also investigated. The series $M(TCNQX_2)(MeCN)_n$ (M = Cu, Ag; X = Br, I; n =1, 2) was discovered and the interconversion of these solvated phases was studied. The effect of coordinated solvent molecules decreases the density of conducting stacks, consequently leading to a decrease of conductivity.

DEDICATION

What doesn't kill you makes you stronger.

ACKNOWLEDGEMENTS

I sincerely acknowledge Professor Kim Dunbar for helping me in my Ph.D studies as well as in my life and career during the past 5 years. Her diligence, self-discipline and pursuit of excellence have provided me with a great role model for learning and growing in the future. Her careful advice and patient education has not only helped me to develop my scientific abilities but has also greatly changed my life by bringing confidence and discipline into my heart. I will always cherish the wisdom she has provided for my career and for my life.

I would also like to express my appreciation to my committee members, Professor François P. Gabbaï, Professor Hongcai Zhou, Professor Winfred Teizer and Professor Joseph Ross for all the help, suggestions and educations they have provided. I deeply appreciate what they have done to help me finish all the Ph.D requirements.

I would like to offer thanks to Professor Kunio Awaga from Nagoya University and Professor Takehiko Mori from the Tokyo institute of Technology for their valuable help as collaborators for a portion of my research work. They have provided great hospitality during my trips to Japan and helped me to gain a deeper understanding of my research.

I would also like to acknowledge the senior group members in Dr. Dunbar's lab for all the help they have provided to me. Dr. Hanhua Zhao helped me enormously by training me in synthesis and general lab skills and took interest in my life and well-being like a father. Dr. Akira Ota and Dr. Xinyi Wang helped me acquire many important skills and to learn critical concepts and Dr. Andrey V. Prosvirin introduced me to the methods

and interpretation of magnetism measurements. Dr. Helen Chifotides provided many great suggestions to my work for which I am most grateful. I offer my sincere thanks and appreciation to my dear colleagues: Dr. Carolina Avendano, Dr. Matthew Hilfiger, Dr. Daphne Aguirre, Dr. Kristen Funck, Dr. Ian Giles, Edward Funck, Dr. Ferdi Karadas, Dr. Nazario Lopez, Sarah Lane, Heather Southerland, Zhanyong Li, Bruno Pena, Amanda David, Mohammed Saber, Andrew Brown, Codi Sanders, Toby Woods, Xuan Zhang, Jill Frank, Francisco Birk, David Kempe, Lei Sun, Maryfer Ballesteros Rivas, Dr. Ming Fang, Dr. Qinglun Wang, Zhaoyang Li and Dr. Dawid Pinkowicz. I take with me many great memories from all these years.

I would like to thank all my friends who have been supportive of me during my Ph.D studies over the years. Thanks to them for their friendship and help in my daily life.

Finally, I would like to acknowledge my parents, Shugong Zhang and Lili Liu for their love over these 27 years. Without their love and support I would not have gotten anywhere in my life.

TABLE OF CONTENTS

Page

LIST OF FIGURES

LIST OF TABLES

CHAPTER I

INTRODUCTION: MOLECULAR CONDUCTORS AND MULTIFUNCTIONAL MATERIALS

Background

Given the rapid development of modern computer technology, there is a great deal of pressure to produce new electronic devices. Until recently, the research frontier of data processing units has focused on traditional materials such as silicon chips, metal oxide semiconductors (MOS) and group IIIA-VA semiconductors (GaAs) with the main issue being the search for processors with smaller domain sizes and faster response speeds. The limitation of fabrication techniques, however, has presented a major obstacle. To date, the smallest reported silicon wafer is 22 nm, but a further scaling of CMOS (complimentary metal-oxide semiconductor) down to 6 nm may take up to 15 years and is not likely to lead to a commercially feasible device.[1,2]

Another approach to solving the problems of miniaturization of electronic devices is to use molecular materials, the study of which has steadily been gaining attention over the past two decades in terms of application of molecules in electronic devices as active (switching, sensing) or passive (current stabilizing or rectifying) components.[3] Molecules possess a natural advantage for electronic devices: (1) they have miniature domain size and a functional unit can be as small as a single molecule, (2) they have confined orbital energies and electron activation or transfer energies can be easily confined by a molecular orbital as opposed to the energy states in traditional materials which are continuous and lead to a range of energy values due to

multi-dimensional transfer pathways, (3) they offer ease of tuning in that the electronic properties and the structures of molecules can be easily manipulated to adjust the properties of the device and (4) they lend themselves to simple fabrication techniques including spin-coating, vapor deposition, and dipping methods which allow for the placement of molecules on the surface of, or sandwiched between, traditional materials such as metal or metal-oxides. Moreover, since molecules are identical, less defects can be expected as compared to the growth of single-crystal silicon chip or GaAs semiconductors.[4]

An elegant example of a molecular device is illustrated in Figure 1.1 which consists of a σ-bonded alkane chain spanning two gold tips [5] The simple device forms a Donor-Bridge-Acceptor (DBA) junction and exhibits unprecedented electronic behavior that can be tuned by modification of the molecule with desire functional groups. Given the obvious power of this approach, the synthesis and device development of molecules in electronic applications is being pursued by chemists, physicists and engineers alike. The materials under investigation in this highly multidisciplinary research field hold great potential for leading to a revolution in micro-sized electronic devices.

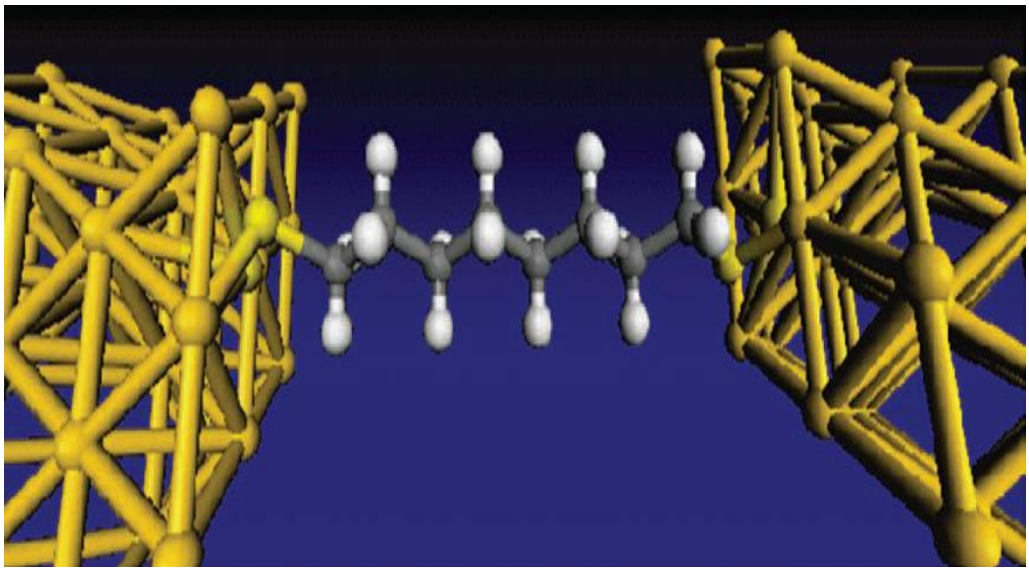

Figure 1.1 A simple device for molecular electronics composed of a $[CH_2\text{-}CH_2]_n$ alkane chain placed between Au{111} tips. The voltage across the bridge is determined by the degree of charge transfer between the tips and the micro-states of the chain.

Molecular Conductors

Molecular conductors with properties that mimic traditional materials have been extensively studied by chemists over the last two decades. Like solid-state materials, molecular conductors can also be classified as metallic conductors, semiconductors or insulators which are distinguished by their energy gaps. Insulators have a huge energy gap (> 5eV) therefore, only a very small number of electrons can be thermally activated to the conduction band. Conversely a metallic conductor exhibits a continuous band structure with no energy gap. As a result, the only obstacle for electron movement is repulsion from the thermal vibration of the lattice, which is much smaller as compared to the thermal energy gap. Therefore, a metallic conductor will exhibit a large, temperature-independent conductivity in an ideal case (if one ignores the lattice vibration). The energy gap of a semiconductor lies between that of insulators and metallic conductors and is ~1 eV. In such a case, the percentage of thermally activated electrons in the conduction band follows the Boltzmann distribution $N_i /N = \exp(-E_g/k_BT)$ (Eg stands for the energy gap). Since the conductivity is proportional to the electrons in the conduction band, an Arrhenius law of conductivity can be expected. The band structure and temperature dependent conductivity diagram are depicted in Figure 1.2.

$$\sigma = \sigma_0 \exp(-E_g/k_BT) \qquad \textbf{Equation 1.1}$$

Although most organic compounds are insulators, McCoy and Moore began discussing the possibility of metallic behavior for organic substances as early as 1911.[6] The first reported molecular semiconductor is a perylene bromine complex reported by Akamatu *et al* in 1954. The material was reported to exhibit good semiconducting

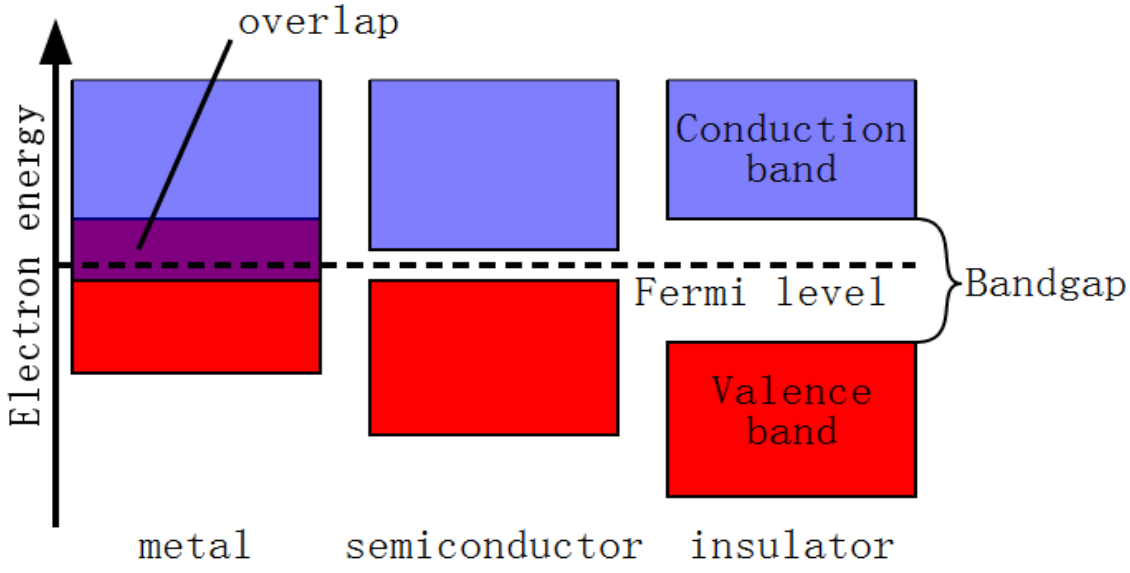

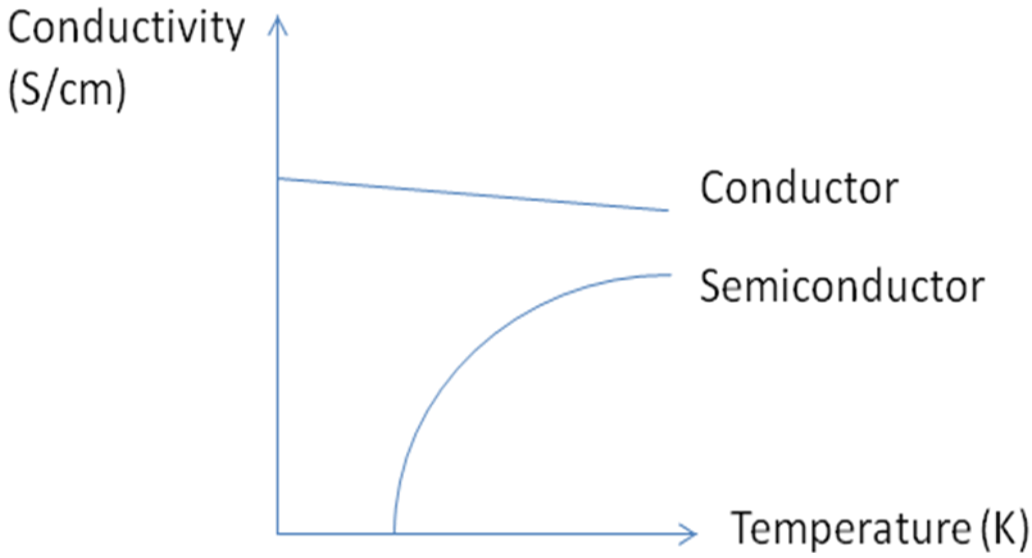

Figure 1.2 Energy band distribution (top) and ideal temperature dependent behavior (bottom) for conductors, semiconductors and insulators.

behavior with a conductivity of approximately 10^{-3} S/cm.[7] This finding eventually led to further investigation of molecule-based conducting materials, especially in the realm of organic metals. A nearly simultaneous discovery was made in the area of organic conductors, namely the preparation of TCNQ (7,7,8,8-tetracyanoquinodimethane) based charge-transfer conducting materials. The research was initiated by chemists working at DuPont.[8] It was not until 1973, however, that the unprecedented metallic conductor, TTF-TCNQ (TTF = tetrathiafulvalene) was reported which sparked enormous interest in the field.[9] In fact, a research on the TTF family of organic donors and the TCNQ family of acceptors continues to be a main focus in the search for improved conducting organic materials.

Charge Transfer Compounds

The definition of a charge transfer compound is a material in which a fraction of charge has been transferred between two different molecular entities or different structural parts. The interest in charge transfer compounds has flourished since the discovery of TTF-TCNQ in which TTF is the electron donor and TCNQ is the electron acceptor. The charge transfer was measured to be 0.59 which means a partial charge transfer which leads to a doping effect of the intrinsic stack of TTF and TCNQ columns. This doping effect results in a mixing of the conduction band and valence band, leading to metallic behavior. Since this discovery, many additional donors related to TTF including TSF (tetraselenafulvalene) and their derivatives were designed and studied in combination with numerous anions to make many different charge transfer salts. In terms of the acceptor-based conductors, TCNQ and related organic acceptors such as DCNQI (*N,N'*-dicyanoquinodiimine) have been studied with various cations including those of the

alkali metals, alkaline earth metals and transition metals. Figure 1.3 depicts the structure of TTF-TCNQ, and Figure 1.4 displays common organic donors and acceptors.

One critical point of the studies of many organic conductors is the solid-state physics theory modeling for examples whose crystal structures could be obtained. With knowledge of the packing diagram, strong anisotropy of these materials can be predicted and a test of the quasi one-dimensional (1-D) model theorem can be performed. Alterations of functional groups lead to crystal structure changes and the resulting differences in energy band and physical properties form the basis for structure-property relationships.[10]

Analysis of Band Structure: Quasi 1-D Model of Molecular Conductors

The quasi 1-D model is a common theoretical treatment suitable for analyzing the band structure of charge transfer salts. The rationale for using such a model stems from the fact that the functional molecules stack in columns which provides a 1-D channel for electron transfer. In this treatment, a frozen orbital hypothesis of functional molecules is adapted, such that the overlap and interaction between the frontier orbitals is the major pathway for electron transfer. As a result, an extended Hückel model treatment of the propagation of frontier orbitals will result in an energy band structure for the material.

With the extended Hückel model, the Hamiltonian for the frontier orbital stacks is as follows:

$$\Sigma(H_{ij} - \varepsilon_i S_{ij})C_i = 0 \qquad \textbf{Equation 1.2}$$

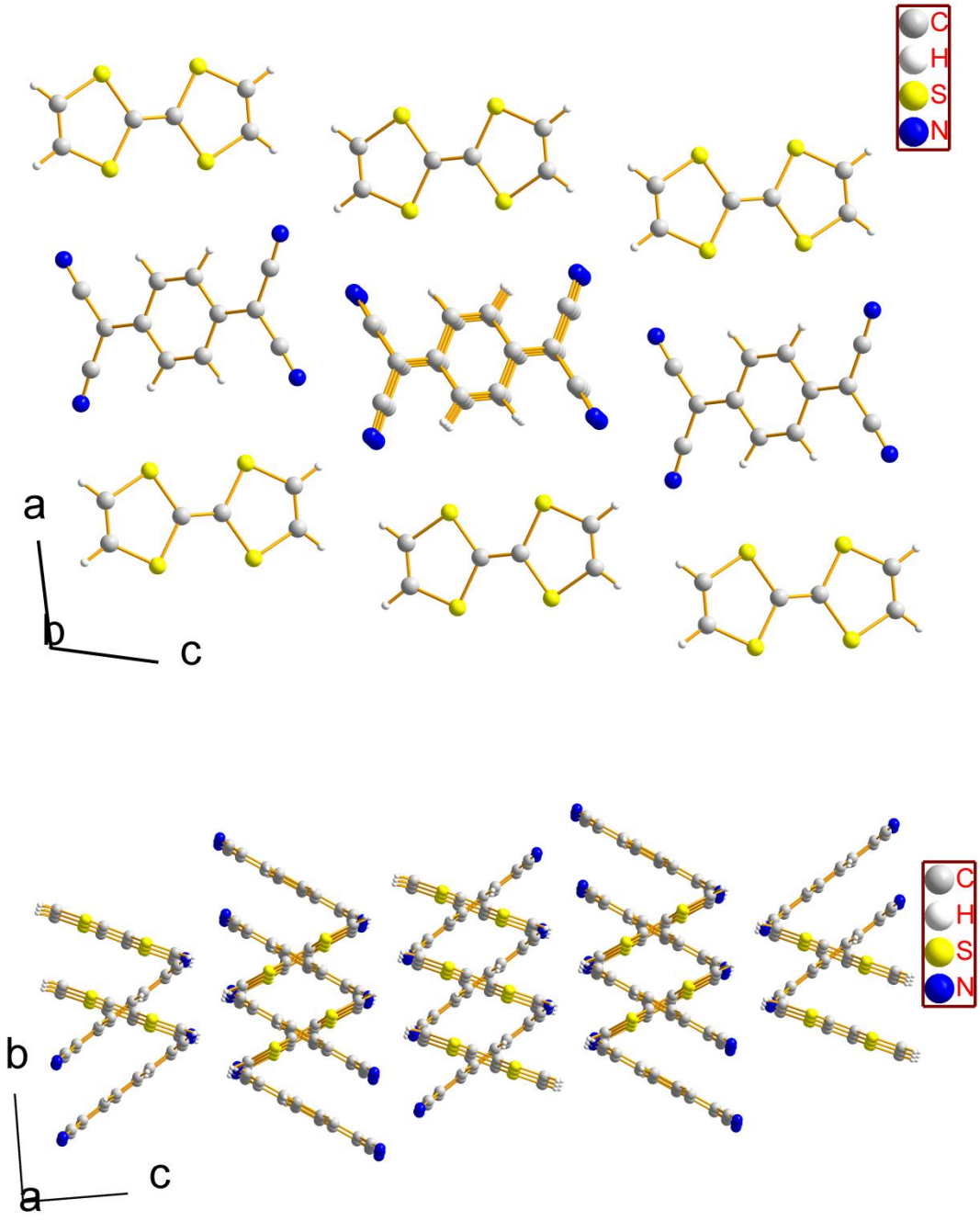

Figure 1.3 The structure of TTF-TCNQ, *ac* plane view (top) and *bc* plane view (bottom).[11]

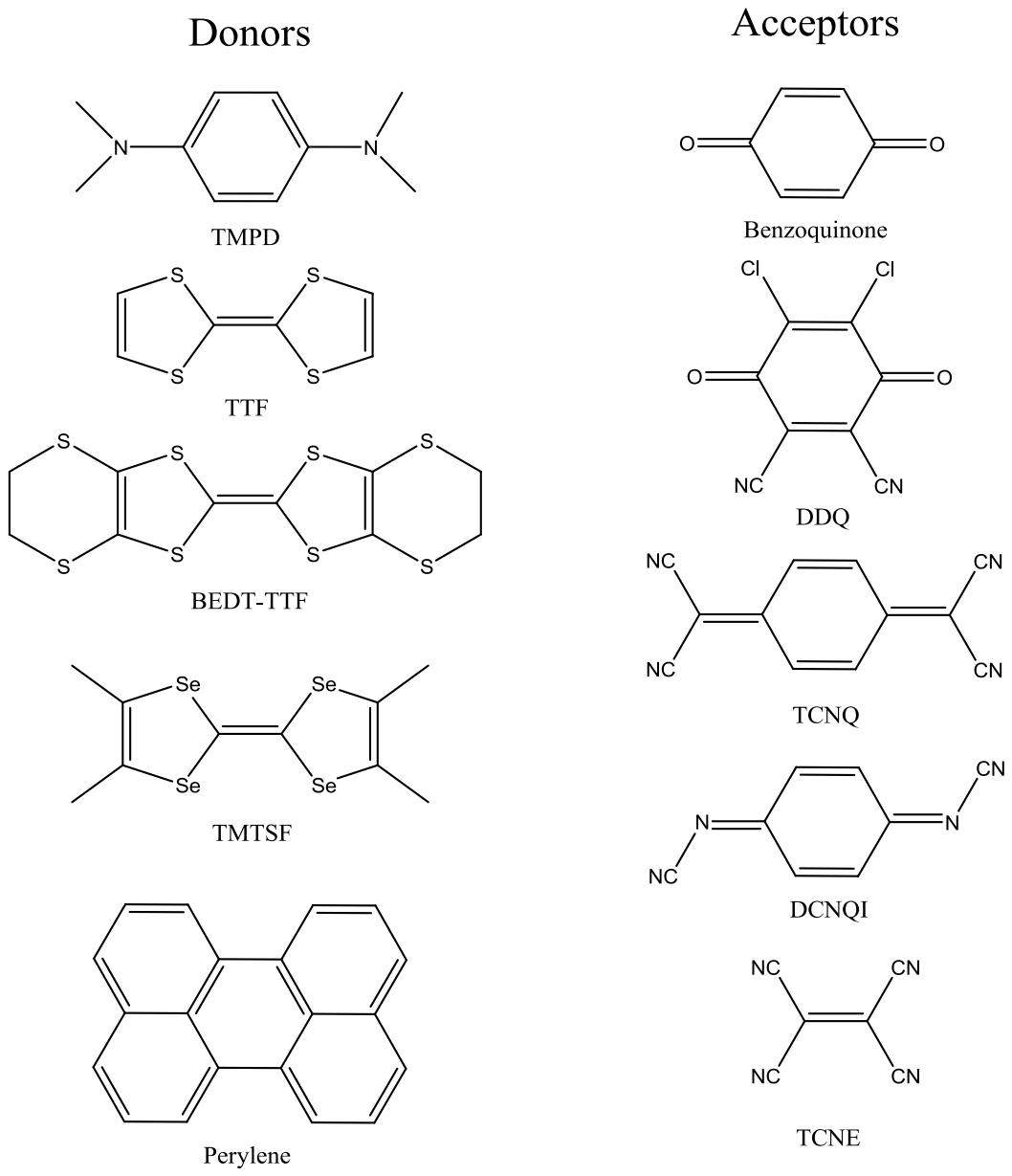

Figure 1.4 Representative donors and acceptors. (TMPD = *N*,*N*,*N*′,*N*′-tetramethylbenzene-1,4-diamine. TTF = tetrathiafulvalene, BEDT-TTF = Bis(ethylenedithio)tetrathiafulvalene. TMTSF = tetramethyltetraselenafulvalene. DDQ = 2, 3-dichloro-5, 6-dicyanobenzoquinone. TCNQ = tetracyanoquinodimethane. DCNQI = *N*, *N*′-dicyanoquinodiimine. TCNE = tetracyanoethylene.)

Here H_{ij} = α (single frontier orbital energy) when i = j, β (transfer integral energy between the adjacent orbital) when i = j-1, 0 for the other case. S_{ij} = 1 when i = j, or 0 when i ≠ j. Therefore, the eigenvalues of the orbitals can be solved as:

$$\varepsilon(k)=\alpha+2\beta cos(k\alpha) \qquad \textbf{Equation 1.3}$$

Therefore, an ideal 1-D energy band structure is a cosine wave which vibrates along the direction of molecular stacking and orbital interactions. In most cases, however, the multi-dimensional interactions cannot be neglected and, actually, higher dimensionality interactions enhance the conductivity by providing more transfer pathways. The common treatment of higher dimensionality interactions is to treat them as perturbations of the ideal 1-D band structure. The perturbation will lead to a wave vibration not only along the major conducting pathway but also along the directions of perturbation which is a "Quasi 1-D model" treatment. The interaction diagram of 1-D and Quasi 1-D models and the resulting band structures are illustrated in Figure 1.5 and 1.6.

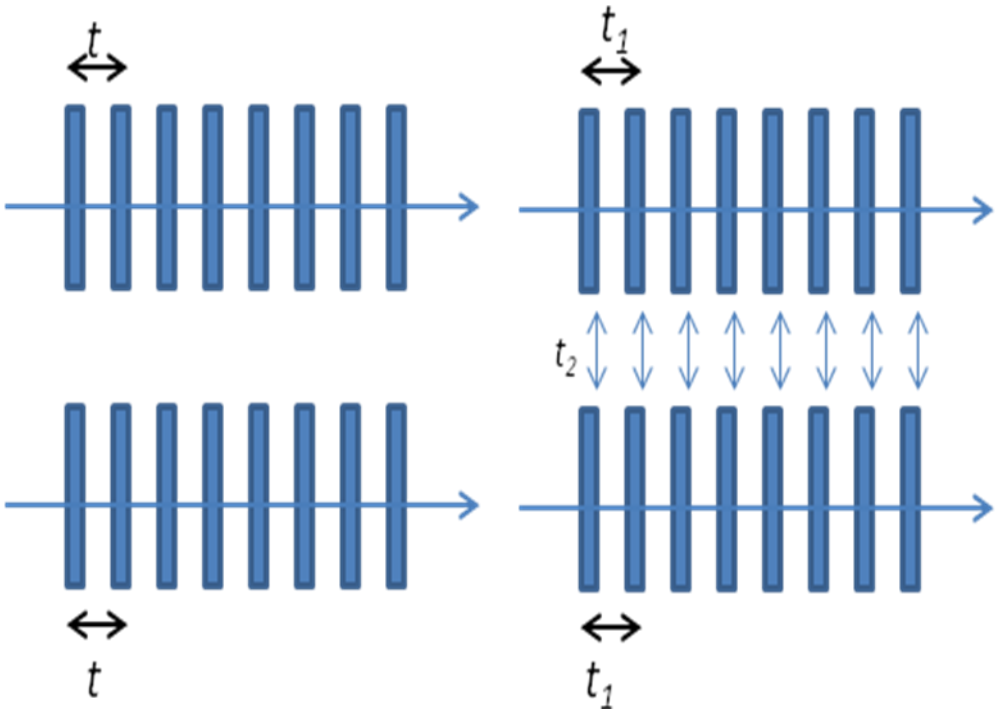

Figure 1.5 The interaction diagram of ideal 1-D model (left) and quasi 1-D model (right) with two types of interactions. The eigenvalues of frontier orbitals will be: $\varepsilon(k)= 2t_1cos(k_1\alpha)+ 2t_2cos(k_2\beta)$.

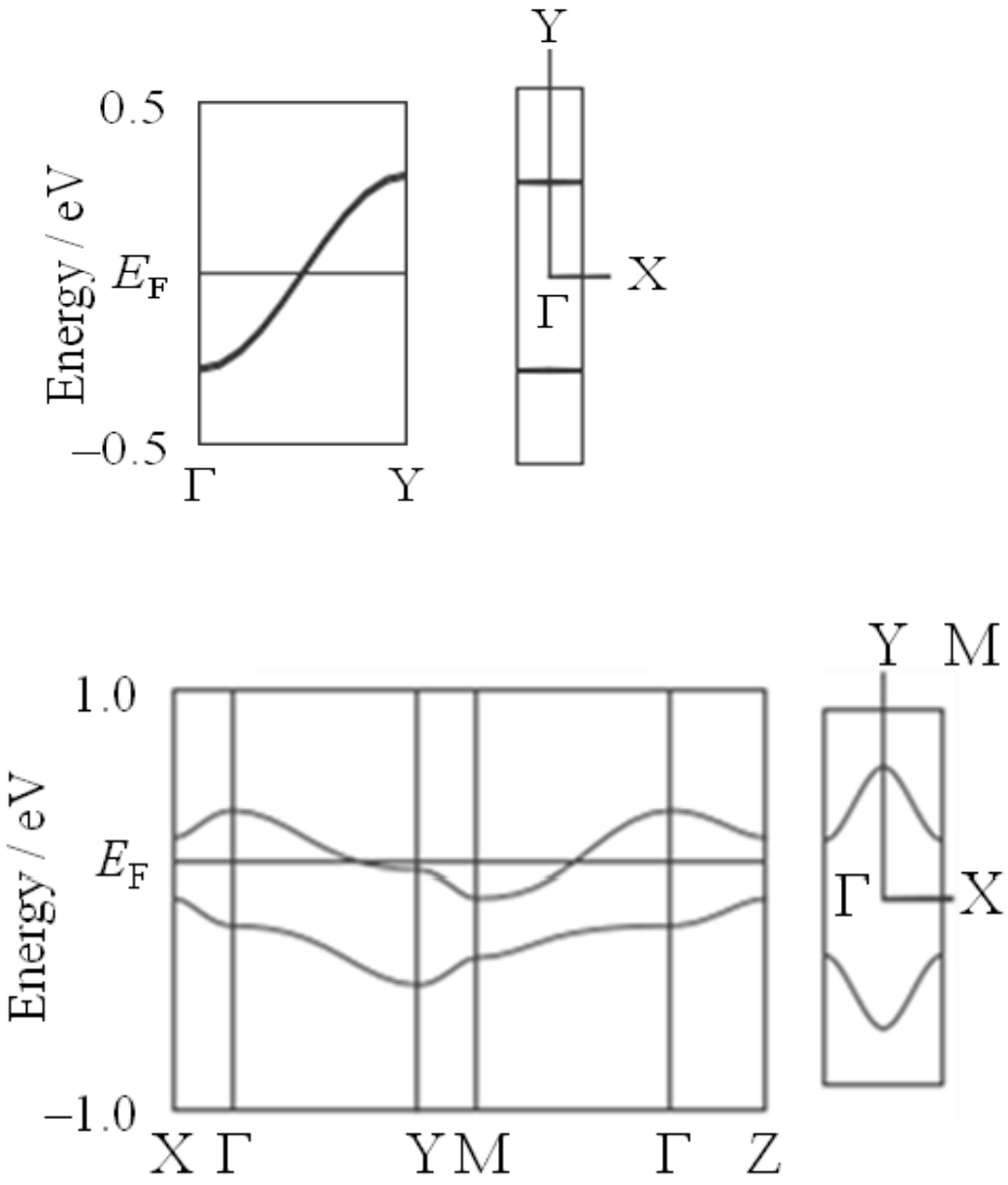

Figure 1.6 Band structure and Fermi surface diagrams for typical 1-D conductor (top) and quasi 1-D conductor (bottom).

Mott Insulators, Peierls Transitions and Charge Density Waves (CDW)

Most of the aforementioned materials are classified as Mott Insulators. A Mott insulator is a material that is a conductor under the prediction of band structure calculations but whose actual conducting behavior is much lower than expected. The decrease in conductivity is caused by electrostatic interactions between the active electrons and local electrons. This phenomenon was first observed in NiO and interpreted by Mott and Peierls.[11] In most of the molecular conductors the functional molecules exist as columnar stacks of radicals which form the pathway for electron transfer (charge mobility). The unpaired electrons in the frontier orbitals play the role of charge carriers. Under these circumstances, the conducting activation energy will be the electron transfer energy between the adjacent molecules and the obstacle of electron transfer is the Coulomb repulsion between the transfer electron and local electron on the radical form. By adopting a Mott-Hubbard theory to the model, and considering the adjacent electrons to be antiferromagnetically coupled, the Hamiltonian can be written and reduced to where t represents the overlapping factor, and U stands for the onsite Coulomb repulsion energy:

$$H = J \Sigma_i S_i \times S_{i+1}, \text{ where } J = -4t^2/U \qquad \textbf{Equation 1.4}$$

Two extreme cases can be derived, namely when t is much larger or much smaller than U. In the first case, the onsite repulsion can be ignored and the material will behave as a conductor. In the latter case, the onsite repulsion dominates which leads to highly localized electron density and the material acts as an insulator and is defined as a Mott insulator.

When the electrons in these molecule-based Mott insulators are perturbed by lattice vibrations, namely when the interactions between the adjacent electrons are coupled with the lattice vibrations, the lattice will be modulated by a function of $2k_F$, where (k_F= a/π) is the period the of original lattice. When this perturbation is operative, an energy gap will be generated at the k_F position of the original band which causes a conductor or semiconductor to turn into an insulator. This transition is called a Peierls transition and the energy gap generated is called a Peierls gap. In this case, the modulated lattice will result in an electron-density modulation which alters the charge density from an even distribution to a ordering wave referred to as a Charge-Density Wave (CDW). The anisotropic conductivity of TTF-TCNQ has been studied in extensive detail and it is believed that the CDW transport contributes to the conductivity as well as the single electron transport and that the Peierls transition at low temperatures merges the CDW with the lattice below 54 K and leads to a metal-to-insulator transition. [12] Figure 1.7 describes the concept of a Mott insulator, a Peierls transition and a Peierls energy gap.

Molecular Conductors and Superconductors Based on TTF-type Donors

The concept of exploring TTF-type donors with different anions began to be fleshed out immediately after the discovery of TTF-TCNQ. The band structure calculation of TTF-TCNQ suggested that the disperse $3p_z$ orbital and $3d_{xz}$ orbital of sulfur atoms greatly contributes to the overlap of the frontier orbitals.[13] Therefore, the design strategy for second generation TTF-type donors has been to introduce more sulfur atoms or, better yet, to substitute sulfur with selenium which has more diffuse orbitals.

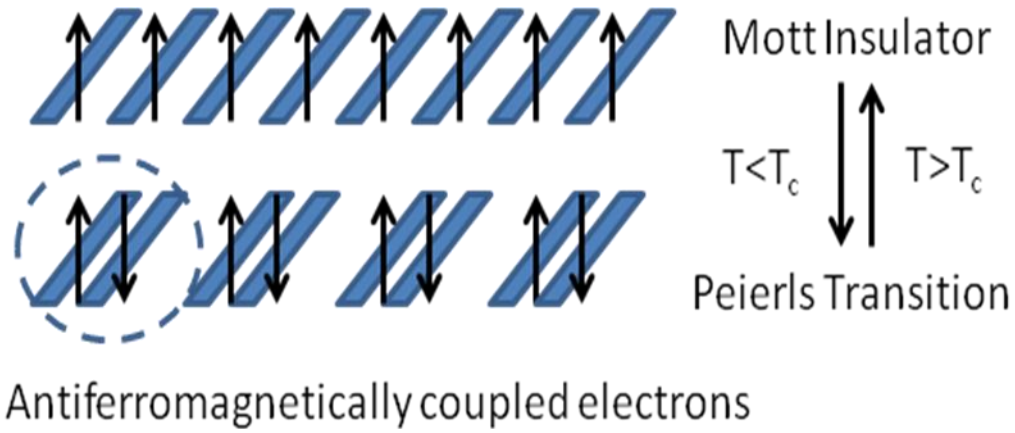

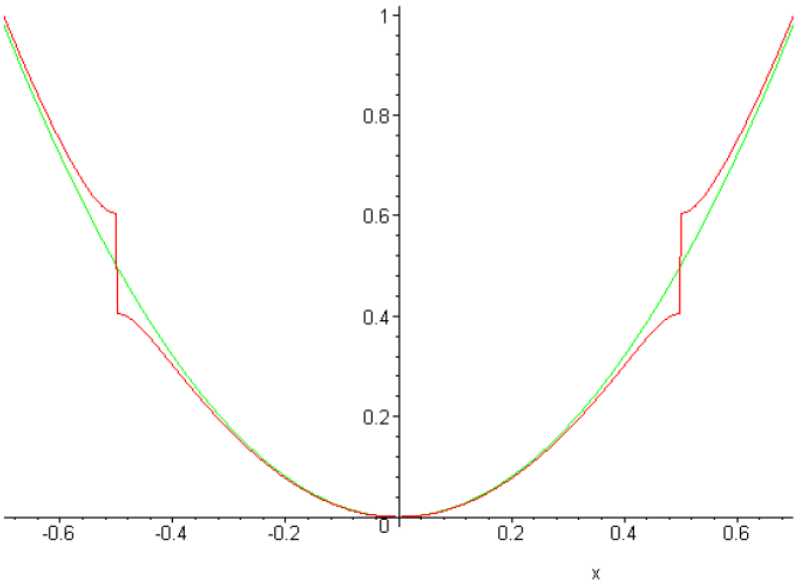

Figure 1.7 Schematic diagram of a Mott insulator state before and after a Peierls transition (top) in molecular materials. The lower diagram depicts the energy state distribution of a Mott insulator state (green) and a Peierls state (red) with an obvious Peierls energy gap.

Apart from the initial interest in the conducting state, the superconducting fluctuations of TTF-TCNQ that were discovered opened up an exciting new research effort in the area organic-based superconductors.[14] The donors that have been used in these efforts are BEDT-TTF (bis(ethylenedithio)tetrathiafulvalene. also known as ET) and TMTSF (tetramethyltetraselenafulvene). Unprecedented superconductivity behavior of various salts of these donors has been observed under high pressure (~10 kbar) and very low temperatures (~1 K). The first example of superconductivity was discovered for $(TMTSF)_2PF_6$ in 1979 which undergoes a phase transition under a hydrostatic pressure of 12 kbar at 0.9K. [15] By combining partially oxidized TMTSF cations with various anions a family of metallic conductors $(TMTSF)_2X$ (X =PF_6, SbF_6, TaF_6, ClO_4, AsF_6, ReO_4, SO_3F) was prepared. Figure 1.8 shows the structure of $(TMTSF)_2(PF_6)$ and Figure 1.9 depicts a conducting phase diagram of $(TMTSF)_2(PF_6)$.

The combination of BEDT-TTF cations with different anions also lead to a series of molecular conductors and a large number of them exhibit superconductivity behavior even under ambient pressure at low temperatures. The first example of an ambient pressure ET superconductor is β-$(ET)_2I_3$ reported in 1984[16] and subsequent work revealed that the application of high pressure increases the critical temperature of the superconducting state.[17] Unlike the TMTSF compounds, ET conductors are often interpreted to be quasi-2D conductors because the sulfur atoms on the expanded ring lead to orbital overlap laterally as well as in along a 1-D stack.

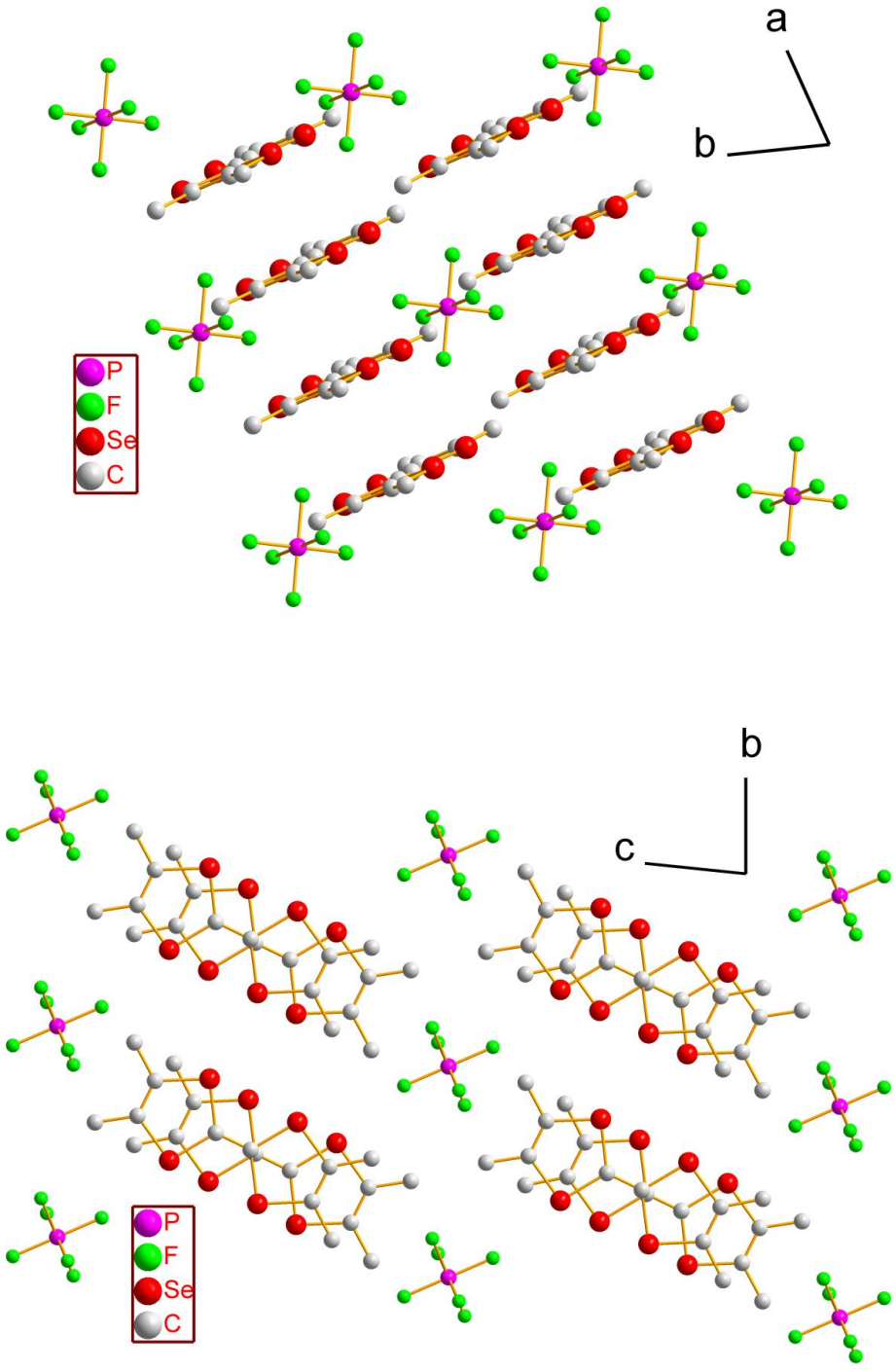

Figure 1.8 The structure of $(TMTSF)_2(PF_6)$ in the *ab* plane and *bc* planes.[17]

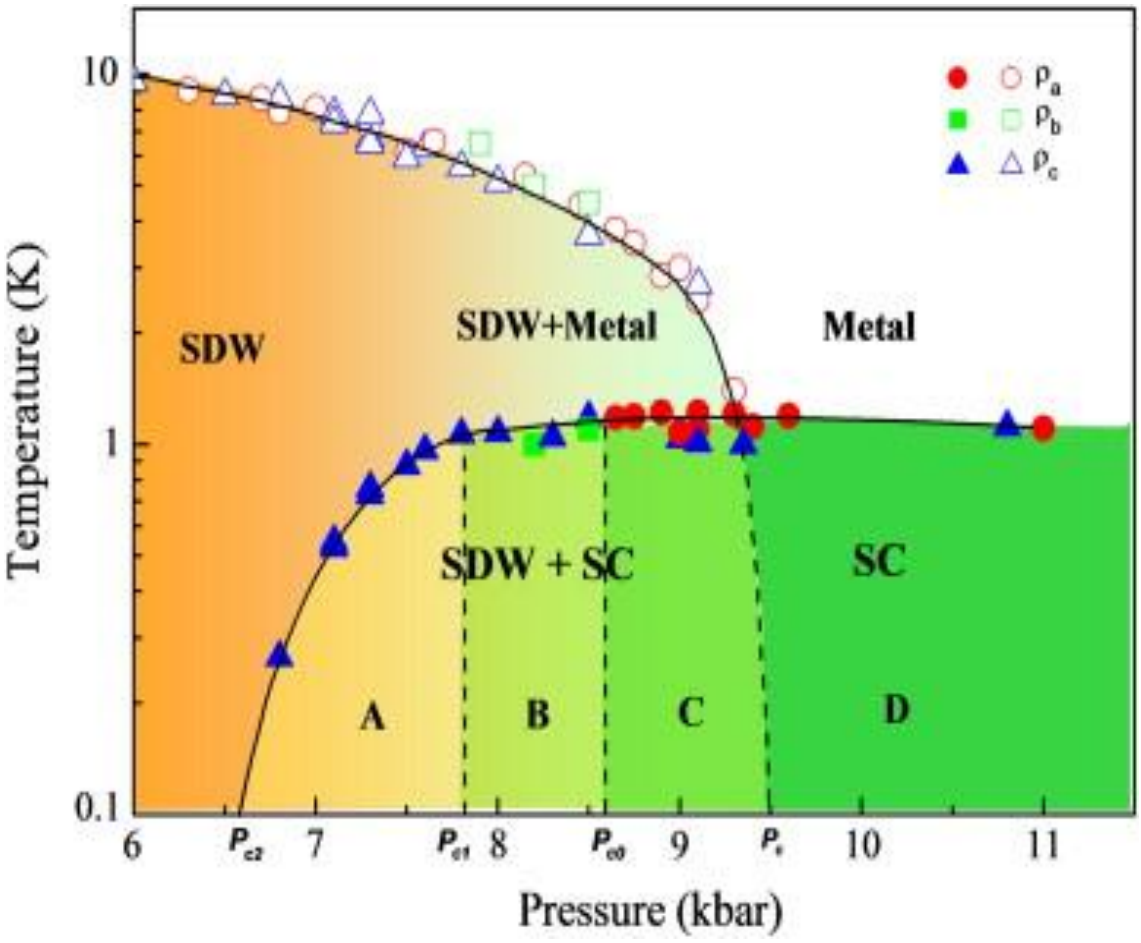

Figure 1.9 A conducting phase diagram of $(TMTSF)_2(PF_6)$ based on variation of temperature and pressure along the *a*, *b* and *c* axes with corresponding data points of ρ_a, ρ_b and ρ_c. SDW = spin-density wave (same as charge density wave when s radical electron is the charge carrier); SC = superconducting.

Molecular Conductors Based on TCNQ and DCNQI

The TCNQ acceptor was the first of its kind to be exploited for organic conductors, but in the 1970s metal cation-TCNQ materials were also investigated. The first series of M(TCNQ) salts to be systematically studied are the alkali metal TCNQ salts. In these studies, Na^+, K^+, Rb^+ $TCNQ^-$ salts were first prepared in 1969,[18] and found to exhibit a magnetic phase transition which was found to be associated with a conducting phase transition in 1972.[19] The structures were analyzed by X-ray diffraction on large single crystals obtained by electrocrystallization methods.[20] Phase transitions were observed for structures at different temperatures which supported the conclusion that increases in magnetization and conductivity are caused by a disruption of the dimerization of the TCNQ anions and antiferromagnetic interactions between the adjacent radicals in the structure. This work underscores the importance of polymorphs for these materials for tuning physical properties.

In the vein of research in this dissertation are conductors based on group 10-TCNQ coordination frameworks, namely Cu(TCNQ) and Ag(TCNQ), and Cu(TCNQ) which became famous after Potember and coworkers reported unique electrical switching behavior of Cu(TCNQ) thin films.[23a,23b] A Cu/Cu(TCNQ)/Al sandwich device was prepared which was found to exhibit dramatically different conducting behavior under different applied voltages: 2MΩ when U<5.5 V, and 200Ω when U>5.5V. In the follow-up investigations by other groups, several problems were found to arise. The most serious one of which was irreproducibility of the resistivity behavior of the sandwich device prepared in different laboratories.[21] This problem was a major obstacle for understanding the behavior of the device until it was solved by the Dunbar group in 1999

who discovered that there are actually two polymorphs of Cu(TCNQ).[22] The kinetic polymorph referred to as Phase I, exhibits semi-conducting behavior in pressed pellet form and is the phase present in the actual switching device. In contrast, the thermodynamic polymorph, Phase II, is an insulator and does not undergo switching. Since Phase I slowly converts to Phase II in the present of acetonitrile, the irreproducibility of sandwich devices is clearly due to varying amounts of Cu(TCNQ) Phase II in the films. Figure 1.10 displays the basic structural motif for Cu(TCNQ) Phase I and Phase II, and Figure 1.11 contains a schematic diagram of the sandwich device and the switching behavior.

A second long-lasting problem in the Cu(TCNQ) research is a lack of understanding of the mechanism for switching. By using *in-situ* spectroscopic techniques on the thin films, such as Raman, infrared, Auger, and XPS, [23]the mechanism was postulated to be partial decomposition of Cu(TCNQ) induced by the external field which leads to a combination of Cu_x^0 + $TCNQ_x^0$ + $[CuTCNQ]_{1-x}$ in the film. The Cu^0 atoms are thought to aggregate into conducting pathways that penetrate the thin film and the Al/Al_2O_3 electrode which lead to the highly conducting state of the device. However, this explanation is not entirely satisfactory because it is known that the switching property is also highly dependent on the fabrication of the device, such as the size of contact areas and the use of different electrode materials.[24] The question is still open as to whether the switching behavior is merely related to the physical structure of the device and the interfacial regions with no relationship to the intrinsic behavior of Cu(TCNQ).

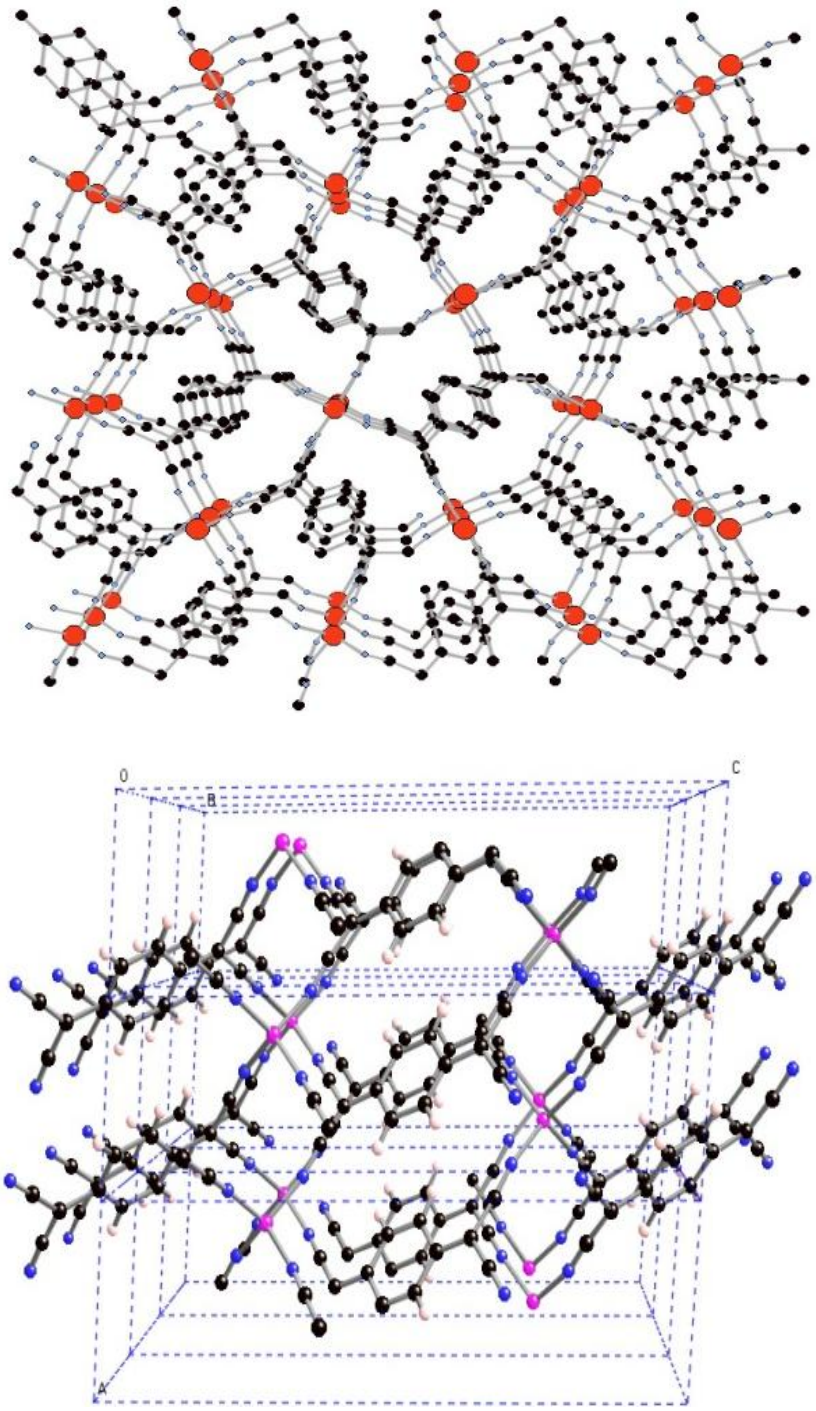

Figure 1.10 Structures of Cu(TCNQ) Phase I (top) and Phase II (bottom).

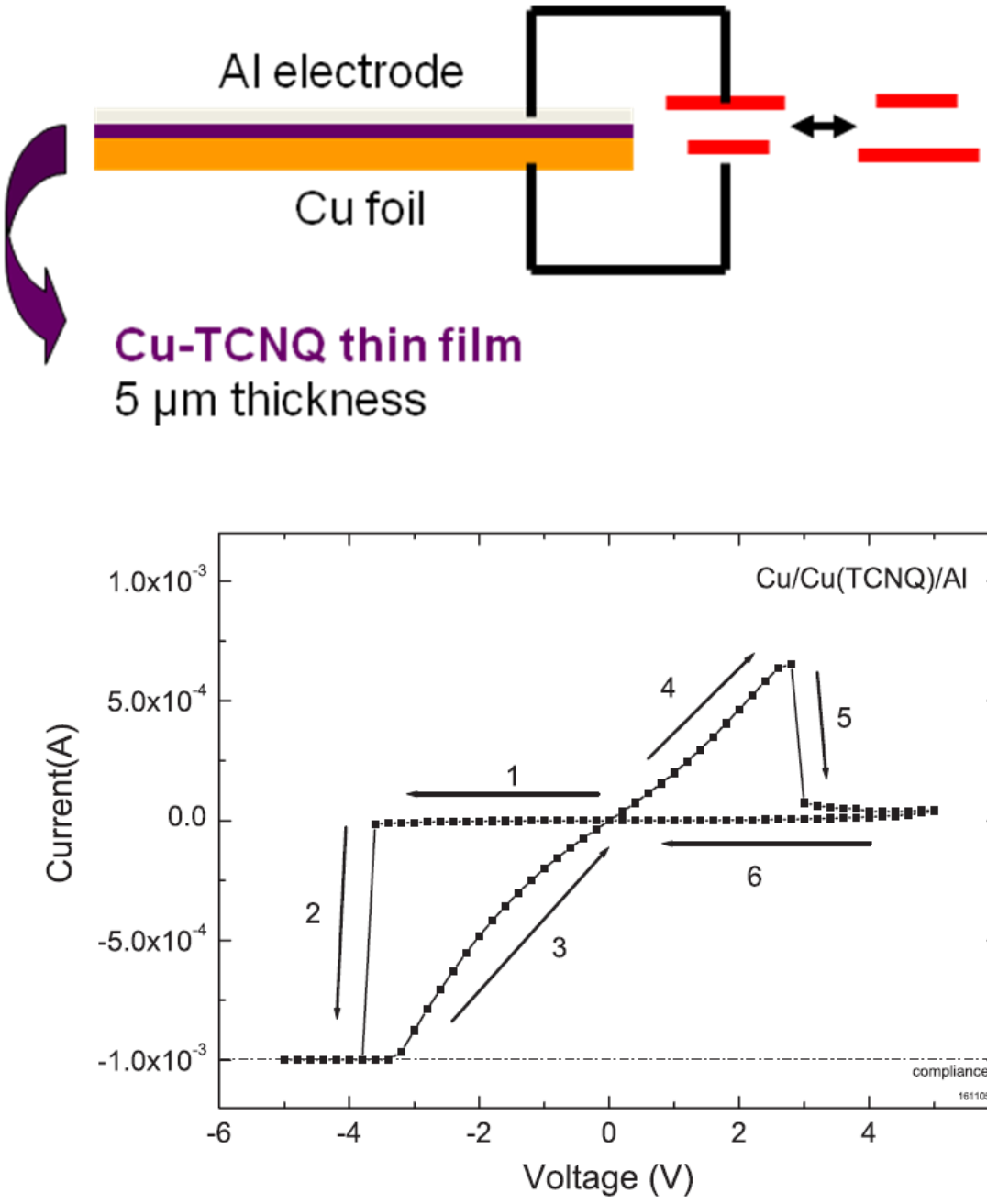

Figure 1.11 Schematic diagram of a Cu/Cu-TCNQ/Al sandwich device (top) and characteristic switching I-V behavior of device (bottom).[25]

The related coinage metal material Ag(TCNQ was also reported by Potember *et al.* to be an optical switching material early in 1982.[25] In contrast to Cu(TCNQ) whose structure was not known until the work from our group, the structure of Ag(TCNQ) was obtained in 1985 by Shields from a crystal grown by electrochemical methods.[26] Polymorphism in this material is also suspected and sparked a controversy,[27] but the properties of Ag(TCNQ) devices have not been found to be irreproducible owing to the fact that the second phase is only a slight variation of the original phase reported by Shields as judged by infrared and powder X-ray crystallography. In spite of the number of years since the original findings, extensive research is still being conducted on device design and applications of Cu(TCNQ) and Ag(TCNQ).

Another excellent organocyanide acceptor molecule is DCNQI and its derivatives. (DCNQI = *N, N'*- dicyanoquinodiimine). DCNQI also behaves as an organic acceptor which is slightly less stable in its radical form. Without substituents, syn- and anti- forms of DCNQI are possible and the crystallization of the compounds are difficult as a result of disorder involving the two isomers. Therefore, investigations have focused on the 2,5-derivatives of DCNQI, 2,5- R1,R2-DCNQI. (R1 = R2 = CH_3,CH_3O, Br, Cl, and R1 = CH_3, R2 = Br, Cl.) In these analogues, the relative position of the cyanide groups is restricted to the anti- form owing to the steric effect which led to greater ease of isolating crystals of a single isomeric product. In combination with different monovalent cations M^+ = Cu^I, Ag^I, Li^+, Na^+, K^+ and NH_4^+, a series of $M(DCNQI)_2$ molecular conductors were prepared and their conductivities were found to be surprisingly high and metallic ranging from 80 S/cm to 1000S/cm.[28] Most of these compounds undergo a metal-to-insulator phase transition in the temperature range of 70-235K, but

$Cu(2,5\text{-}R_1,R_2\text{-}DCNQI)_2$ ($R_1 = R_2 = CH_3$) was found to retain its metallic behavior down to 1.5 K! The unprecedented high conductivity is based on the presence of partially reduced DCNQI anions (calculated to be -2/3 for each DCNQI), which create holes in the conducting pathway and decrease the on-site Coulomb repulsion between activated electrons and local electrons on the molecules. Band structure calculations indicate that the overlap integrals between 3*d* orbitals of Cu and the LUMO of DCNQI species are considerably larger than the interactions between adjacent DCNQI molecules. This situation means that the 3d orbital of Cu contributes an important perturbation to the band structure in 2-D which has a profound effect on the conductivity of the material.[29] Figure 1.12 displays the structure of $Cu(2,5\text{-}Me_2\text{-}DCNQI)_2$.

Tuning the Conductivity with Structure

One of the attractive aspects of this chemistry is the level of control that one can exert over the properties of the materials. With even a minor change in the crystal structure, the physical properties will be drastically altered. Several factors affect the properties, the main one being the stacking distance between the functional molecules which, itself, directly affects the degree of orbital overlap, and, consequently, the electron transfer energy between the adjacent molecules. Another important issue is the degree of the electron accepting capabilities of the organic molecule which affects the local charge density on the donating functional molecules and the number of charge carrier in the conducting pathway. Higher dimensionality interactions can be triggered by structural changes that promote better overlap between metal ions and the organic acceptors.

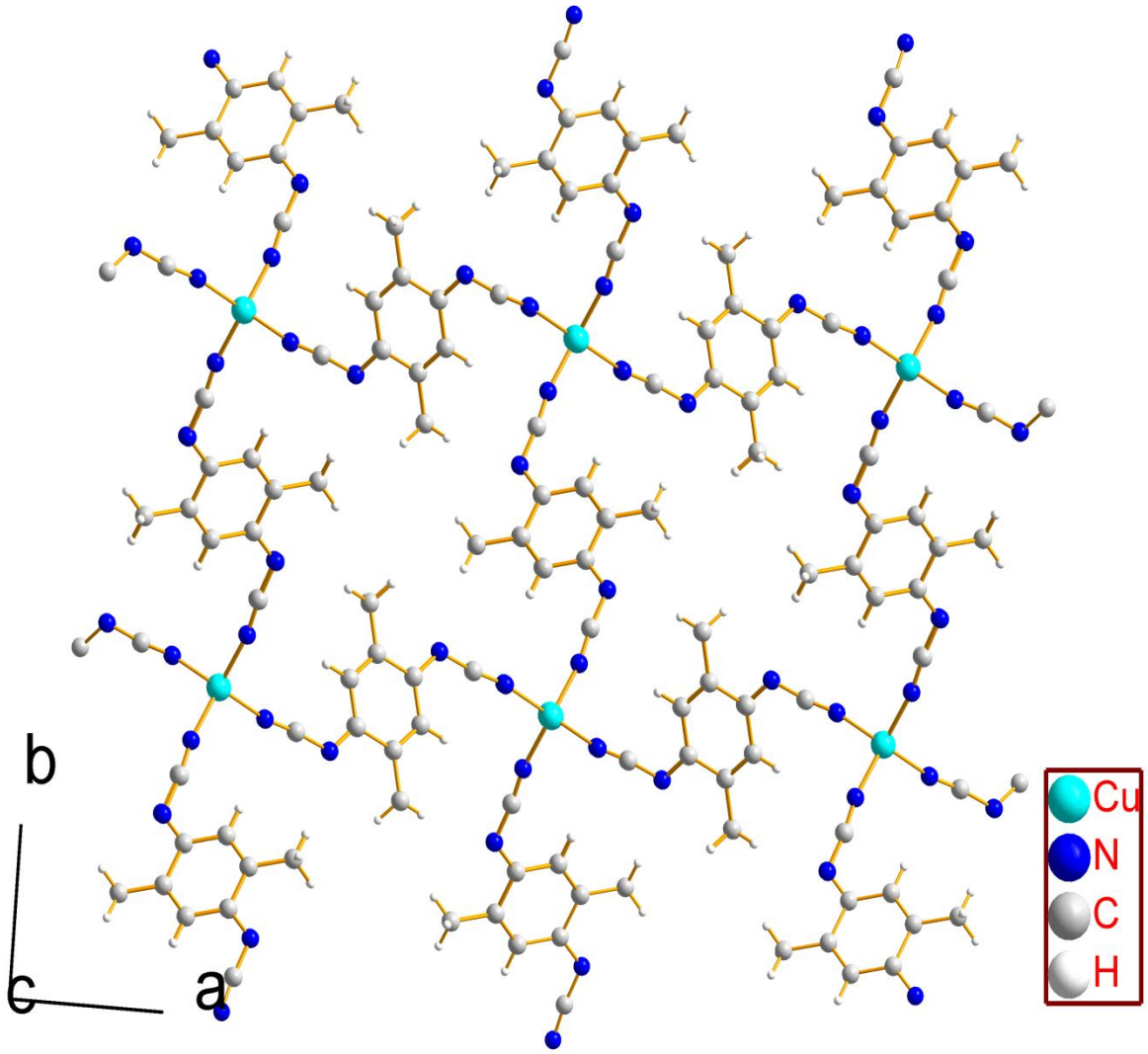

Figure 1.12 The structure of Cu(2,5-Me_2-DCNQI)$_2$ in the *ab* plane.

One elegant example of the possibilities available to chemists working in this area is the recent work of Dunbar *et al.* on the semiconductors $Cu(TCNQX_2)$ (X = Br, Cl). With only the very simple substitution of the 2,5 hydrogen atoms with halogens, the structures of $Cu(TCNQX_2)$ are very different from either Cu(TCNQ) polymorph and exhibit higher conductivities than Cu(TCNQ) Phase I.[30] The structure of the $Cu(TCNQX_2)$ materials is shown in Figure 1.13 and their conductivities are compared to Cu(TCNQ) phase I in Figure 1.14.

Another example that is excellent for the understanding of structure-property relationships is the aforementioned $Cu(DCNQI)_2$ series. As mentioned earlier the $Cu(2,5\text{-}Me_2\text{-}DCNQI)_2$ compound exhibits a much higher conductivity and retains its metallic behavior down until 1.5 K whereas other derivatives undergo a metal-insulator transition at ~200 K. Since their structures are almost identical, the reason is attributed to the slightly more acute N-Cu-N angles which result in a weaker crystal field and a less distorted tetrahedral coordination environment for the Cu cations. The result is a change in the relative energies of the Cu d_{xz} and d_{yz} orbitals which overlap to different degrees with the DCNQI ligands; if the overlap is increased, the result is a multi-Fermi surface character which leads to higher conductivities and lower phase-transition temperatures.[30]

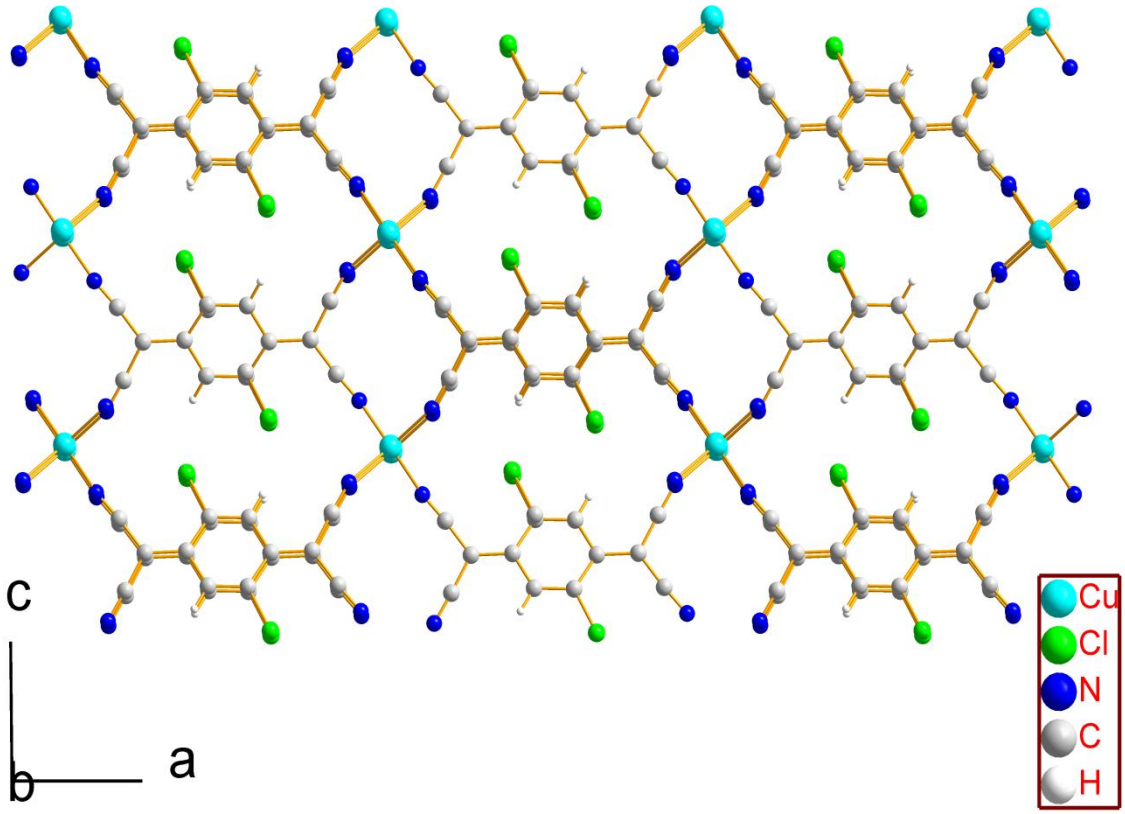

Figure 1.13 The structure of $Cu(TCNQCl_2)$, in the *ac* plane. $Cu(TCNQBr_2)$ is isostructural with $Cu(TCNQCl_2)$.

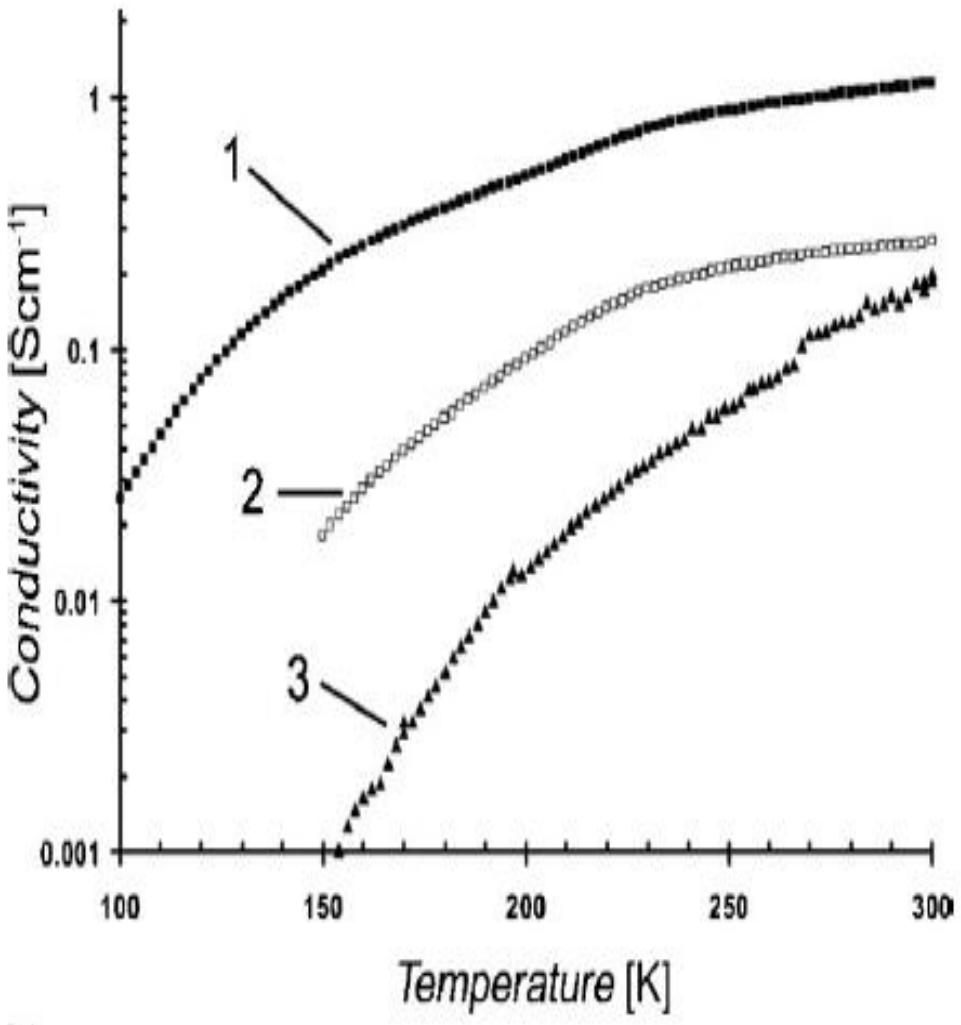

Figure 1.14 Comparison of temperature dependent conductivities of $Cu(TCNQCl_2)$, (1), Cu(TCNQ) Phase I, (2), and $Cu(TCNQBr_2)$, (3).

Multifunctional Molecular Electronics: Beyond Conducting

From the aforementioned examples of molecular conductors, one can extrapolate the design strategy of using open-shell organic molecules in conducting phases to the use of functional groups that could lead to multifunctional materials. One interesting goal for tuning the properties involves studying the interplay between conductivity and other phenomena. For example, conductivity can be perturbed by the application of an external magnetic field to induce magnetoresistivity and the application of pressure to study piezoresistivity. In the case of perturbation of the conductivity by light, the result is photoresisitivity. Moreover, alternating the applied electric field can potentially lead to a change in conductivity. Such behavior is called as non-linear conducting behavior and is generally considered to be the origin of intrinsic switching behavior. In the field of molecular conductors, the research is mainly focused on the non-linear behavior, and the interplay of molecular magnetism and molecular conductivity because redox active molecules or magnetic spin centers molecules are relatively easy to be introduced into the material.

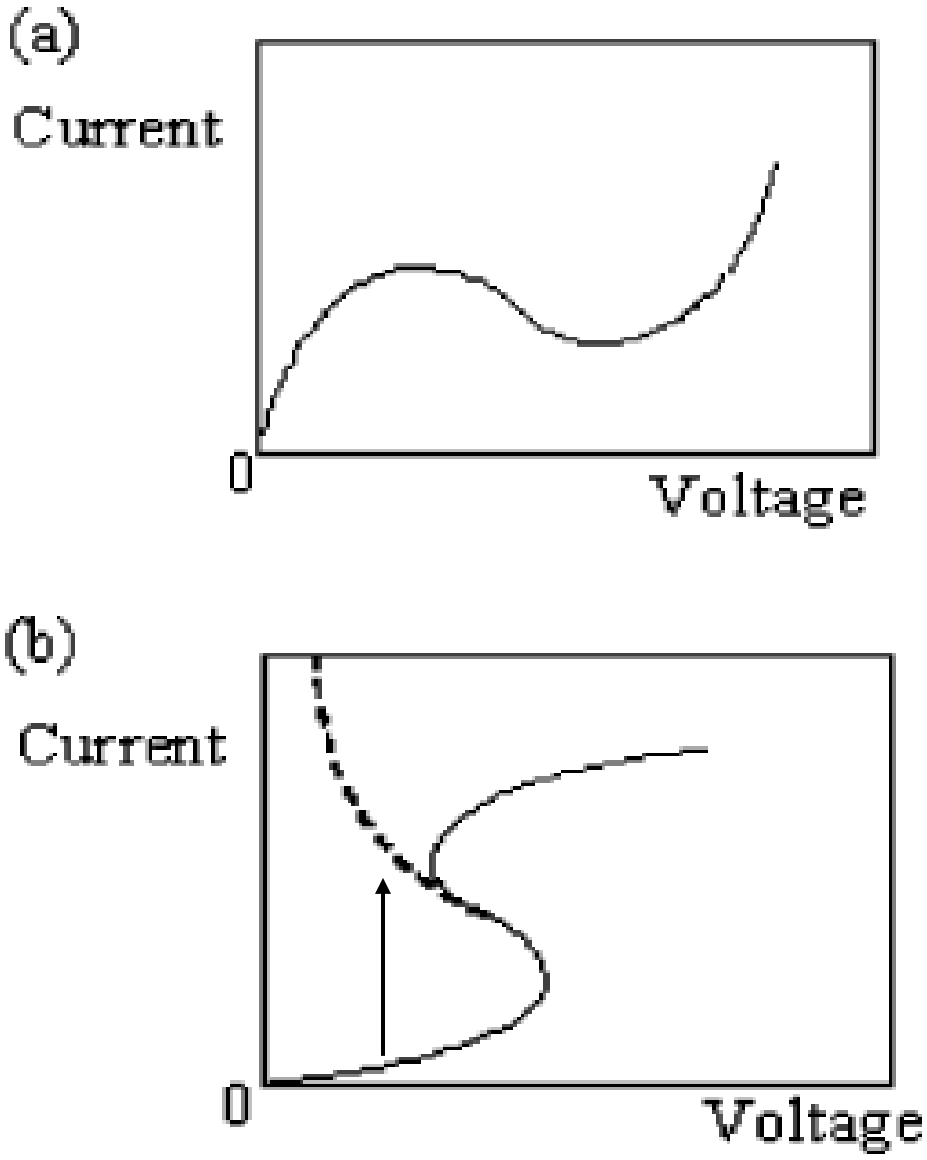

Figure 1.15 Typical I-V behavior illustrating non-linear conductivity. (a) represents the first type, which is commonly observed in GaAs or metal-oxides. (b) illustrates the typical behavior of charge transfer compounds. The solid line represents the theoretical model and the dashed line represents experimental measurements. The arrow indicates a potential pathway for a phase transition.

Non-linear Conductivity and Non-Volatile Memory

Traditional conductors obey Ohm's Law, namely the current that passes through the material is proportional to the applied voltage and the slope is the resistance of the material. In some special cases, the material will deviate from Ohm's Law and exhibit different resistance with the variation of applied voltages. From the different I-V behavior of these materials, two types of non-linear conductivity are observed as displayed in Figure 1.15. From the I-V curve, both types contain a region where the slope of V/I is negative. In this region, the resistivity is called negative differential resistivity (NDR), and is believed to be the origin of switching behavior.

The first type of non-linear behavior is mostly observed for bulk semiconductors such as GaAs or metal oxides, whereas most of the molecular conductors with non-linear behavior fall into the second category. Saito *et al.* has investigated a large number of charge transfer molecular conductors and pointed out that the second type of non-linear behavior may be universal for charge transfer compounds. [31] Generally speaking, the mechanism of non-linear behavior is a result of positive feedback of charge carrier number with an increase of external field caused by a field-induced structural change or domain movement. [32] One example that nicely illustrates this point is the non-linear behavior of K(TCNQ). With an increase in current density, the voltage across the sample decreases and exhibits a negative differential resistivity after the threshold field of 1920 V/cm with a stripe pattern being observed on the single crystal. This stripe pattern travels along the crystal with the applied current and disappears with the removal of current,

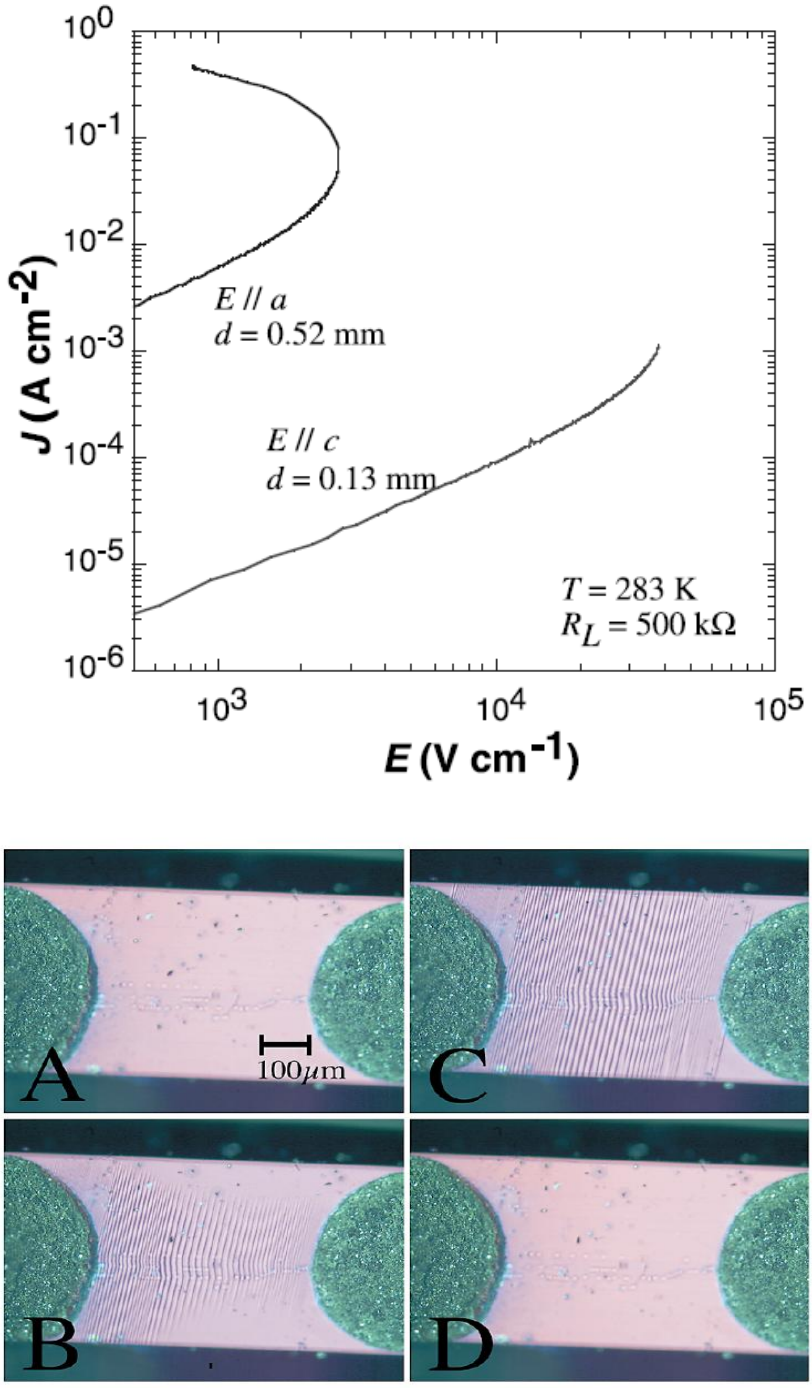

Figure 1.16 Non-linear behavior of K(TCNQ) (top) and the stripe pattern induced by current (botton). The voltage applied in the A, B, C, D cases is 0 V, 800 V, 1000cV, and 0 V respectively.

which suggests a current-induced structural phase change from dimerized (high resistivity) to non-dimerized TCNQ (low resisitivity) stacks. Figure 1.16 depicts the non-linear behavior of K(TCNQ) below 283 K, and the stripe pattern under the applied current.[33]

An important application of non-linear behavior is for non-volatile memory devices. (NVM) Non-volatile memory is widely used in modern computers as temporary data storage such as RAMs (random-access memory). The memory effect is retained even after removal of the external field and will maintain the state (conducting or insulating, or "1" and "0") until erased by another applied field. By this definition, many molecular conductors with non-linear behavior can be used as non-volatile memory units since they undergo field-induced phase transitions. As displayed in Figure 1.11, the Cu(TCNQ) device is a non-volatile memory in the “ON” state when it is highly conducting and the conductivity will not revert to the low conducting state until a sufficiently strong reverse field is applied. From the beginning of the field, Cu(TCNQ) has been considered as a classic example of non-linear conductivity and non-volatile memory.

Co-Existence and Synergism of Magnetism and Conductivity

Molecular magnetism is a rapidly developing field. As compared to conventional magnets such as metals and metal oxides, molecule-based magnets have similar advantages to molecular conductors, namely miniature domain size, tunable design features and ease of processing. Targets of modern research in the area of molecular magnets are extended phase materials with high ordering temperatures and discrete molecules that exhibit magnetic hysteresis similar to bulk magnets, which are referred to as single-molecule magnets (SMMs).[34] The great potential for applications in the mass

data storage, fast processing devices and quantum computing is driving scientists to keep developing new molecular magnets, especially low dimensional materials such as single molecule magnets, SMMs, which are 0-D[35] and single-chain magnets, SCMs, which are 1-D.[36]

Since most of the charge carriers in molecular conductors are electron spins, it is not unusual that researchers are interested in the co-existence of magnetic and conducting properties. Interactions between localized spins and itinerant spins provide an opportunity for tuning the conducting behavior with an external magnetic field. The simplest design strategy in this vein is to combine magnetic cations or anions with electron donors or acceptors.[37] The first organic conductor with magnetic anions was prepared by Day *et al.* who reported (BEDT-TTF)$_4$Fe(C_2O_4)$_3$·A·C_6H_5CN (A=H_2O, K^+, NH_4^+). For A = H_2O, the compound undergoes a semiconducting to superconducting transition at ~ 7K, and the transition temperature is sensitive to the applied magnetic field along the conducting axis.[38] In 1999, Kobayashi *et al.* prepared κ-$BETS_2(FeBr_4)$, (BETS=bis-(ethylenedithio)-tetraselenafulvalene), which is a metallic conductor with an antiferromagnetic transition at 2.5 K and a metal-to-superconducting transition at 1.1 K.[39] Later, (BEDT-TTF)$_3$[$Mn^{II}Cr^{III}(C_2O_4)_3$] was synthesized by Coronado *et al.* in 2000 as the first conductor with concomitant ferromagnetic ordering.[40] In the structure (Figure 1.17), the columns of BEDT-TTF are responsible for the conducting property whereas the layers of oxalate-bridged 3d cations exhibit ferromagnetic behavior.

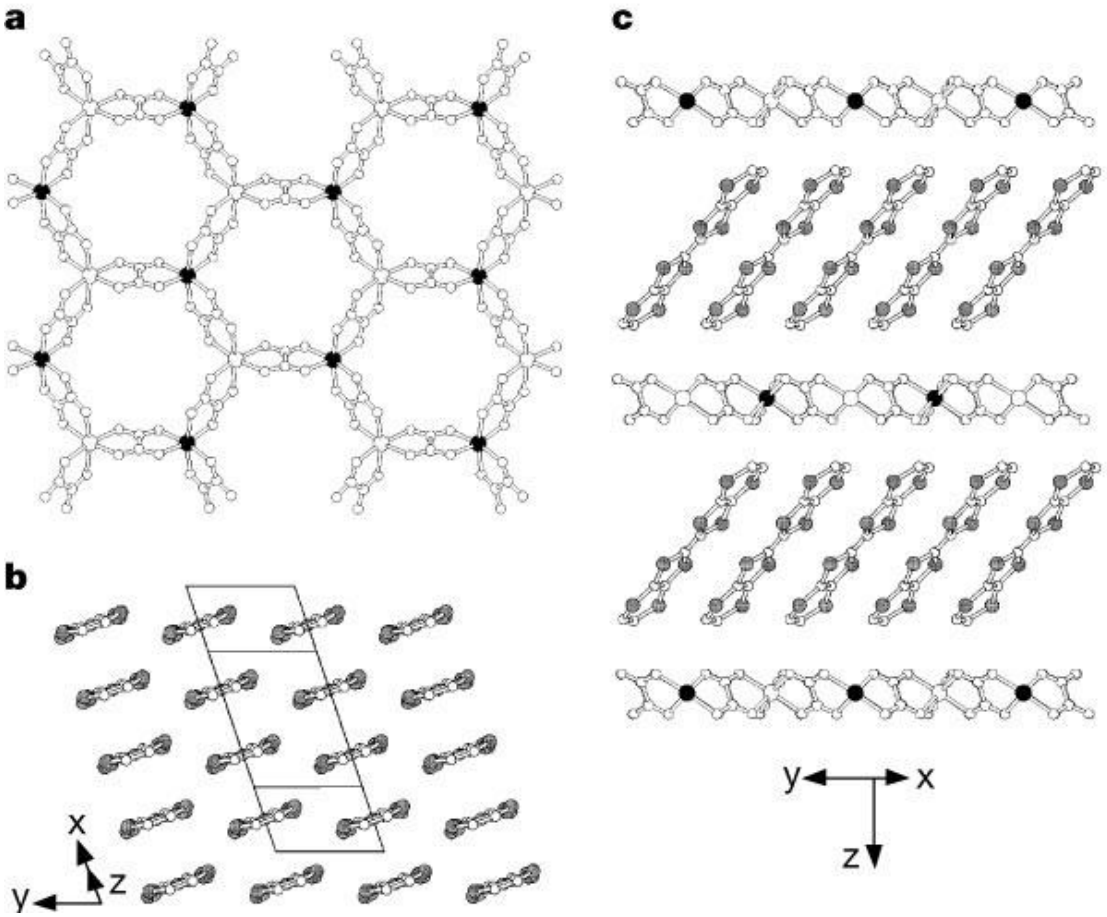

Figure 1.17 The structure of two sub-lattices of the hybrid material: $(BEDT\text{-}TTF)_3[Mn^{II}Cr^{III}(C_2O_4)_3]$. (a), the honeycomb-shape layer of Mn^{II} and Cr^{III} cations bridged by oxalates (b), the columnar stack of BEDT-TTF cations (c), the relative position of BEDT-TTF stacks and metal-oxalate frameworks.

After the molecule $[Mn_{12}O_{12}(OOCCH_3)_{16}(H_2O)_4]\cdot 4H_2O\cdot 2CH_3COOH$, commonly refered to a "Mn_{12}-acetate", was characterized as the first single-molecule to exhibit magnetic hysteresis,[41] the field of single molecule magnets (SMMs) has blossomed in the past decade. Consequently, the co-existence of SMM behavior and conducting properties in a single multifunctional material has become a new target. This strategy has been embraced by Yamashita and coworkers who combined the tetranuclear SMM cation $[Mn_2^{II}Mn_2^{III}(hmp)_6(MeCN)_2(H_2O)_4](ClO_4)_4\cdot 2MeCN$ (hmp= 2-hydroxymethylpyridine)[42] with $[NBu_4][Pt^{III}(mnt)_2]$ (mnt= 2,3-dimercaptomaleonitrile), a metal-dithiolene anion known for exhibiting high conductivity,[43] the results of which is the material $\{Mn_2^{II}Mn_2^{III}(hmp)_6(MeCN)_2(H_2O)_4[Pt(mnt)_2]_4\}[Pt(mnt)_2]_2$ with a coexistence of SMM and semiconducting properties.[44] The attempt of combining dimerized Mn-salen-type SMM catins [45] with $[Ni(dmit)_2]^-$ (salen = *N*, *N*′-ethylene-bis(salicylideneiminate), dmit = 4,5-dimercapto-1,3-dithiole-2-thione), another SMM semiconductor, leads to $[Mn(5\text{-}Rsaltmen)Ni(dmit)_2]_2$ (R=MeO, Me) with room temperature conductivities of 7×10^{-4} S/cm and 1×10^{-4} S/cm, respectively. [46] The coexistence of molecule magnetism and conductivity provides the opportunity for interplay between the magnetization and electron conduction, which leads to the potential of using external magnetic field to control the conducting state, consequently the application in the field of data storage and modern computing. The structure of $[Mn(5\text{-}MeOsaltmen)Ni(dmit)_2]_2$ and the frequency-dependent AC susceptibility data are displayed in Figure 1.18.

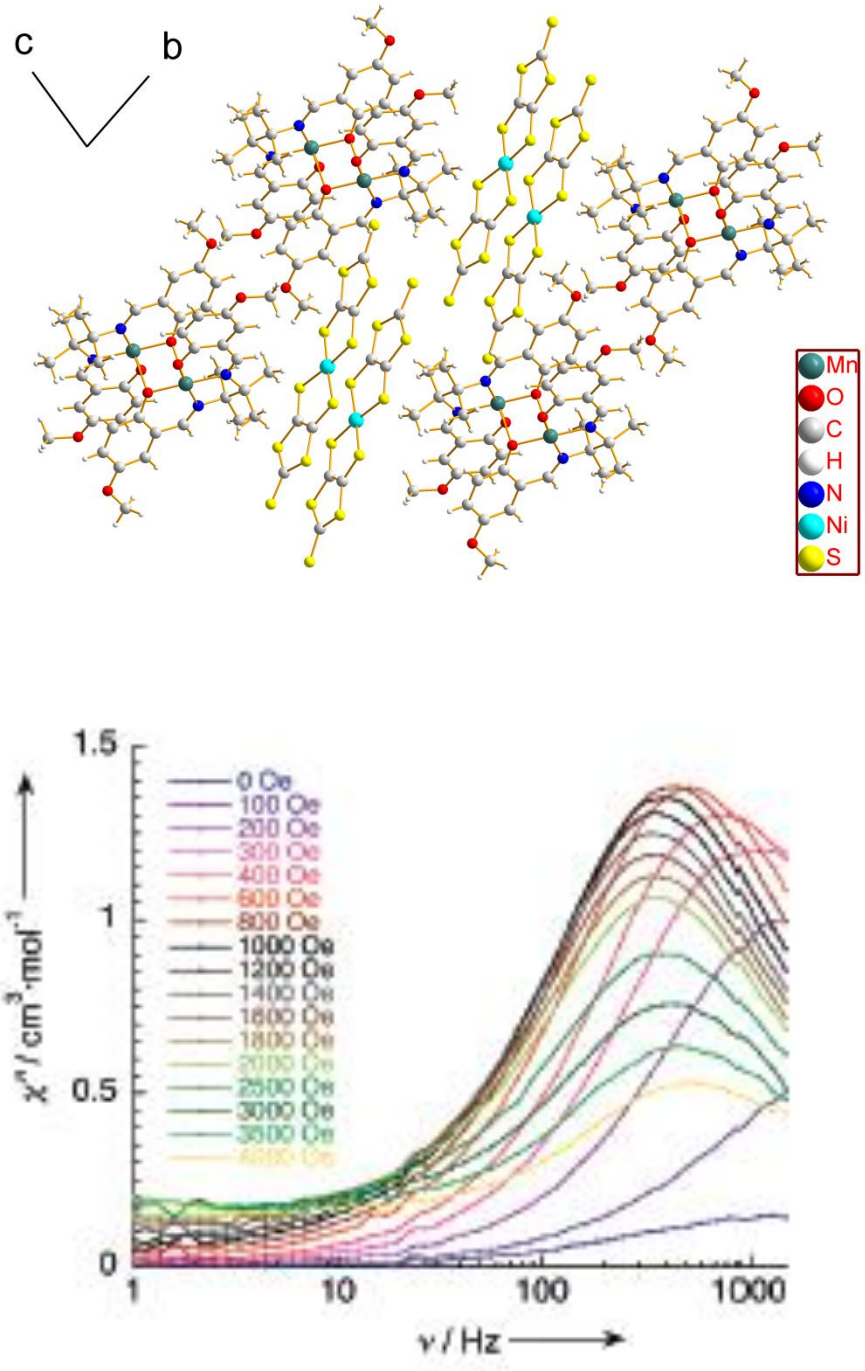

Figure 1.18 The *bc* plane view of $\{Mn(5\text{-MeOsaltmen})[Ni(dmit)_2]\}_2$ (top) and its frequency-dependent out-of-phase component of AC susceptibility (bottom).

Molecular Conductors with Non-Electron Charge Carriers

The field of porous metal-organic frameworks (MOFs) became a topic of high interest in recent years,[47] and chemists have started looking into the conducting materials in which the charge carriers are not electrons but rather protons or lithium cations. These carriers are bigger than electrons but are relatively smaller than the channels or pores in the MOF structures, therefore the transport of carriers is feasible due to the porosity of these frameworks. For conductors with proton carriers, the major pathway is considered to be hydrogen bonding through guest water molecules in the MOF channels. As a result, the strategy of introducing non-electron conductivity into MOF chemistry is to expose MOFs to humid air (for less water-stable MOFs), water or lithium salt solutions, and take advantage of the absorption of water molecules and lithium cations as transporting guests in the frameworks.

Recent results of MOF conductors involving lithium charge carriers were reported by Long *et al.*, By soaking the desolvated MOF, Mg_2(dobdc) ($dobdc^{4-}$ = 2,5-dioxido-1,4-benzenedicarboxylate) in solutions of $LiBF_4$, LiO^iPr, and ($LiBF_4$ + LiO^iPr mixtures, a series of lithium conducting materials were obtained with a room-temperature conductivity up to 3.1×10^{-4} S/cm.[48] With the proper concentration of LiO^iPr, the $^iPrO^-$ anion is attracted by polar Mg^{2+} ions in the structure, and the hydrophobic ^{i}Pr group protects the channel from polarization and enhances the mobility of impregnated Li^+ cations which is important for potential applications as a conducting separator in a lithium battery.

Several examples of water-absorbed MOFs acting as proton conductors have been reported by H. Kitagawa and coworkers in recent years;[49] an elegant example of a

compound that exhibits a proton conducting pathway is $Mn(DHBQ)(H_2O)_2$ (DHBQ=2,5-dihydroxy-1,4-benzoquinone). The structure of $Mn(DHBQ)(H_2O)_2$ consists of a chain of Mn(II) ions connected by $DHBQ^{2-}{}_{ligands}$ in the equatorial position with two coordinated water molecules in the axial positions. In the structure (Figure 1.19), the axial water molecules from different chains and the hydroxy groups on the ligands are connected through hydrogen bonding which forms a pathway for proton conduction. The compound exhibits a room temperature conductivity of 4×10^{-5} S/cm whereas the anhydride compound is completely insulating. [50a] Since the occupancy of water in MOFs is determined by the humidity of environment, it is believed that MOF proton conductors are promising in humidity sensor applications.

Perspective of TCNQ-based Conductors and Molecular Electronics

As already mentioned in the background section, TCNQ has the potential to be a critical building block in novel molecular conductors and multifunctional molecular electronics. Playing both roles as anion and ligand, TCNQ radicals can be combined with functional cations, including transition metal and lanthanide metal ions, which may potentially lead to a coexistence of conductivity and other properties. On the other hand, with all the fascinating behavior that TCNQ-based conductors can potentially exhibit, such as non-linear behavior, switching properties and phase transitions; the mechanisms of these responses need to be unearthed. Part of the reason for the lack of understanding stems from the difficulty of separating and structurally characterizing a pure, single domain crystal of the material, thereby prevents anisotropic measurements and theoretical simulations to be applied to the materials. Therefore, it is essential to prepare crystalline,

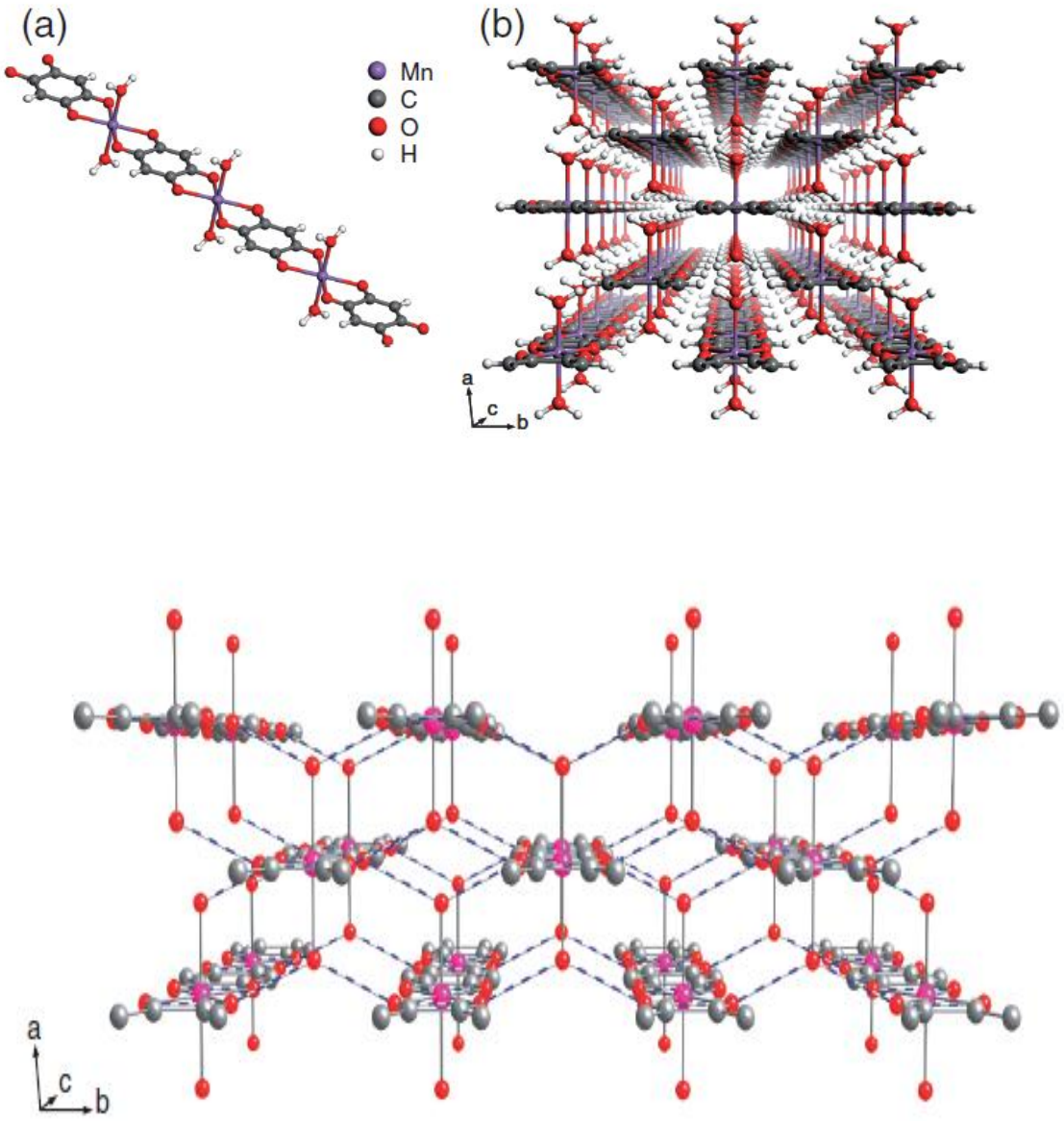

Figure 1.19 The structure of $Mn(DHBQ)_2(H_2O)_2$ as single chain (a), packing diagram (b), and the illustration of hydrogen bonding (bottom).

pure materials of TCNQ-based materials, to investigate their properties, and understand the relationship between their properties and structures.

With this overarching goal in mind, this dissertation focuses on the syntheses, characterization, and modeling of molecular conductors based on TCNQ and its derivatives. The purpose of this research is to gain a better understanding of the mechanism of molecular conductivity, and to develop a design strategy for future molecular electronic devices with enhanced conductivities and multifunctionality.

CHAPTER II

DRAMATICALLY DIFFERENT CONDUCTIVITIES FOR POLYMORPHS OF THE MAIN-GROUP TCNQ BINARY MATERIAL Tl(TCNQ)*

Background

With the conventional materials used for memory storage approaching their size limit in the near future,[2] advances in technology demand new types of nanoscale materials with higher storage densities and faster response times. In this vein, materials that respond to the application of an electric field or changes in light, pressure, or temperature are being sought for incorporation into electronic devices with ultra-fast operating speeds.[50] Examples of molecule-based materials that exhibit fascinating properties with promise as bistable switches are the spin crossover complex $Fe(abpt)_2(TCNQ)_2$ [51] (abpt = 4-amino-3,5-bis(pyridin-2-yl)-1,2,4-triazole), the single component conductors, $Ni(tmdt)_2$ and $Ni(dmit)_2$ (tmdt = trimethylenetetrathiafulvalenedithiolatedmit, dmit = 4,5-dimercapto-1,3-dithiole-2-thione.), [52] the metallo-organic conductor $Cu(DM\text{-}DCNQI)_2$,[31, 53] (DM-DCNQI = Dimethyl-*N*,*N*′- Dicyanoquinonediimine) and the organo-sulfur cation salt

---

*Part of this chapter is reprinted with permission from *Angew. Chem. Int. Ed.* Avendano, C.; Zhang, Z.; Ota, A.; Zhao, H.; Dunbar, K. R.; *"Dramatically different conductivity properties for MOF polymorphs of Tl(TCNQ): an unexpected room temperature crystal-to-crystal phase transition that alters Tl•••Tl contacts and TCNQ—TCNQ stacking interactions."* **2011**, *50*, 6543-6547. DOI: 10.1002/anie.201100372. Copyright 2011 by WILEY-VCH Verlag GmbH & Co. KGaA, Weinheim.

$(EDO\text{-}TTF)_2PF_6$,[54] (EDO-TTF = ethylendioxy-tetrathiafulvalene). These examples constitute compelling evidence that molecular solids are highly promising for use in future device applications.

As mentioned in chapter I, the most extensively studied example among molecule-based materials in the case of electric-field-induced switching behavior is the organocyanide 3-D coordination polymer Cu(TCNQ). This material converts from an insulting state to a highly conducting state with the application of an external electric field or upon irradiation with light.[27] Interestingly, a similar current induced conducting state transition was also observed for the simple alkali metal salt K(TCNQ).[34] The key structural issues driving the properties of these materials is the arrangement of fully reduced TCNQ radicals in columns. In the evenly separated case, the material is characterized as a "Mott insulator" and exhibits a relatively high conducting state. The typical phase transition, known as the spin-Peierls transition, occurs when the temperature is decreased and involves π-dimerization of adjacent radicals in the column; the result is a relatively poor conductor as the electrons become highly localized. The metastable nature of the stacking arrangements in metal-TCNQ binary compounds depends on temperature and the synthetic conditions used to prepare them. These "soft" materials exhibit rich polymorphism and their conducting behavior is dictated by the particular structure of each phase.

In the quest for TCNQ-based conducting salts, it is instructive to capitalize on the rich chemistry of alkali metals, for example thallium which behaves as an pseudo-alkali metal. In contrast to other Group 13 elements, Tl prefers the 1+ oxidation state (although Tl^{3+} is known), and many similarities between the chemistry of

alkali-metal ions and Tl^+ have been noted.[55] The electronegativity of Tl (2.04) is much higher than that of any alkali metal, which should lead to less ionic compounds with smaller band gaps and thus higher carrier mobility. Moreover, unlike alkali metals, Tl^I possesses a stereoactive lone pair which is expected to lead to greater structural diversity than that found for alkali metals.[55b,56] When we began our work in this area, we discovered that Hünig *et al.* had reported the reaction of the organic donor DM-DCNQI in its radical anion form with Tl^I which led to the isolation of the one-dimensional semiconductor, $Tl(DM\text{-}DCNQI)_2$, with a room temperature conductivity comparable to a metal (σ_{RT} = 50 S/cm).[57] Given that main-group organocyanide chemistry is essentially an unexplored area with the only example being the aforementioned material, we elected to study the chemistry of thallium(I) with $TCNQ^{-\bullet}$ and the physical properties of the binary phase(s). In this chapter, the syntheses, structures and properties of two distinct polymorphs of Tl(TCNQ) aree described. The project was initiated by Dr. Avendaño and completed by Zhongyue Zhang in his dissertation research. The individual contributions will be mentioned in the following paragraphs.

Experimental Section

General considerations. The TCNQ and $TlPF_6$ (98%) starting materials were purchased from TCI and used without further purification. Methanol was purified by distillation with magnesium turnings and a small amount of I_2 to initiate the Grignard reaction. Acetonitrile was pretreated with 3Å molecular sieves and purified by re-distillation with molecular sieves. Infrared spectra were obtained on a NEXUS 470 FT-IR using KBr plates and Nujol. Magnetism and conductivity data were collected on a Quantum Design MPMS model SQUID. For the conductivity measurements, the four-probe method was

used with four 50 μm diameter gold wires being attached with gold paste to a rectangular shaped pressed-pellets of microcrystalline powders of Phase I and Phase II.

Bulk preparation of Tl(TCNQ) Phase I. A dark green solution of LiTCNQ (0.211 g, 1.0 mmol) in 5 mL of methanol was slowly added to a colorless solution of $TlPF_6$ (0.350 g, 1.0 mmol) in 5 mL of water. The mixture was then diluted with an additional 10 mL of water and stirred for 5 minutes. The resulting dark purple powder was quickly filtered and dried *in vacuo*. Yield = 0.113 g (0.28 mmol), 28%.

Single crystals of Tl(TCNQ) Phase I. Single crystals were grown over the course of 1 week in a 3 mm diameter sealed glass tube by slow diffusion of 10 mL of a methanol solution of LiTCNQ (0.042g, 0.2mmol) into a 15 mL water/methanol (4:1 v/v) solution of $TlPF_6$ (0.070g, 0.2mmol). Elemental analysis calcd. for **1** $C_{14}N_4H_4Tl$: C, 35.21; H, 0.99; N, 13.69; Found: C, 35.89; H, 0.94; N, 13.89%. IR(Nujol): ν(C≡N) 2181, 2164, 2151 and δ(C-H) 823 cm^{-1}. Elemental analysis and infrared spectra were performed on single crystal samples prepared by Dr. Avendaño .

Bulk preparation of Tl(TCNQ) Phase II. A dark blue solution of LiTCNQ (0.150 g, 0.7 mmol) in 10 mL of methanol was slowly added to a colorless solution of $TlPF_6$ (0.175 g, 0.5 mmol) in 10 mL of water. The mixture was stirred in air for 20 minutes to yield a dark purple powder which was filtered, washed with copious amounts of water and diethyl ether and finally dried in air. Yield = 0.180 g (0.41 mmol), 82 %. Elemental analysis calcd. for **2** $C_{14}N_4H_4Tl$: C, 35.21; H, 0.99; N, 13.69; Found: C, 35.83; H, 0.98; N, 13.90%. IR(Nujol): ν(C≡N) 2180, 2149 and δ(C-H) 822 cm^{-1}.

Single crystals of Tl(TCNQ) Phase II. Single crystals of Tl(TCNQ) Phase II were obtained as a by-product during the isolation of single crystals of Phase I. Two types of

crystals formed in the thin tube as determined by inspection of the material under a microscope. A small amount of dark purple, needle-like crystals of Phase I were observed along with very small, dark blue dendrites which are aggregates of Phase II crystals.

Single crystal X-ray data collection and refinement. Single crystal structure diffraction data were collected on a Bruker APEX II diffractometer for Phase I and on the ChemMatCars synchrotron beamline at the Advanced Photon Source (APS), Argonne National Laboratory. Unit cell refinement and integration was performed with a Bruker APEX II software package. Absorption corrections were performed with the SADABS program in the Bruker SHELX software package. Structure solution and refinement procedures were performed with the SHELX program along with the graphical interface XSEED.

Structural Discussion

Tl(TCNQ) Phase I. Phase I crystallizes in the $P2_1/c$ space group as a 3-D network polymer consisting of metal ions arranged in linear strings, each surrounded by four stacks of TCNQ acceptor molecules and with adjacent TCNQ stacks being rotated by 90° with respect to each other, as in the case of Cu(TCNQ) Phase I. In contrast to the latter, the TCNQ units in **1** propagate along the a axis with alternating distances of 3.16(1) Å and 3.35(1) Å between the π-stacked TCNQ radicals. Each Tl^I center is coordinated to eight TCNQ molecules; the stereoactive lone pair forces the Tl^I centers to be in a distorted cubic geometry (Tl-N distance: 2.70-3.27 Å). The distance between adjacent Tl metal ions along the short axis alternates between 3.46(1) and 3.70(1) Å. The packing

diagram of Phase I is displayed in Figure 2.1, and a side-view of Phase I that illustrates the separation between the TCNQ radicals is displayed in Figure 2.2.

Tl(TCNQ) Phase II. Crystals of Phase II could not be obtained other than as very small crystallites, therefore structural data were collected at the ChemMatCars APS synchrotron facility at Argonne National Laboratories. Phase II crystallizes in the P2/c space group as a 3-D network polymer whose structure consists of Tl^{I} ions surrounded by four stacks of TCNQ acceptor molecules as found in Phase I, but with adjacent TCNQ stacks arranged in a parallel orientation with respect to each other. Another important difference between the polymorphs is that the distances between the adjacent TCNQ radical and adjacent Tl metal ions in Phase II are equivalent (3.22(2) Å and 3.79(2) Å respectively. As in the case of Phase I, the Tl^{I} ions in Phase II adopt a distorted cubic coordination environment as indicated by the inequivalent Tl-N bond distances. The larger differences in the Tl-N bond lengths for Phase I reflect a higher degree of distortion than Phase II. The more elongated Tl-N bonds observed for both polymorphs reflect the presence of Tl s-orbital lone pair electrons. In addition, in both structures, the distance between metal ions is slightly less than the sum of the van der Waals radii of two Tl^{I} ions (3.92 Å). Interactions between Tl atoms are quite rare and have only been documented in two other Tl compounds, $(Tl(DM\text{-}DCNQI)_2$ and Tl_2(phthalocyanine) with Tl••Tl contacts of 3.81Å 3.69Å respectively which are longer than those in the new Tl(TCNQ) phases.[57,58] The packing diagram of Phase II is displayed in Figure 2.3. Pertinent crystallographic data for Phase I and Phase II are listed in Table 2.1. The distorted cubic coordination environment of the Tl^{I} cations is depicted in Figure 2.4.

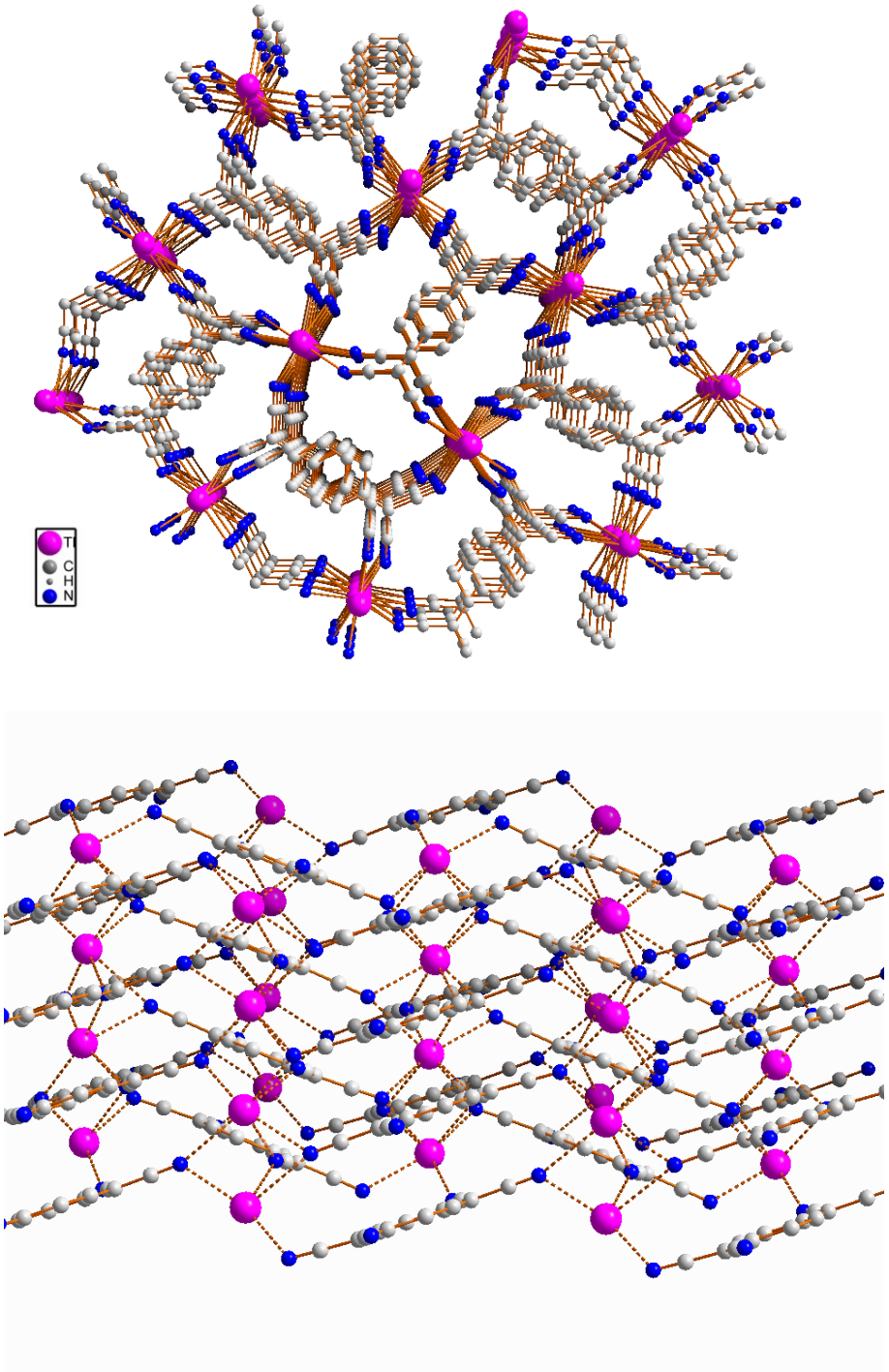

Figure 2.1 The top view (top) and side-view (bottom) of Tl(TCNQ) Phase I. The Tl-N bonds are represented by dashed lines.

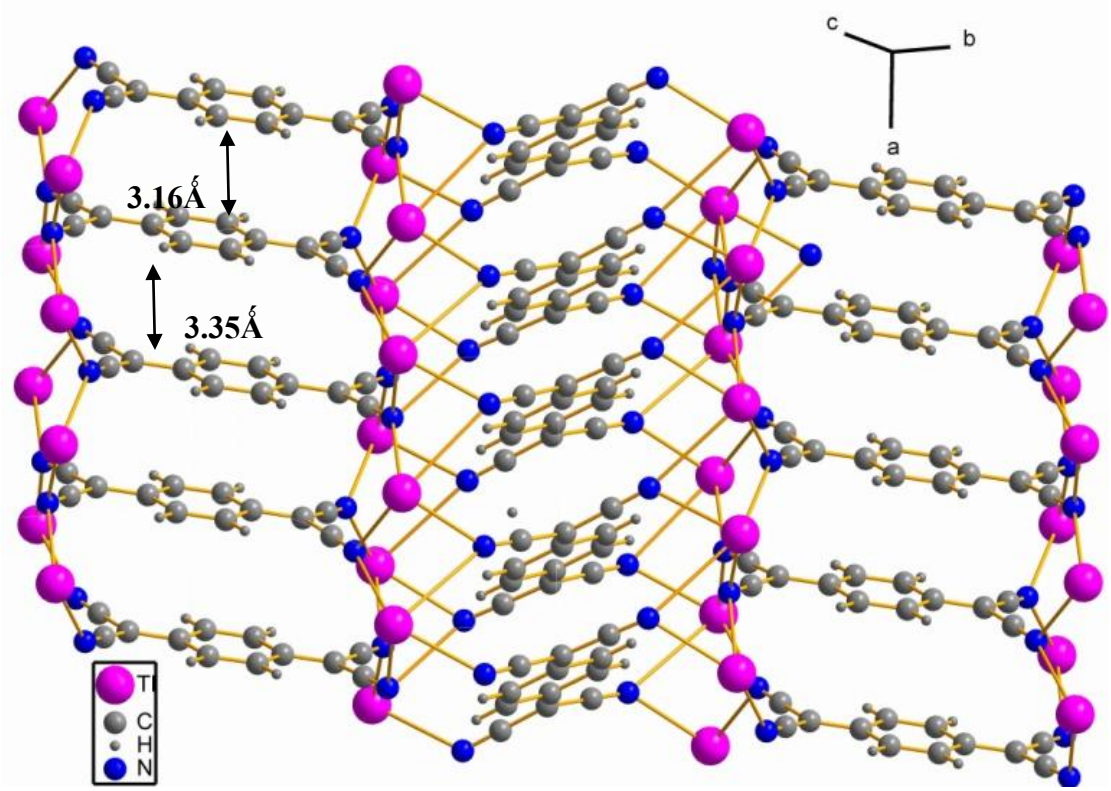

Figure 2.2 A side view of Phase I that illustrates the TCNQ interplanar separations.

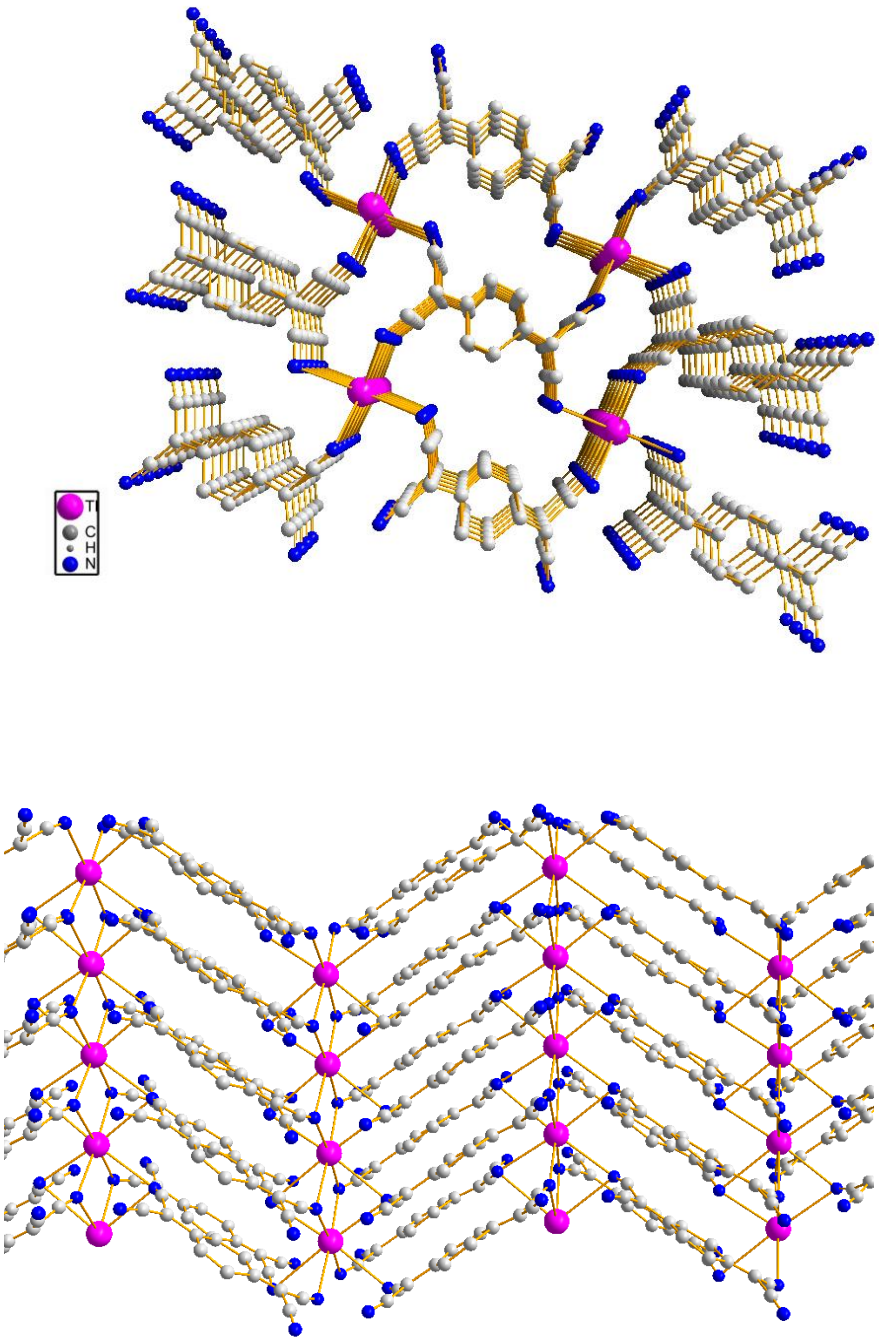

Figure 2.3 The structure of Tl(TCNQ) Phase II, top view (top) and side-view (bottom).

Structural comparisons with reported metal-TCNQ frameworks. The similarity of the structural and chemical properties between the Tl^+ cation and K^+ and Ag^+ is well-known as evidenced by many reports.[56] An inspection of the structures of Tl(TCNQ) Phase I, Na(TCNQ) (Phases I & II), K(TCNQ) (Phases I & II), Rb(TCNQ) (Phases I & III), Cu(TCNQ) Phase I, Ag(TCNQ) reveals that they adopt a similar structural motif. In all of these structures, the TCNQ radicals are stacked in columns with adjacent TCNQ radicals in the same layer being nearly perpendicular to each other. The major differences among these materials are the metal-nitrogen distance ($d_{M\text{-}N}$), the spacing of the TCNQ radicals, and the space group; a compilation of these data is found in Table 2.2. The metal-nitrogen distances for Cu(TCNQ), Ag(TCNQ) and Tl(TCNQ) are smaller than the sum of van der Waals radii which suggests the existence of M-N coordination bonds for transition and main-group metal-TCNQ frameworks; meanwhile, the sum of van der Waals radii and $r_{M\text{-}N}$ are nearly identical in the case of M(TCNQ) series (M = Na, K, Rb), which indicates a purely electrostatic interaction between the metal cations and TCNQ radicals. In contrast to all of these phases, Tl(TCNQ) Phase II and Rb(TCNQ) Phase II adopt a similar structure with the TCNQ radicals being oriented in a parallel fashion. Interestingly, for both alkali metals and Cu^I materials, evenly spaced and short-long spaced TCNQ columns have been observed in their polymorphs which we have found is also possible for Tl(TCNQ) polymorphs.

Table 2.1 Pertinent crystallographic parameters and data for Tl(TCNQ) Phase I and Phase II.

Compound	Phase I	Phase II
Formula	$C_{12}H_2N_4Tl$	$C_{12}H_2N_4Tl$
F_w [g mol^{-1}]	408.56	408.56
Crystal size mm^3	0.21 x 0.13 x 0.10	0.02 x 0.015 x 0.01
Crystal system,	Monoclinic, $P2_1/c$	Monoclinic, P2/c
a [Å]	7.1656(14)	7.703(1)
b [Å]	12.441(3)	3.7883(8)
c [Å]	12.999(3)	19.526(4)
α [°]	90	90
β [°]	97.82(3)	97.75(3)
γ [°]	90	90
V [$Å^3$]	1148.0 (4)	518.45(18)
Z	4	2
ρ_{calc} [g cm^{-3}]	2.364	2.617
μ ($Mo_{K\alpha}$ and Synchrotron) [mm^{-1}]	0.71073	0.41328
Reflns collectged	12987	7699
Unique Reflns	2788	1234
Reflns with I >2σ(I)	2233	1061
Parameters	170	63
R(int)	0.0359	0.1189
$R1^{[a]}$	0.0395	0.1056
$wR2^{[b]}$	0.1062	0.2485
GOF	1.087	1.802
Compound	Phase I	Phase II

[a] $R1 = \Sigma||F_o| - |F_c||\Sigma|F_o|$. [b] $wR2 = [\Sigma[w(F_o^2 - F_c^2)^2]/\Sigma[w(F_o^2)^2]]^{1/2}$.

Phase I

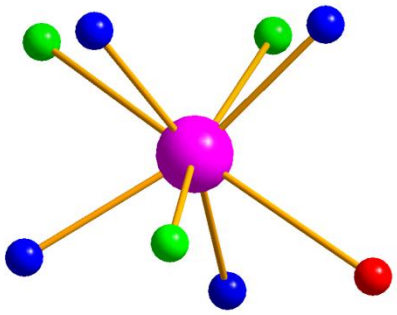

N-Tl bond distances	Å
Blue	2.68(1)
	2.70(2)
	2.75(1)
	2.81(1)
Green	3.25(2)
	3.25(1)
	3.26(1)
Red	3.42(2)

Phase II

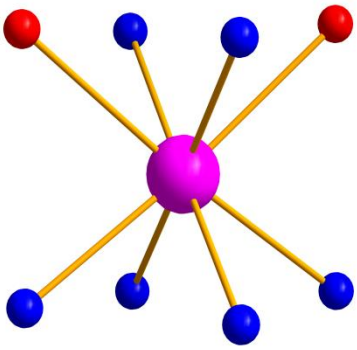

N-Tl bond distances	Å
Blue	2.92(2)
	2.92(2)
	2.97(2)
	2.97(2)
	3.05(2)
	3.05(2)
Red	3.23(2)
	3.23(2)

Figure 2.4 The coordination environment of Tl^{I} cations in Phase I and Phase II.

Table 2.2 Comparison between Tl(TCNQ) polymorphs and M(TCNQ) polymorphs (M = Na, K, Rb, Cu, Ag) with respect to metal-nitrogen distance, separation distance, space group and physical properties.[a][22, 24, 28]

Relative position of TCNQ radicals: perpendicular

Metal (Phase)	r_i+r_N(Å)	***d*(M – N)(Å)**	***d*(A – A)(Å)**	**Space group**	**Activation Energy(eV)**
Cu(I)	2.10	1.95	3.24	*Pn*	0.16
Ag	2.50	2.30-2.34	3.50	*Pnnm*	0.14
Tl(I)	3.09	2.68-3.42	3.16/3.35	$P2_1/n$	0.28
Na(I)	2.52	2.50	3.22/3.50 3.20/3.48	*C*-1	0.23-0.32
Na(II)	2.52	2.42-2.56	3.385	$P2_1/n$	0.16-0.22
K(I)	3.09	2.86-3.02	3.24/3.55 3.23/3.58	$P2_1/n$	0.23-0.45
K(II)	3.09	2.93-3.00	3.479	$P2_1/c$	0.15-0.31
Rb(I)	3.15	2.98-3.10	3.16/3.48	$P2_1/c$	0.41-0.53
Rb(III)	3.15	3.08	3.33	*P4/m*	0.28-0.37

Relative position of TCNQ radicals: parallel

Metal (Phase)	r_i+r_N(Å)	***d*(M – N)(Å)**	***d*(A – A)(Å)**	**Space group**	**Activation Energy(eV)**
Tl(II)	3.09	2.92-3.23	3.22	*P2/c*	0.13
Rb(II)	3.15	2.30-2.34	3.43	*P-1*	0.16-0.19

[a] r_i+r_N=sum of van der Waals radii of the cation and N atoms, d(M–N)= distance between metal ion and nitrile N atoms, d(A–A)=average distance between acceptor molecules. Nitrogen radius r_N=1.50 Å.

Powder X-ray Diffraction Study

The polymorphism issue for Tl(TCNQ) was made evident by the extremely different conductivities that were observed for single crystal and pressed pellet samples. The single crystal of Tl(TCNQ) exhibits a weak semiconducting behavior with a room temperature conductivity of ~10^{-4} S/cm, but a pressed pellet of the powder product obtained by directly mixing $TlPF_6$ and LiTCNQ in methanol/water exhibits a much higher conductivity with a r.t. value of 10^{-1} S/cm. Generally, given that the resistance of a pressed pellet should be the sum of the intrinsic resistance of sample and resistance of the inter-particle contact distances, we expected that the pressed pellet would exhibit a lower conductivity than a single crystal product. The fact that the opposite is actually the case prompted us to investigate the nature of polymorphism in the Tl(TCNQ) phases.

A comparison of the powder X-ray pattern of the powder product obtained from the bulk synthesis and the pattern obtained from a powder simulation of the single crystal X-ray solution for Tl(TCNQ) Phase I conformed the polymorphism of Tl(TCNQ) as most of the peaks, especially with $2\theta<25^{o}$ do not coincide. With the help of synchrotron radiation, the structure of Phase II was obtained, and a comparison between the powder pattern of the bulk product and pattern simulated from the structure of Phase II indicates that the product from the bulk preparation is actually Phase II. Figure 2.5 displays an overlay of the X-ray powder diffraction patterns of Phase I and Phase II. Figure 2.6 displays the experimental powder diffraction data for Phase I and II along with the patterns simulated from the corresponding X-ray structure.

At this point, it is instructive to discuss the results of our investigations concerning the factors that influence the phase transition of Phase I. A time-dependent

powder diffraction study was performed on a sample prepared from a bulk reaction between $TlPF_6$ and Li(TCNQ) in water. After intervals of 5 min, 10 min, 30 min, 1 hour and 2 hours, portions of the powder precipitate were removed from the flask using a pipette, filtered and dried *in vacuo*. From the X-ray powder diffraction data of these samples (Figure 2.7), one can see the evolution in the patterns as evidenced, for example, by a decrease in intensity of the peak at $2\theta = 9.8^{o}$ and an increase in intensity of the peak at $2\theta = 9.0^{o}$. A simulation of these two phases supports the conclusion that the bulk reaction first produces Phase I which then slowly transforms to Phase II.

A tandem powder X-ray diffraction study of the effect of temperature on the phase transition was also performed by collecting data after reactions were performed for 30 minutes at 0 ^{o}C, 20 ^{o}C and 40 ^{o}C (Figure 2.8). The data reveal that, at low temperatures, the product contains mainly Phase I and that with increasing temperature, the percentage of Phase II is greater with the phase transition being complete in 30 minutes. Another study was initiated after the surprising observation that storage of samples in moist air affects the structure. A pure powder sample of Phase I was placed in ambient laboratory air and powder diffraction experiments were performed after 1 day, 2 days, 3 days, and 2 weeks (Figure 2.9). It is obvious from the evolution of the data and the fact that a pure sample does not exhibit any transformation in a dry atmosphere that Phase I undergoes a phase transition in the presence of moist air. The comparison suggests that the major driving force of the phase transition is the difference on the solubility of two different phases. Apparently, Phase I is more soluble than Phase I, therefore, a dissolution-recrystallization process occurs at the surface of the crystal of Phase I which slowly leads to a complete transition to Phase II. The scanning electron microscopy

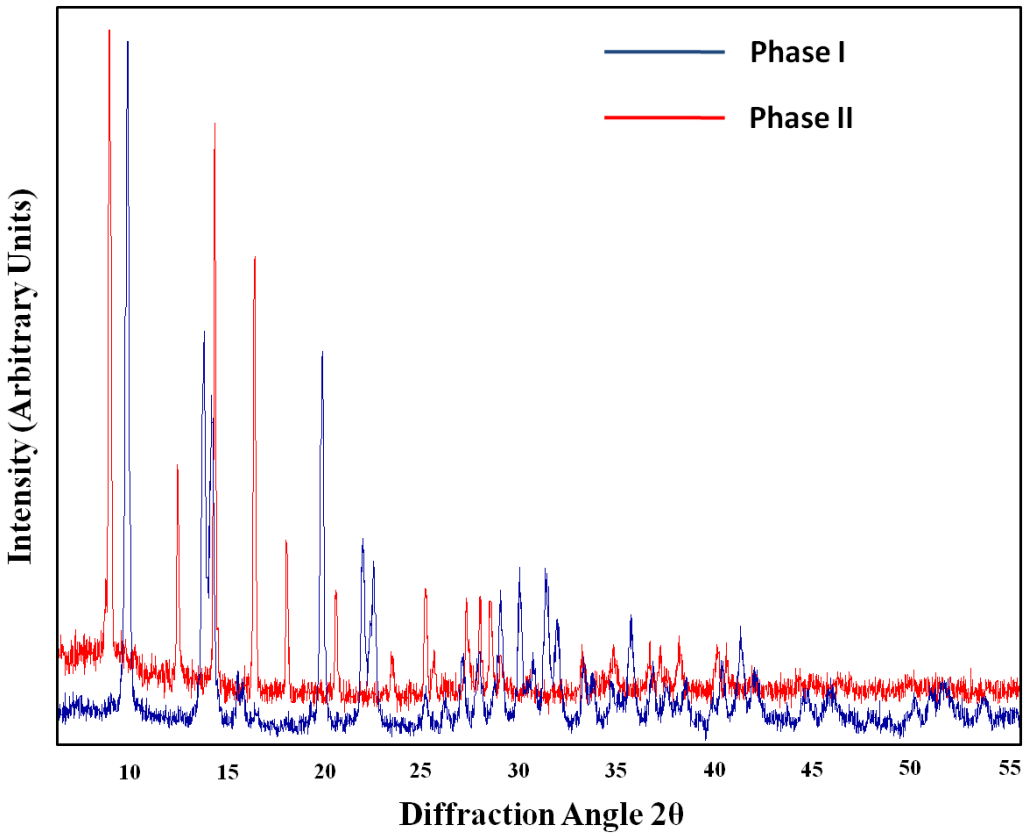

Figure 2.5 Overlay of the powder X-ray diffraction patterns of Phase I and Phase II.

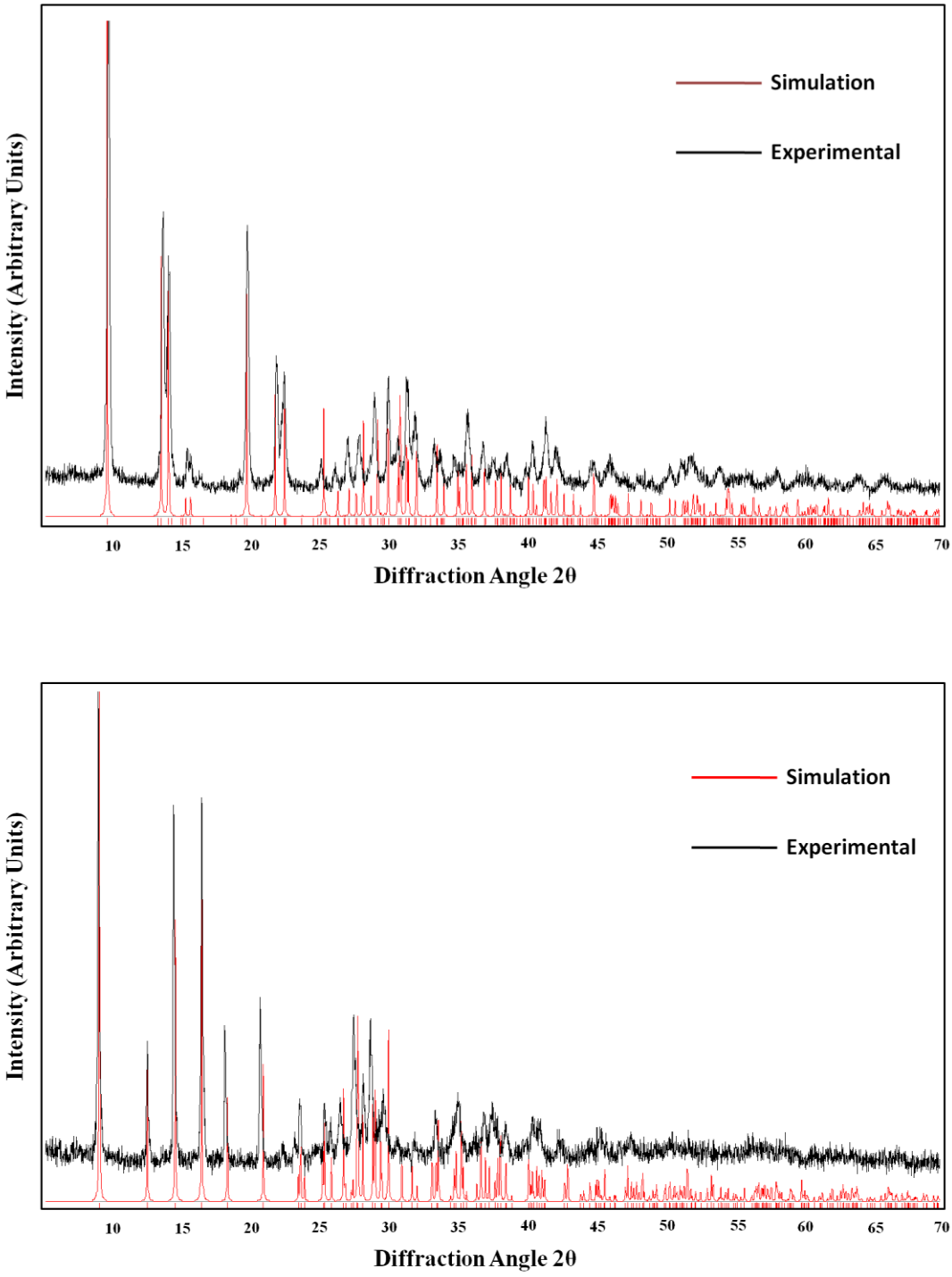

Figure 2.6 Experimental powder X-ray diffraction pattern of bulk microcrystalline samples (black) and simulated patterns (red) of Tl(TCNQ) Phase I (top) and Phase II (bottom).

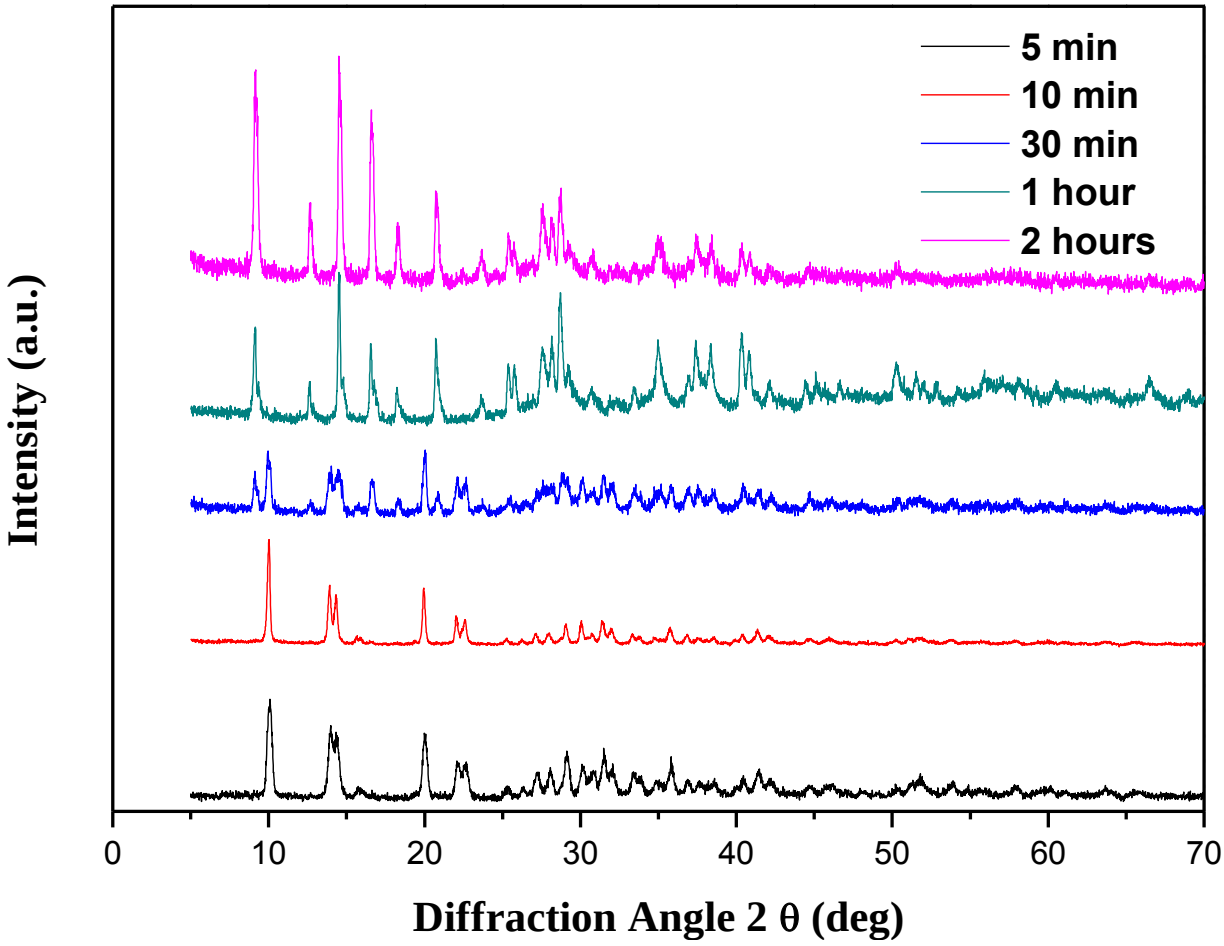

Figure 2.7 X-ray diffraction powder patterns of a sample of Tl(TCNQ) crystals obtained from a bulk reaction between $TlPF_6$ and LiTCNQ in water/methanol. After being soaked in water for the indicated time periods, the sample converts from Phase I to Phase II.

(SEM) images of Phase I and Phase II (Figure 2.10) revealed the difference in the morphologies of Phase I and Phase II.

Infrared Spectral Study

The infrared spectra of M-TCNQ compounds provide information on the coordination mode and the oxidation states of the TCNQ ligands.[59] The $\nu_{C\equiv N}$ stretching modes and the δ_{C-H} out-of-plane bending modes of the TCNQ moieties are both useful in this regard. The $\nu_{C\equiv N}$ modes of Phase I appear at 2181, 2164 and 2151cm^{-1} whereas the $\nu_{C\equiv N}$ stretches of Phase II are at 2180 and 2149cm^{-1}. Both polymorphs exhibit a δ_{C-H} mode at ~823 cm^{-1} which, according to reported compounds,[60] is indicative of a singly reduced TCNQ radical as expected. The minor differences in the $\nu_{C\equiv N}$ modes is expected on the basis of the slightly different coordination environments of the two polymorphs.

Conductivity Measurements

Conductivity data were collected on pressed pellets of the samples, as large single crystals of Phase II are very difficult to obtain. The four-probe method was used in which four 50 μm diameter gold wires were pasted evenly on a rectangular pressed pellet with gold paste. From the measurements (Figure 2.11), it can be seen that Phase I exhibits a room temperature (r.t.) conductivity of 2.4×10^{-4} S/cm and Phase II exhibits a r.t conductivity of 5.4×10^{-1} S/cm;

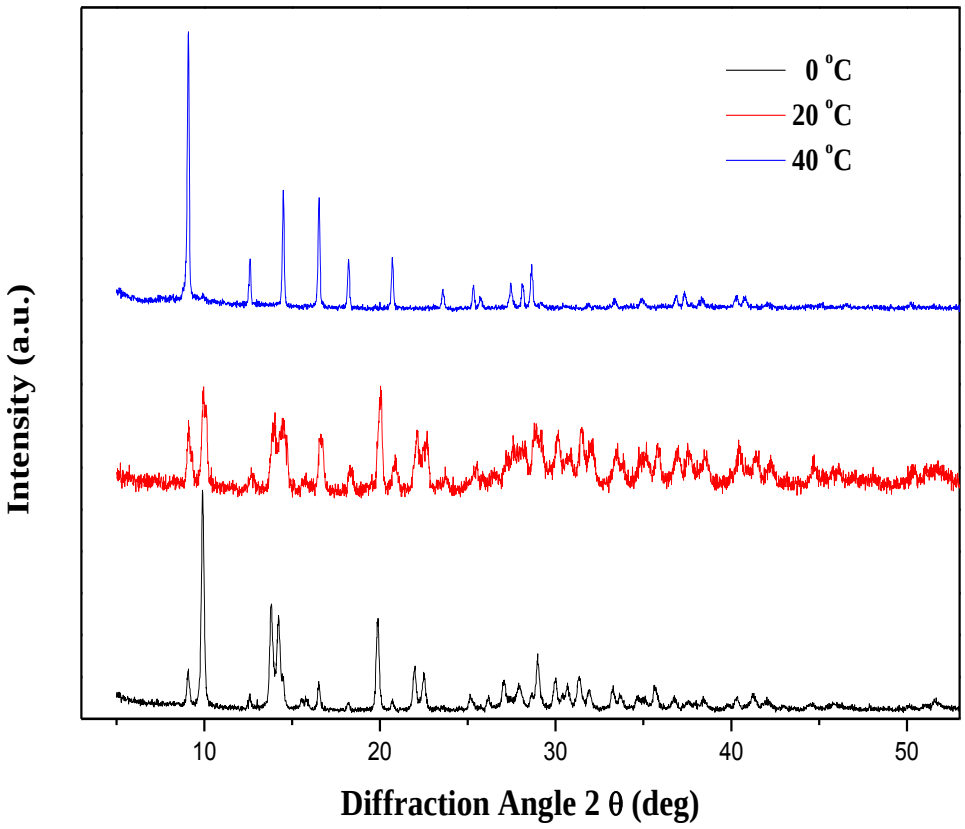

Figure 2.8 Powder diffraction patterns of a bulk product of Tl(TCNQ) prepared at 0, 20 and 40 °C, and soaked in mother liquor for 30 minutes. At low temperature, Phase I dominates, with an increase in temperature, the component of Phase II has increased.

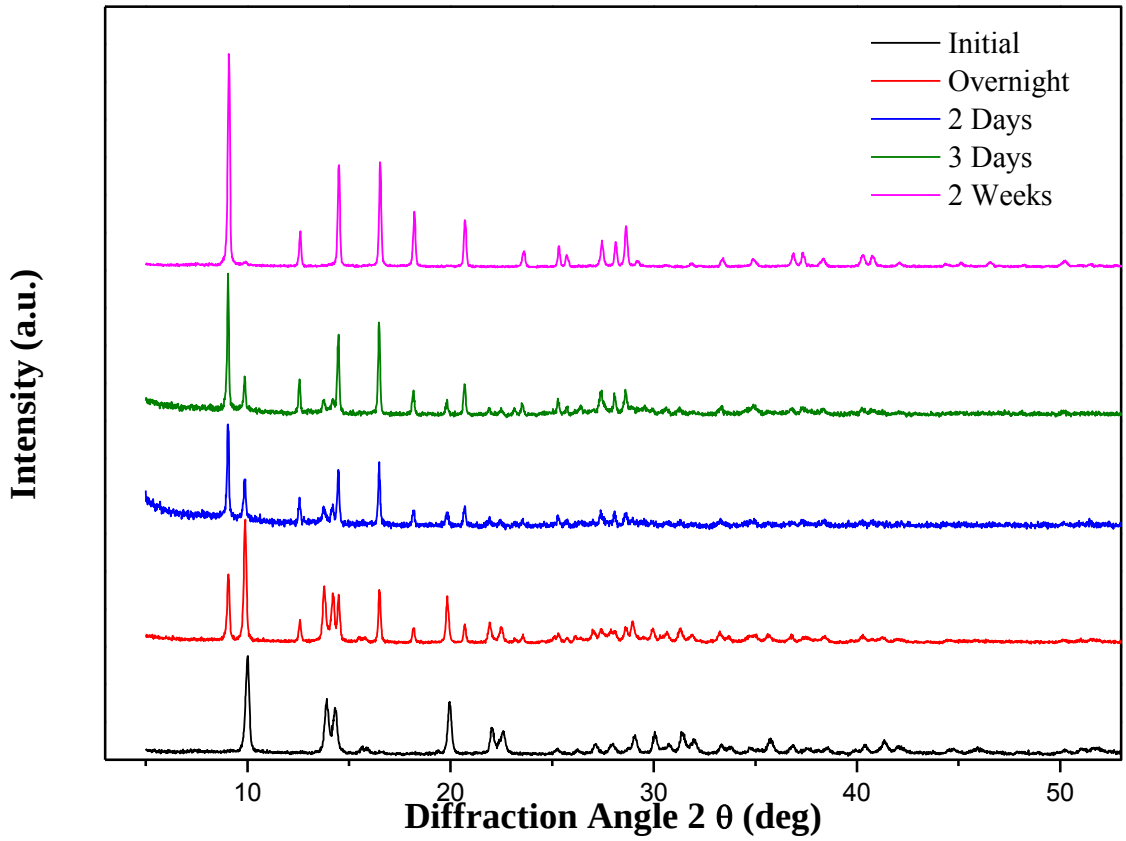

Figure 2.9 The powder diffraction pattern of Tl(TCNQ) of Phase I after exposure to the ambient air of laboratory.

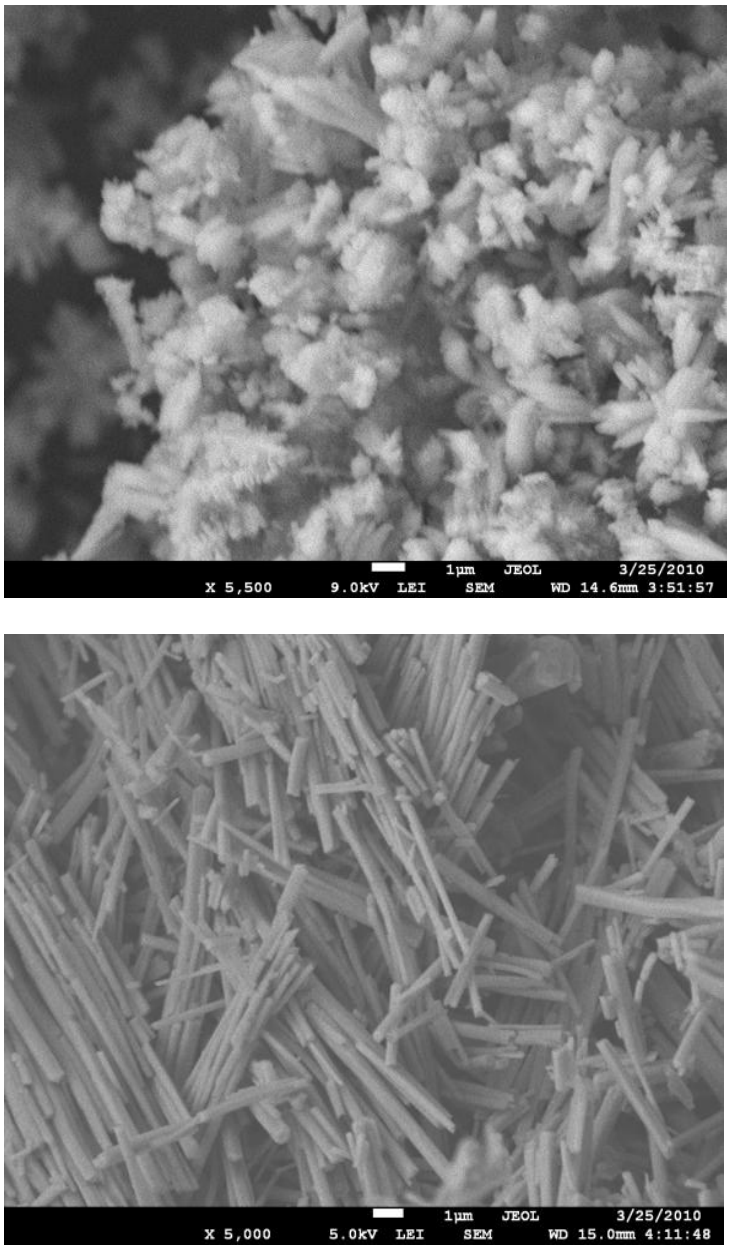

Figure 2.10 SEM images that depict the morphology of Phase I (top) and Phase II (bottom).

from their temperature dependent behavior, both compounds are semiconductors which is not surprising considering the structures of Phase I and II. Phase I exhibits an alternating separation distance for TCNQ radicals in the columns, namely 3.17(1) Å and 3.35(1) Å, and Phase II contains evenly stacked columns with a distance of 3.22(2) Å between the neighboring TCNQ radicals. The separation distance of Phase II is similar to that found in Cu(TCNQ) (3.24 Å), which, not unexpectedly, leads to similar r.t. conductivity properties, specifically the value is 0.24 S/cm versus 0.25 S/cm. The partial dimerization in the structure of Phase I indicates a localization of charge carriers in the stack the consequence of which is a relatively low conductivity as compared to Phase II.

By fitting the variable temperature conductivity data for Phase I and Phase II to the Arrhenius Law, $\sigma = \sigma_0 \, exp(-E_g/k_BT)$, E_g (the effective energy gap) was estimated for both Phase I and Phase II. Phase I and Phase II exhibit energy gaps of 280 meV and 135 meV respectively. The results correspond well with the partially dimerized TCNQ radicals in Phase I, and evenly separated TCNQ radicals in Phase II. The partial dimerization in Phase I leads to a secondary band gap which arises from a Peierls transition; as a result, the effective energy gap is larger in the case of Phase I.

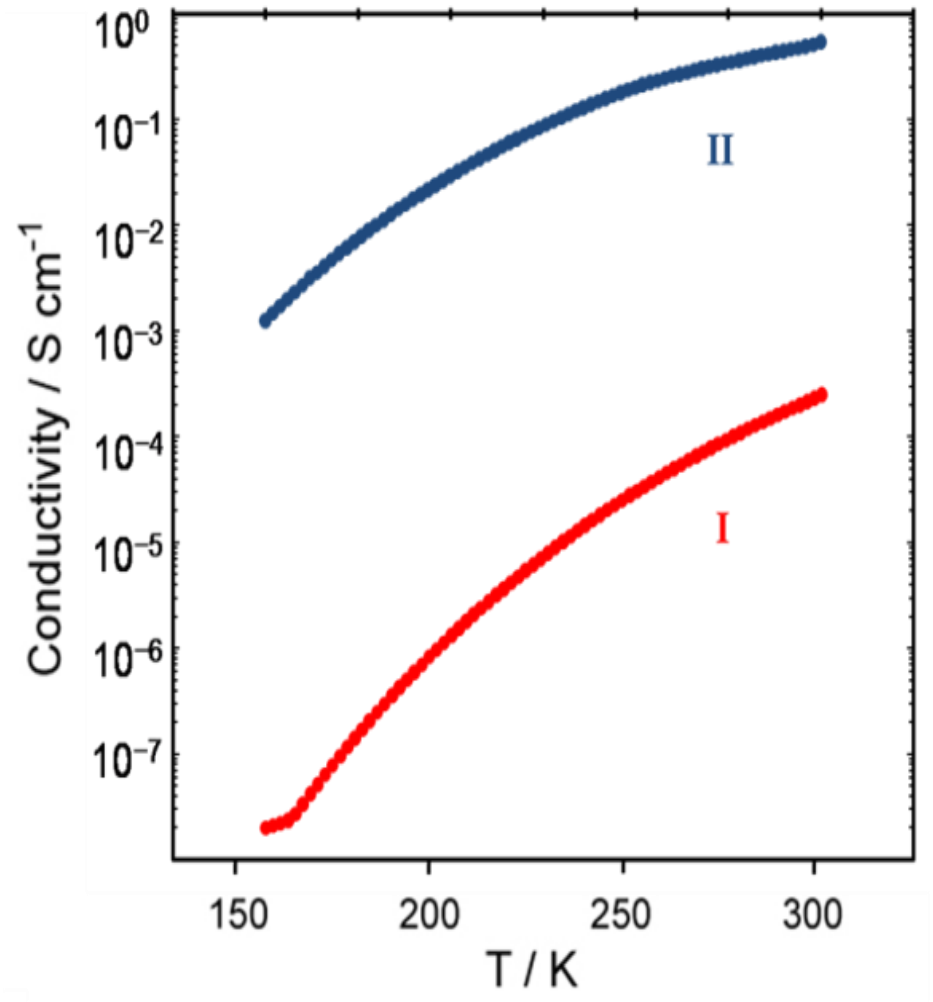

Figure 2.11 Variable temperature conductivity data for Phase I and Phase II.

Band Structure Calculations

The band structure calculations were performed by our collaborators Hirotaka Kojima and Professor Takehiko Mori from the Tokyo Institute of Technology. The simulation was based on the refined crystal structures of Phase I and Phase II. In the calculation, the neighboring neutral dimer levels were evaluated by Gaussian 09 at B3LYP/6-31G(d,p) levels,[61] and the transfer integral (t) was estimated from the energy level splitting of the LUMO according to $t = (E_{LUMO} - E_{LUMO+1})/2$. The sign of t is always positive by this method. In another approach, the transfer integral was estimated as $t = E \times S$ from the intermolecular overlap integrals (S) between the molecular orbitals according to the reported method,[62] where the energy of the molecular orbital E was assumed to be -10 eV. The same method has been applied to evaluate the transfer integral between the TCNQ molecules and the metal atoms.

The first step of simulation takes only the organic-organic interactions into consideration, therefore the transfer integrals between adjacent TCNQ radicals in one column and in neighboring columns were calculated. The interaction diagrams, band structures and Fermi surface diagrams of Phase I and Phase II are displayed in Figures 2.12 and 2.13. From the diagram for Phase I, strong dimerization is evidenced by the small inter-dimer transfer integral (45meV) and large intra-dimer transfer integral. (171meV). As a result, the band structure is split into two bands as shown in 2.12d. The dimerization band gap was calculated to be 252 meV, which is close to the experimental value of 280 meV. In the case of Phase II, since TCNQ radicals are evenly distributed, the integral is a single value of t_b = 160meV. Weak inter-columnar interactions were observed as described in 2.13b. Two types of weak interactions were identified and

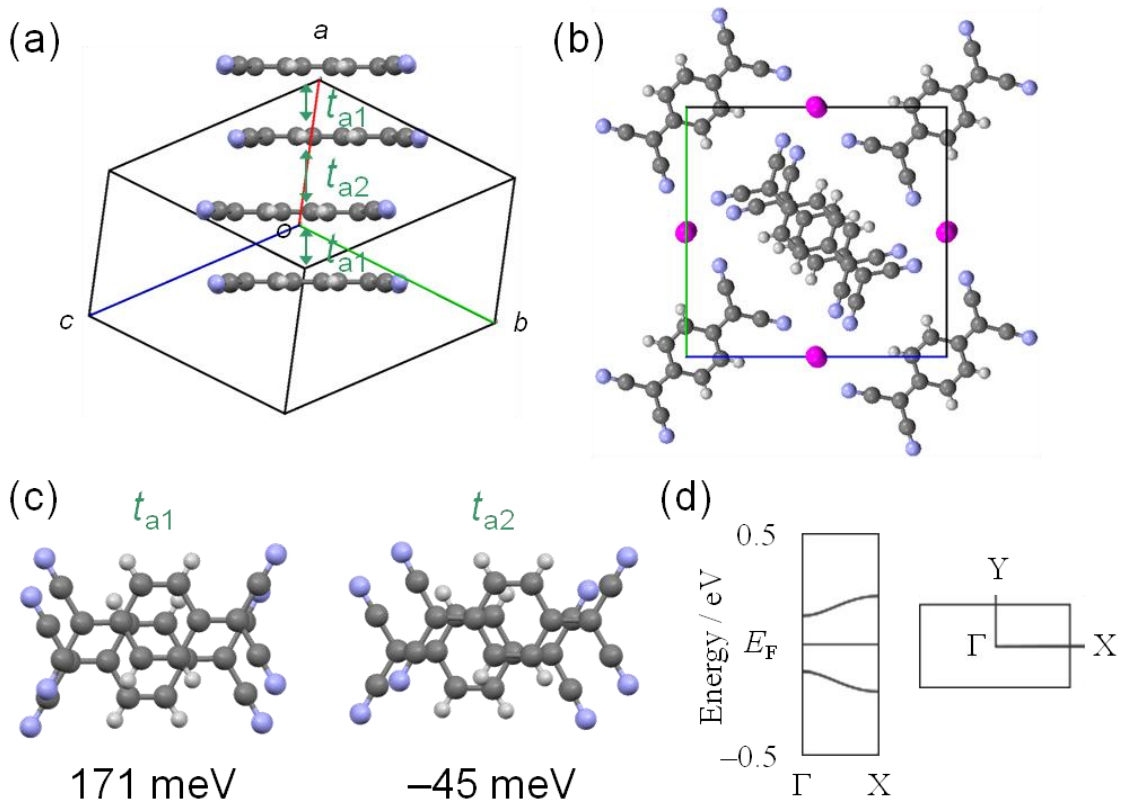

Figure 2.12 The interaction diagram (a, b and c), calculated band structure and Fermi surface (d) for Tl(TCNQ) Phase I.

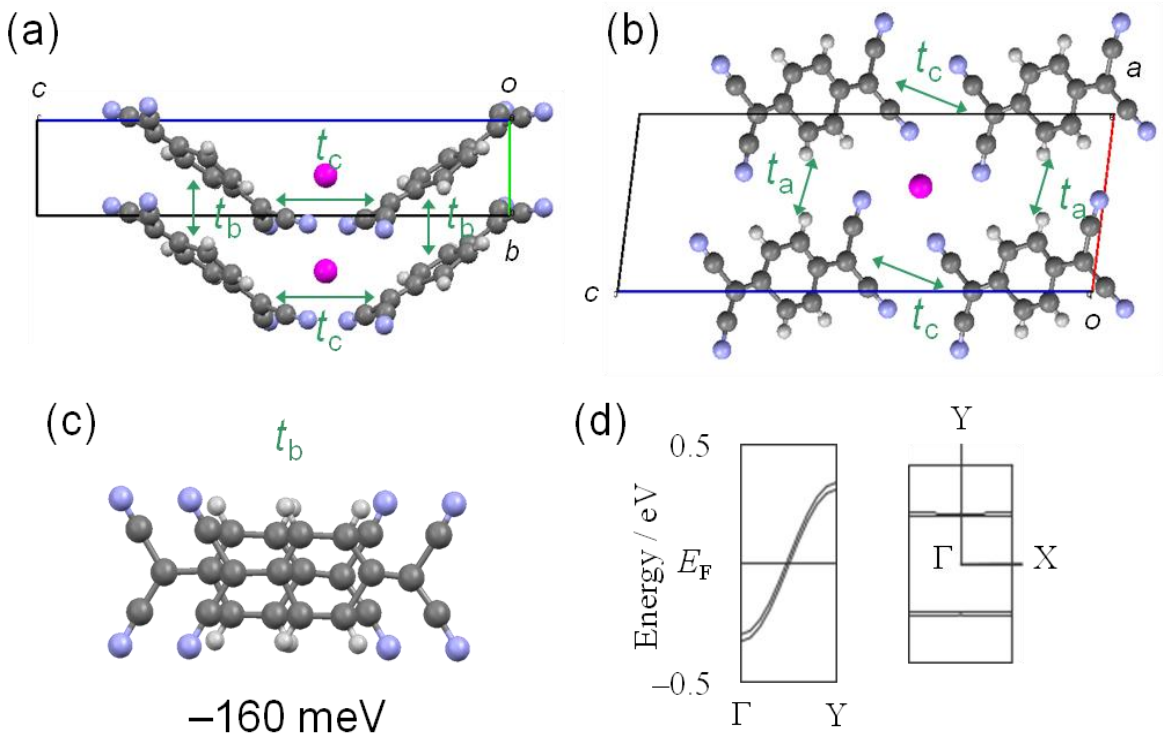

Figure 2.13 The interaction diagram (a, b and c), calculated band structure and Fermi surface (d) for Tl(TCNQ) Phase II.

calculated to be t_a = 1 meV and t_c = 7 meV. Therefore, the Fermi surface is slightly modulated but not so much that it alters the 1-D conducting features of Tl(TCNQ) Phase II.

Conclusions

The results of this study establish the existence of two markedly different polymorphs of Tl(TCNQ). Powder X-ray diffraction studies revealed that subtle differences in the reaction conditions (e.g. time, temperature, solvent;) lead to variable quantities of the two phases. With some effort, pure samples of both phases were obtained as crystalline powders and single crystals. Their structures were determined by single crystal X-ray diffraction with synchrotron radiation methods being required for Phase II. Conductivity data obtained on pressed pellets of bulk samples of the two phases revealed that Phase I is a weak semiconductor, a finding that is not unexpected given the pronounced π-dimerization of the $TCNQ^-$ units along the stack. On the other hand, the Tl(TCNQ) Phase II polymorph exhibits much higher conductivities as a result of the regular and short spacing between the $TCNQ^-$ radicals along the stack which leads to increased electron mobility. These findings add valuable information to the small database of single crystal X-ray data available for binary TCNQ materials and provide valuable insight into structure-property relationships in such materials. These compounds constitute the first examples of a main-group metal-TCNQ framework. The potential charge transfer between the organocyanide acceptors and Tl^I cations are of continued interest in future studies, given the previous report of $Tl(DM\text{-}DCNQI)_2$[57] by Hünig who reported a Knight shift in ^{205}Tl NMR and EPR and magnetic data that support that this type of electronic interaction between the Tl^I ion and organocyanide radicals is possible.

CHAPTER III

INVESTIGATION OF THE STRUCTURE-PROPERTY RELATIONSHIP OF MAIN-GROUP WITH TCNQ DERIVATIVES SEMICONDUCTORS*

Background

The design of molecule-based materials with interesting electronic, optical or magnetic properties is a central theme of modern materials science research.[63] A particularly compelling goal in the pursuit of functional materials is the realization of new generation memory devices with higher information density and increased operation speeds. In this vein, considerable efforts are being directed towards the design and fabrication of tunable nanoscale materials and nanodevices.[50] One of the highly successful strategies in this area is the co-assembly of metal ions and organic radicals to prepare solids that exhibit electrical or magnetic bistability. In these materials, the metal donors (D) and organic acceptors (A) are intimately organized into extended architectures that are often highly one-dimensional in terms of the arrangement of the organic radicals.

Among the organocyanide acceptors that have been extensively studied by materials chemists is 7, 7, 8, 8-tetracyanoquinodimethane (TCNQ). This acceptor undergoes two accessible reversible reductions and is air stable in the radical anion form.

---

*Part of this chapter is reprinted with permission from *Chem. Eur. J.* Zhang, Z.; Zhao, H.; Kojima, H.; Mori, T.; Dunbar, K. R.; *"Conducting Organic Frameworks Based on a Main Group Metaland Organocyanide Radicals."* **2013**, DOI: 10.1002/chem.201203422
Copyright 2013 by WILEY-VCH Verlag GmbH & Co. KGaA, Weinheim.

The versatility of the TCNQ molecule has led to its incorporation into a variety of important materials and devices, such as the metallic conducting charge-transfer material $TTF^{\delta+}(TCNQ)^{\delta-}$ which was discovered in 1973 by Ferraris *et al*, [8] the extraordinary material Cu(TCNQ) reported by Cowan and coworkers to form a sandwich device composed of Cu/Cu(TCNQ)/Al that undergoes voltage-induced switching,[22a,22b] and a series of alkali metal binary TCNQ frameworks (M(TCNQ), M = Na, K, Rb) that exhibit temperature-induced structural changes associated with a magnetic and conducting phase transition. [19,20]

An obvious issue in this field of study has persisted since TCNQ was first prepared at Dupont in the 1960's,[64] namely that a general understanding of the properties of simple binary M_xTCNQ_y materials have been stymied due to a lack of structural information. The few binary TCNQ compounds whose structures have been determined exhibit extraordinary structural complexity and polymorphism. Subtle changes in crystallization conditions, temperature and even humidity can trigger a phase change. Moreover, facile interconversions between polymorphs under mild conditions lead to difficulty in the isolation and purification of pure materials. On the other hand, the interconversion of polymorphs is accompanied by drastic changes in semiconducting behavior, but, in many cases the structures have not been determined due to the difficulty in obtaining crystals of the rapidly precipitating phases. Therefore an understanding of what is driving the properties is lacking. The dearth of structural information on known binary TCNQ materials with transition metals and the absence of main group analogues is unfortunate, as such light-weight conductors hold great promise for device applications especially if they can be properly tuned as to their steric and electronic properties with

substituents on the TCNQ radicals. In this vein, our group recently initiated a broad investigation of various 2,5 halogenated TCNQ derivatives with the goal of obtaining more single crystal phases and, possibly, enhanced conducting properties. Indeed, these studies have led to new semiconductors with previously unknown structures including the materials $Cu(TCNQCl_2)$ and $Cu(TCNQBr_2)$ with the chloro- derivative setting the record among the conducting 1:1 $M^+(TCNQ)^-$ salts with a room temperature conductivity of 1.15 $S \cdot cm^{-1}$. [32] An analysis of the structure-property relationships revealed that the steric and electronic effects of the substituent has a profound influence on the structures and properties as compared to the original Cu(TCNQ) phases. Given the promising discoveries over the decades with s and d block binary TCNQ phases, we decided to expand the field of TCNQ materials by exploring the chemistry of the "pseudo-alkali metal" main-group element thallium. Given the fascinating results in hand with TCNQ, I undertook the syntheses of thallium(I) materials with the 2, 5-subsituted derivatives, $TCNQX_2$ (X=Cl, Br, I), and report the new semi-conductors $Tl(TCNQX_2)$ along with their structures and a theoretical analysis and comparisons to the related TCNQ phases in this chapter.

Experimental Section

General Consideration. All reactions and manipulations were carried out under a dry nitrogen atmosphere. Deionized water was boiled and purged with nitrogen for 1 hour to remove dissolved oxygen. Dry methanol was obtained by distillation over Mg turnings under a nitrogen atmosphere. Acetonitrile was dried over 3 Å molecular sieves and distilled under an atmosphere of nitrogen prior to use. The TCNQ sample was purchased from TCI and $TlPF_6$ was supplied by Aldrich. The derivatives $TCNQX_2$ (X = Cl, Br, I),

their lithium salts (including LiTCNQ) and [Bu_4N] salts were synthesized according to literature methods.[64] Elemental analyses were performed by Atlantic Microlab, Inc. on bulk prepared powders. Single-crystal X-ray data were collected on a Bruker-AXS APEX-II CCD 3-circle X-ray diffractometer with the exception of Tl(TCNQ) Phase III data which were collected at the synchrotron facility at ChemMatCars in the Advanced Photon Source, Argonne National Lab. Powder X-ray data were collected on a Bruker D8-Focus Bragg-Brentano X-ray powder diffractometer. Variable temperature conductivity measurements over the range 150 K - 300 K were obtained on a Quantum Design model MPMS SQUID magnetometer by using gold paste to connect two 15 μm diameter gold wires to each end of the long axis of the needle-shape single crystals which is the (011) face of the single crystal and the direction of columnar stacking of TCNQ radicals. Infrared spectra were recorded as Nujol mulls between KBr plates using a Nicolet IR/42 FT-IR spectrometer.

Syntheses. Tl(TCNQCl_2) (Phase I), (1). A quantity of Li(TCNQCl_2) (0.028g, 0.1mmol) was dissolved in 10 mL of methanol and $TlPF_6$ (0.035g, 0.1mmol) was dissolved in a mixture of 10 mL of methanol/5 mL of water. The two solutions were slowly diffused into each other by layering them in a 6 mm outside diameter thin tube. Dark purple needle crystals formed over the course of two days.

Tl(TCNQCl_2) (Phase II), (2). Samples of LiTCNQCl_2 (0.028 g, 0.1 mmol) and $TlPF_6$ (0.035 g, 0.1 mmol) were dissolved in 10 mL of methanol and the mixture was stirred for 2 hours. The resulting precipitate was collected by filtration and dried *in vacuo*: yield 0.038 g, 80%. Anal. Calcd for $C_{12}H_2N_4Cl_2Tl$, %: C, 30.19; H, 0.42; Cl, 14.85; N, 11.73. Found : C, 30.01; H, 0.24; Cl, 14.59, N, 11.70.

$Tl(TCNQBr_2)$, (3). Separate samples of $LiTCNQBr_2$ (0.037 g, 0.1 mmol) and $TlPF_6$ (0.035 g, 0.1 mmol) were dissolved in 10 mL of methanol and the mixture was stirred for 2 hours. The resulting precipitate was collected by filtration and dried *in vacuo*: yield 0.052 g, 93%. Anal. Calcd for $C_{12}H_2N_4Br_2Tl$, %: C, 25.45; H, 0.36; Br, 28.22; N, 9.89. Found: C, 25.57; H, 0.32; Br, 28.14; N, 9.94; Single crystals were obtained by slow diffusion of $Li(TCNQBr_2)$ (0.051g, 0.1 mmol) in 10 mL of methanol and $TlPF_6$ (0.035g, 0.1mmol) in a mixture of 10 mL of methanol/5mL in a 6 mm O.D. thin tube. Dark purple needle crystals were harvested after two days.

$Tl(TCNQI_2)$, (4). A sample of $Li(TCNQI_2)$ (0.051 g, 0.1 mmol) was dissolved in 10 mL of methanol and $TlPF_6$ (0.035 g, 0.1 mmol) was dissolved in a mixture of 10 mL of methanol/5 mL of water. The two solutions were layered in a 6 mm O.D. thin tube. Dark purple block crystals formed by slow diffusion after two days.

Tl(TCNQ) Phase III, (5). Quantities of $[Bu_4N](TCNQ)$ (0.044 g, 0.1 mmol) and $TlPF_6$ (0.035 g, 0.1mmol) were dissolved in 10 mL of acetonitrile and the solution was stirred for 2 hours. The resulting precipitate was collected by filtration and dried *in vacuo*. Yield: 99%, Anal. Calcd for $C_{12}H_2N_4Tl$, %: C, 35.28; H, 0.99; N, 13.71. Found: C, 34.68; H, 0.86; N, 13.41; Single crystals were obtained by dissolving $[Bu_4N](TCNQ)$ (0.022 g, 0.05 mmol) in 5 mL of acetonitrile and $TlPF_6$ (0.035g, 0.1 mmol) in 10 mL of acetonitrile and carefully layering the solutions in a thin tube (6 mm O.D.). After slow diffusion had taken place over the course of a week, a very small crop of dark purple dendritic needle crystals were obtained.

Theoretical Calculations. The transfer integrals were calculated on the basis of the molecular orbital calculations. The frozen orbital approximation was adopted and the

intermolecular overlap integrals were evaluated from overlap of the Slater orbitals by using the extended Hückel Slater exponents in order to consider the intermolecular interaction correctly.[65,66,67] The transfer integrals (t) were estimated by $t = E \times S$, where S is the overlap integral of the LUMOs between the TCNQ molecules, and E is assumed to be –10 eV which is the energy of the molecular orbital. The organic-metal interactions were estimated similarly from the transfer integrals between the TCNQ LUMO and the Tl 6s orbital. The electronic configuration of a Tl^+ ion is $6s^26p^0$, so since the Tl 6p levels (–5.0 eV) are located far above the TCNQ LUMO (–11 eV), the transfer integrals to the Tl 6s orbitals (–11.6 eV) are considered.

Structural Discussion

X-ray Crystallographic Analyses. Tl(TCNQCl$_2$) Phase I, (1), and Tl(TCNQBr$_2$), (3). Single crystal X-ray data collected on compounds **1** and **3** revealed that these isostructural compounds crystallize in the monoclinic space group P2/c. The projections in the *ab* and *bc* planes are depicted in Figure 3.1. The Tl^I ions reside in a distorted cubic environment with a coordination number of eight and are arranged in chains located between the TCNQ layers. The Tl···Tl separations are 3.42(1) Å (**1**) and 3.41(1) Å (**3**), which are less than the Tl···Tl van de Waals contact of 3.92 Å. The $TCNQX_2^-$ radical anions are arranged in a columnar stack with the $TCNQX_2$ units being situated with halogen groups alternating from one side of the stack to the other as can be clearly seen in Figures 3.1a and 3.1b. One interesting feature is that the adjacent TCNQ radicals along the stack are not perfectly parallel (dihedral angle = 0.5° for Tl(TCNQCl$_2$) and 1.5° for Tl(TCNQBr$_2$)). The average stacking distances are 3.30(1) Å for $TCNQCl_2^-$ and 3.28(1) Å for $TCNQBr_2^-$. Given the non-zero dihedral angles between adjacent planar radicals,

the π-π interactions are expected to be less prominent than found in a perfect parallel arrangement.

Tl(TCNQI$_2$), (4). Compound **4** crystallizes in the monoclinic space group P-1 with a different structure than the others in this family. The material adopts a two dimensional layered motif in which the Tl^I metal ions are situated in layers surrounded by four $TCNQI_2^-$ radical anions. The projection in the bc plane (Figure 3.2a) reveals that the $TCNQI_2^-$ groups are arranged with the iodine substituents pointing in the same direction. Owing to the bulk of the iodine atoms, the $TCNQI_2$ units are slipped as can be seen in Figure 3.2b; the I···I and Tl···Tl separations are identical at 4.12 Å. The six-coordinate Tl^I metal ions are in a distorted octahedral environment with Tl···N bonds in the range *Tl(TCNQ) Phase III, (5).* Crystals of a new phase of the material were unexpectedly obtained during an attempt to prepare a bulk sample of Tl(TCNQ) phase I. When the reaction between $TlPF_6$ and $(Bu_4N)^+TCNQ^-$ is performed in dry acetonitrile, the result is a dark purple powder whose powder XRD pattern is very similar to the simulated spectrum obtained from the single crystal data of Tl(TCNQ) phase I, but, surprisingly, unlike phase I, the new material does not undergo a phase transition when suspended in water or methanol for several days. By using a thin-tube diffusion method, tiny crystals of **5** were obtained and structurally characterized at the Advanced Photon Source facility at Argonne National Lab. Surprisingly, the structure is nearly identical to the Tl(TCNQ) phase I in stacking mode and space group ($P2_1/c$) (Figure 3.4a, 3.4b), but the dimensions and of the unit cell are slightly decreased. For the new phase, the cell parameters are a = 6.987 (1) Å, b = 12.332(3) Å, c = 12.947(3) Å, β = 97.75(3)º, V = 1105.9(4) $Å^3$ as compared to the original structure of Tl(TCNQ) phase I (a = 7.165(1) Å, b = 12.441(3) Å,

c = 12.999(3) Å, β = 98.03(1)º, *V* = 1148.0(4) Å^3.) The decrease in volume leads to increased overlap of frontier orbitals and stronger interactions between adjacent TCNQ radicals. This subtle, but important, difference leads to increased stability of phase III. with no further phase transition being observed. In support of this conclusion are the separations between adjacent TCNQ radicals of 3.13 Å and 3.29 Å, evidence of strong dimerization. Table 3.1 summarizes the Pertinent crystallographic parameters and data for compounds 1, 3, 4 and 5.

Comparison of the 1:1 binary TCNQ Complexes. As mentioned in the previous section, the co-assembly of Tl^I cations and TCNQ radicals results in a variety of structure types. To put these new results into perspective, it is instructive to examine the diversity of structures of 1:1 binary TCNQ materials, (excluding the alkali metals) depicted in Figure 3.5. [24,28,32,68] The particular architecture is characterized by the coordination number of the metal cations and the orientation motif and stacking of the TCNQ radicals. A four-coordinate environment is observed for the Cu^I and Ag^I materials, with a perpendicular arrangement of TCNQ ligands being observed for the Cu(TCNQ) phase I and Ag(TCNQ) phase II. In contrast, Cu(TCNQ) phase II and Cu(TCNQX_2) (X = Cl, Br) adopt a parallel packing mode for the TCNQ moiety with different relative positions of adjacent columns (non-coplanar versus co-planar). The Tl^I ion is in an 8-coordinate environment in Tl(TCNQ) phase I, phase II and Tl(TCNQX_2) (X = Cl, Br) with perpendicular, parallel/non-coplanar, and parallel/co-planar arrangements of the TCNQ radicals respectively. An exceptional case is the six-coordinate Tl(TCNQI_2) which adopts a layered architecture, presumably as a result of the steric effect of the iodine substituents.

Polymorphism in Binary M(TCNQ) Phases. An overarching theme in metal binary TCNQ compounds is that of polymorphism. Slightly different preparation conditions can lead to materials whose properties are vastly different. For example, the initial kinetic polymorph of Cu(TCNQ), which is an excellent semiconductor, undergoes a first order phase transition in warm acetonitrile without apparent dissolution to form a thermodynamic phase which is nearly insulating.[23] The more ionic compounds with alkali metals ions form a polymorph that undergoes a secondary transition to a spin-Peierls phase at a critical temperature (348 K for Na(TCNQ), 395 K for K*(*TCNQ), 381 K for Rb(TCNQ), and 210 K for Cs(TCNQ)), with a concomitant magnetic phase transition and a change in semiconducting behavior. [20,21] Given these issues with polymorphism, it is important to compare the powder X-ray pattern of products from bulk reactions with the simulated pattern from the corresponding single crystal data. Recently we communicated a preliminary report of the preparation of two distinct Tl(TCNQ) polymorphs which constitute another entirely new class of 1:1 M:TCNQ polymorphs. Single crystals of Tl(TCNQ) phase I are obtained by thin tube layering of a Li(TCNQ)/MeOH solution and a $TlPF_6/H_2O$/MeOH solution. A microcrystalline form of Tl(TCNQ) phase II can be prepared by stirring Li(TCNQ) and $TlPF_6$ in water for 2 hours. [69] The difference between the powder X-ray diffraction patterns of the bulk powder and the data simulated from the corresponding single crystals revealed the existence of polymorphs.

(a)

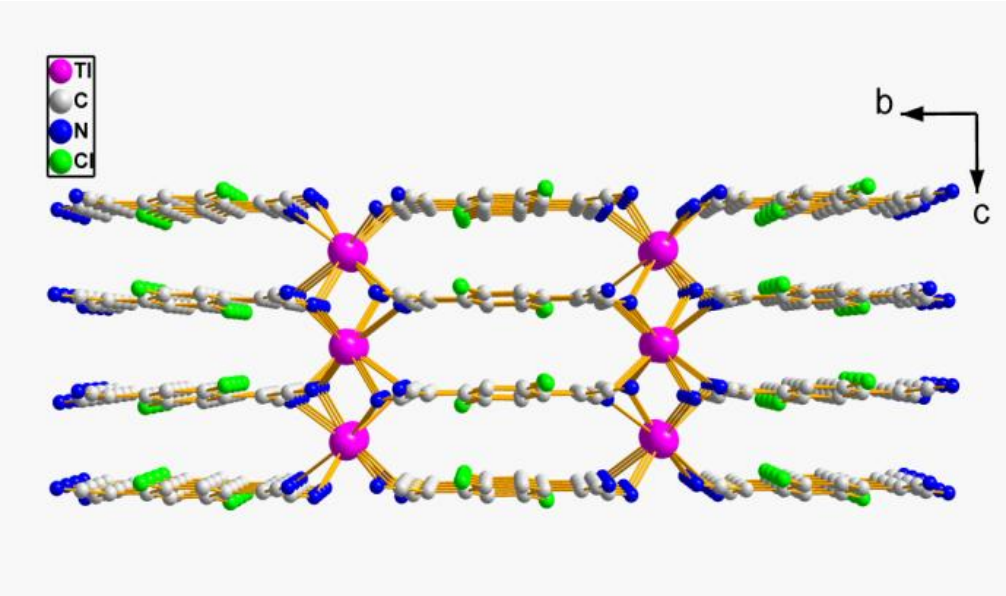

(b)

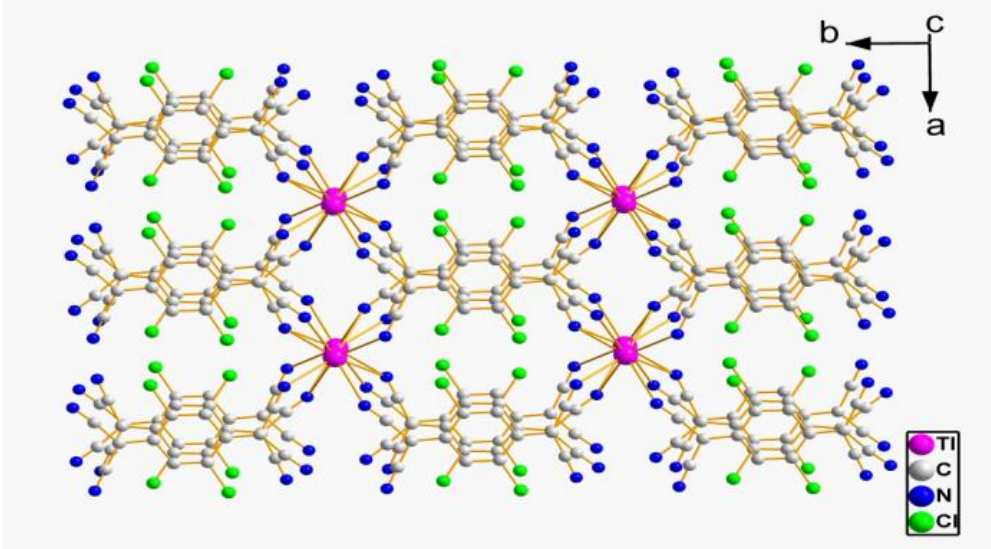

Figure 3.1 Views of the structure of Tl(TCNQCl$_2$) Phase I (1) in (a) the *ab* plane and (b) the *bc* plane. Tl(TCNQBr$_2$), (3), adopts the same structure.

(a)

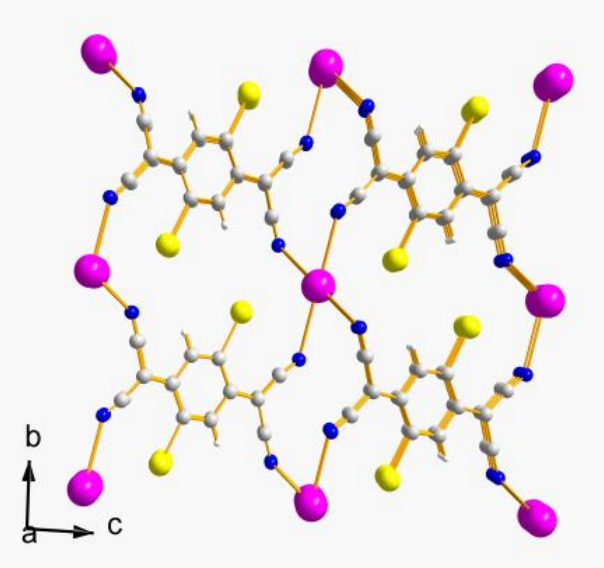

(b)

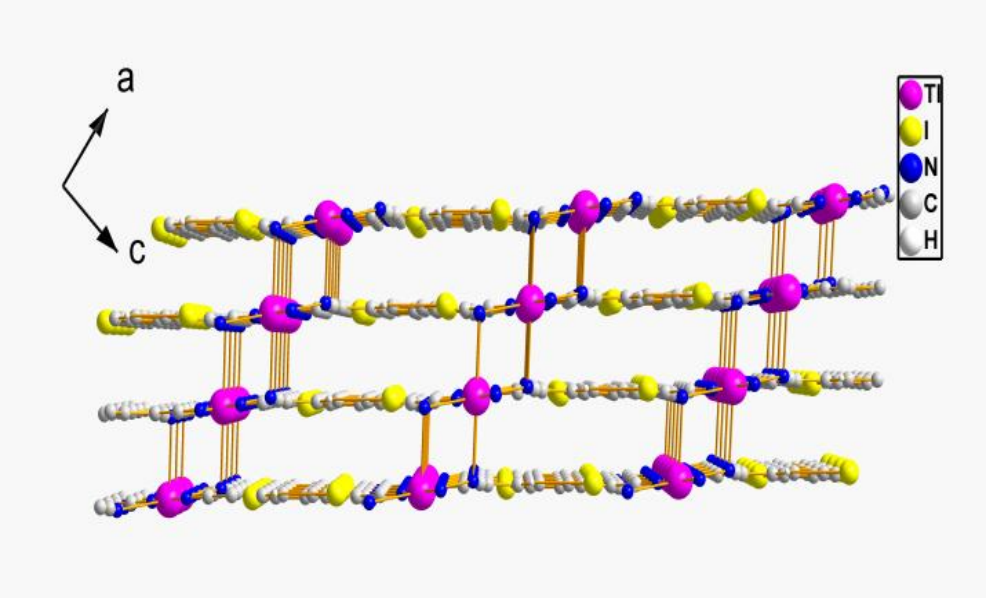

Figure 3.2 Views of the structure of $Tl(TCNQI_2)$ (4), in (a) the *bc* plane and (b) the *ac* plane.

$Tl(TCNQCl_2)$ Phase I (**1**)

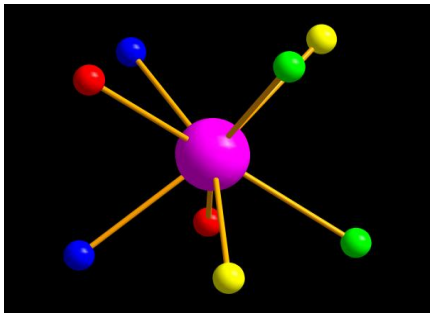

Tl-N bond distances	Å
Blue	2.914
Green	2.993
Red	2.999
Yellow	3.074

$Tl(TCNQBr_2)$ (**3**)

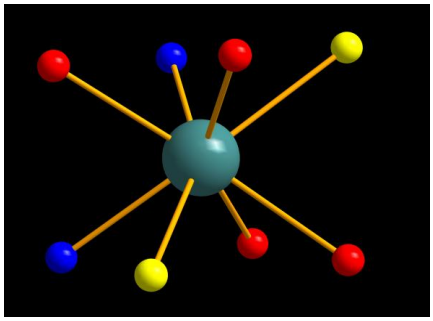

Tl-N bond distances	Å
Blue	2.916
Red	2.999
Yellow	3.182

$Tl(TCNQI_2)$ (**4**)

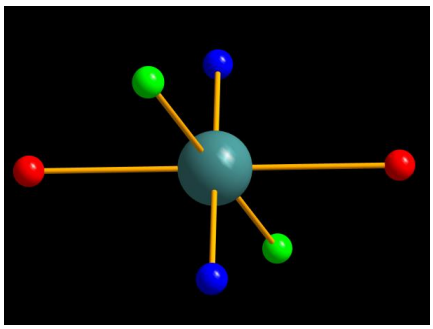

Tl-N bond distances	Å
Blue	2.915
Green	2.976
Red	3.198

Figure 3.3 The coordination environment of Tl in $Tl(TCNQCl_2)$ (1**),** $Tl(TCNQBr_2)$ (3**)** and $Tl(TCNQI_2)$ (4**).** In both 1 and 3, the Tl cations adopt a distorted cubic coordination environment with a coordination number of 8. Inequivalent Tl-N bond distances are listed in the table. In compound 4, Tl cations adopt a distorted octahedral environment with two elongated Tl-N bonds (3.198 Å), which are the "interlayer" Tl-N bonds with the other Tl-N distances being considered as the " in-planar" Tl-N bonds.

(a)

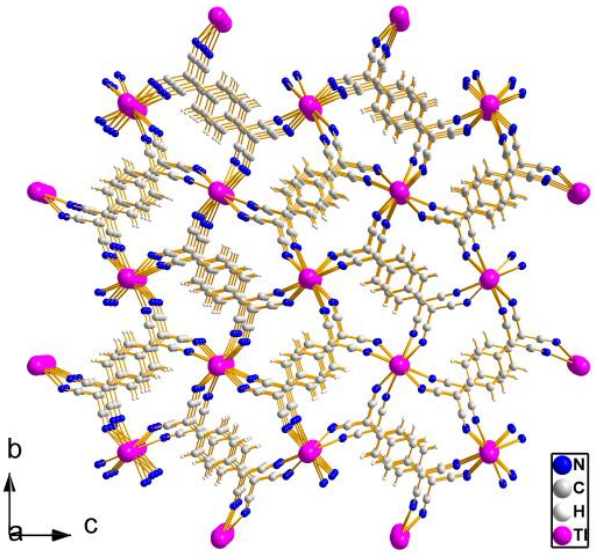

(b)

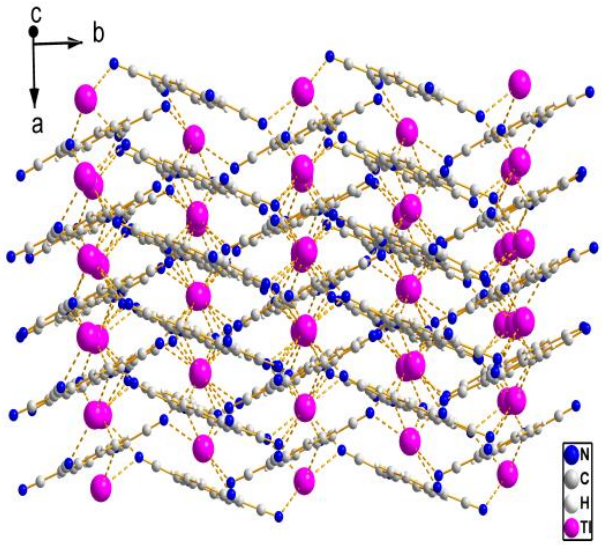

Figure 3.4 Views of Tl(TCNQ) Phase III (5), prepared in CH_3CN in the (a) *bc* and (b) *ab* planes.

Table 3.1. Pertinent crystallographic parameters and data for $Tl(TCNQX_2)$ (X= Cl (1), Br (3) , I (4)) and Tl(TCNQ) Phase III (5) . [a]

Compound	1	3	4	5
Formula	$C_{12}H_2N_4Cl_2Tl$	$C_{12}H_2N_4Br_2Tl$	$C_{12}H_2N_4I_2Tl$	$C_{12}H_4N_4Tl$
F_w [g mol^{-1}]	477.46	566.36	660.37	408.57
Crystal size mm^3	0.40 x 0.30 x 0.20	0.34 x 0.24 x 0.16	0.33 x 0.30 x 0.22	0.08 x 0.02 x0.01
Crystal system, SG	Monoclinic, P2/c	Monoclinic, P2.c	Monoclinic, P-1	Monoclinic, $P2_1/c$
a [Å]	7.538(2)	7.756(2)	4.120(1)	6.987(1)
b [Å]	11.804(2)	11.640(2)	8.494(2)	12.332(3)
c [Å]	6.843(1)	6.813(1)	9.099(2)	12.947(3)
α [°]	90	90	91.12(3)	90
β [°]	96.85(3)	97.72(3)	95.55(3)	97.75(3)
γ [°]	90	90	95.74(3)	90
V [$Å^3$]	604.59(7)	609.47(3)	315.26(4)	1105.4(6)
Z	2	2	1	4
ρ_{calc} [g cm^{-3}]	2.645	3.086	3.478	2.454
μ ($Mo_{K\alpha}$) [mm^{-1}]	0.711	0.711	0.711	0.413(synchrotron)
Reflns collectged	6610	1456	2942	2892
Unique Reflns	1468	1456	1429	2892
Reflns with I >2σ(I)	1350	1362	1255	1980
Parameters	47	88	88	69
R(int)	0.0359	0.0309	0.0297	0.0642
$R1^{[a]}$	0.0277	0.0485	0.0393	0.0877
$wR2^{[b]}$	0.1159	0.1178	0.0919	0.0823
GOF	1.001	1.150	1.051	1.054
Compound	1	3	4	5

[a] $R1 = \Sigma||F_o| - |F_c||\Sigma|F_o|$. [b] $wR2 = [\Sigma[w(F_o^2 - F_c^2)^2]/\Sigma[w(F_o^2)^2]]^{1/2}$.

Four-Coordinate -Type I

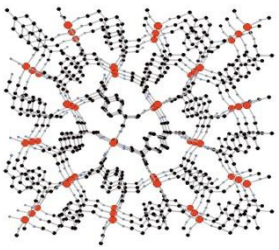

Cu(TCNQ) Phase I

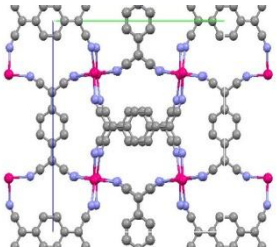

Ag(TCNQ) Phase II

Four-Coordinate -Type II

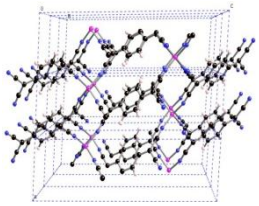

Cu(TCNQ) Phase II

Four-Coordinate -Type III

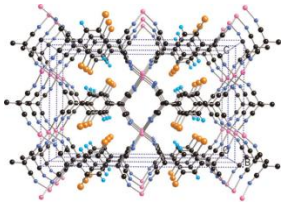

Cu(TCNQX$_2$) (X=Cl, Br)

Six-Coordinate

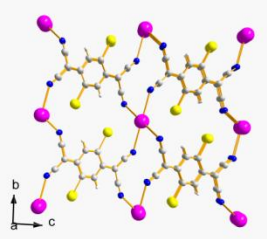

Tl(TCNQI$_2$)

Eight-Coordinate-Type I

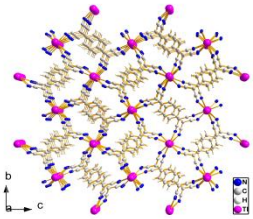

Tl(TCNQ) Phase I & III

Eight-Coordinate- Type II

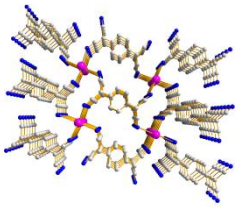

Tl(TCNQ) Phase II

Eight-Coordinate-Type III

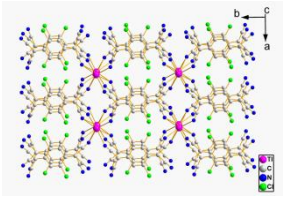

Tl(TCNQX$_2$)(X=Cl,Br)

Figure 3.5 Structures of known polymorphs of binary M(TCNQ) phases determined by single crystal X-ray diffraction.

Interestingly, although two polymorphs of $Tl(TCNQCl_2)$ were obtained (Figure 3.6a), only one phase of $Tl(TCNQBr_2)$ was detected regardless of the conditions (Figure 3.6b). All attempted bulk preparations of $Tl(TCNQI_2)$ led to amorphous powders. Since the electron withdrawing properties of halogen substituents are similar as judged by the first reduction potentials being similar ($E_{1/2}$ = 0.48 for $TCNQCl_2$, 0.49 for $TCNQBr_2$ and 0.46 for $TCNQI_2$), it is reasonable to expect that the stacking models of TCNQ moieties are primarily dictated by the steric effect of the halogen atoms. For example, in addition to the compound which is isostructural with $Tl(TCNQBr_2)$, a second phase of $Tl(TCNQCl_2)$ was discovered which hints at improved flexibility in terms of stacking options available for the chlorine derivative. In the case of $Tl(TCNQI_2)$, the much larger iodine atoms lead to a less stable crystal packing arrangement and, as a result, only amorphous solids were obtained despite many attempts to grow crystals.

Infrared Spectroscopy

Infrared spectroscopy is a useful technique for characterizing TCNQ charge transfer salts, especially with respect to distinguishing the presence of TCNQ in its various redox states. The pertinent data for known binary phases as well as the new $Tl(TCNQX_2)$ compounds (X = H, Cl, Br, I) are provided in Table 3.2. As expected, compounds 1 and 3 exhibit ν(C≡N) stretching modes similar to their counterparts $Cu(TCNQX_2)$ (X = Cl, Br,) at 2143, 2132 and 2121 cm^{-1} and at 2185, 2169 and 2154 cm^{-1} respectively. The similarity of the ν(C≡N) modes indicates an analogous coordination environment for the

(a)

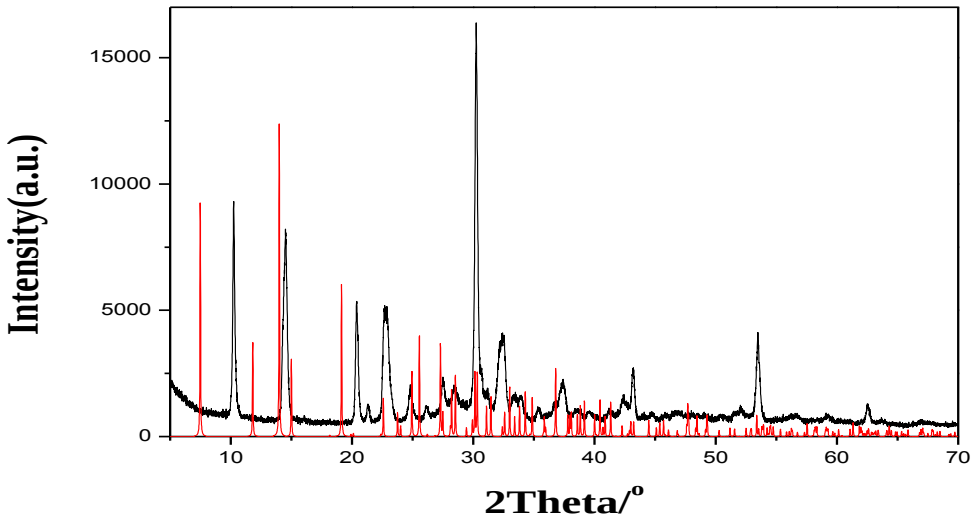

(b)

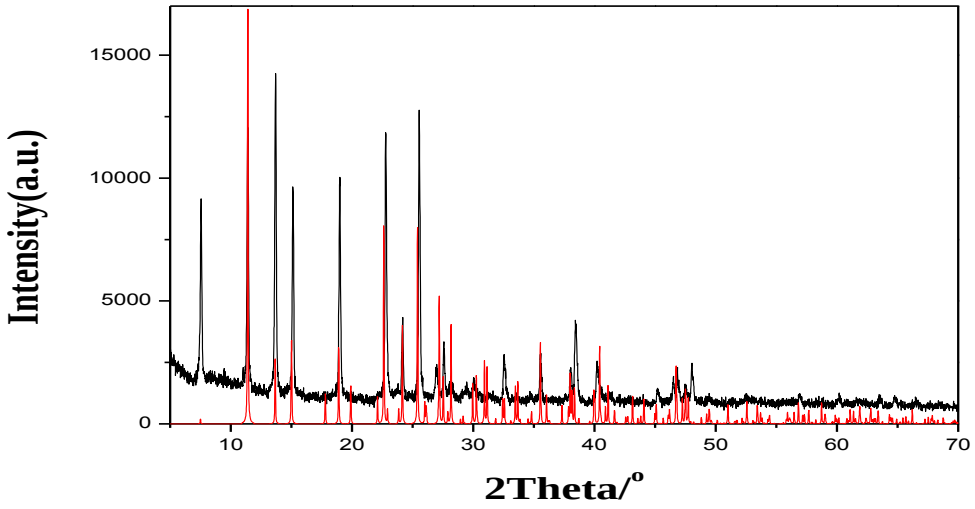

Figure 3.6. Powder X-ray data on (a) bulk sample of Phase II of Tl(TCNQCl$_2$) (black trace) overlaid with data simulated from single crystals of Phase I (red trace) indicating that they are different phases (b) bulk sample of Tl(TCNQBr$_2$) (black trace) overlaid with the simulation from the single crystal data (red trace) verifying that the two phases are identical.

Table 3.2 Infrared data for $Tl(TCNQX_2)$ compounds.

	$\nu(C\equiv N)$ / cm^{-1}	$\delta(C\text{-}H)$ /cm^{-1}
Tl(TCNQ) Phase I[69]	2181, 2164, 2151	823
Tl(TCNQ) Phase II[69]	2180, 2149	822
Tl(TCNQ) Phase III (5)	2182, 2165, 2151	823
$Tl(TCNQCl_2)$ Phase I (1)	2143, 2132, 2121	834
$Tl(TCNQCl_2)$ Phase II (2)	2183, 2154	835
$Tl(TCNQBr_2)$ (3)	2185, 2169, 2154	845
$Tl(TCNQI_2)$ (4)	2176, 2145	846

cyanide groups which we know to be the case for 1 and 3. Compound 2, however, exhibits a strong and sharp ν(C≡N) absorption at 2183 cm^{-1}, with a shoulder at 2154cm^{-1}. In the case of compound 4, the ν(C≡N) modes appear as strong and broad absorptions at 2176 cm^{-1} and 2145 cm^{-1}. The differences in the infrared spectra of 1 and 2 data are a result of polymorphism as found in the Tl(TCNQ) phase I and II compounds as well. In all cases, the data support the conclusion of the one-electron reduced radical forms of the TCNQ molecules.

It is also instructive to examine the out-of-plane δ(C-H) bending mode in these compounds which is very sensitive to the oxidation state of TCNQ moiety. The δ(C-H) modes appear at 834 cm^{-1}, 835 cm^{-1}, 845 cm^{-1}, and 846 cm^{-1} for 1, 2, 3 and 4, respectively which confirms the existence of the radical form of TCNQ moiety in the structure. In terms of comparison, the δ(C-H) modes of $TCNQCl_2$, $TCNQBr_2$ and $TCNQI_2$ appear at 848 cm^{-1}, 874 cm^{-1} and 870 cm^{-1} and the bending modes for the reduced form as the lithium salt occur at 828 cm^{-1}, 847cm^{-1} and 846 cm^{-1} respectively.

Conductivity Measurements

Most binary TCNQ salts are semiconductors due to the stacking interactions that produce columns of TCNQ radicals, the existence of which leads to overlap between the singly-occupied molecular orbital (SOMO) and the lowest unoccupied molecular orbital (LUMO) of adjacent radicals which facilitates electron hopping. Typically the band structure and conductivity data can be predicted by taking into account the charge, stacking motif and structural parameters of the material. For example, in our preliminary work, we discovered that one polymorph of Tl(TCNQ), phase I, exhibits alternating distances between both the adjacent TCNQ molecules (3.16(1) Å and 3.35(1) Å and the

Tl^{I} ions (3.63(1) Å and 3.45(1) Å), a signature of a typical spin-Peierls material in which adjacent TCNQ radicals are partially dimerized. Antiferromagnetic interactions between the spins lead to a secondary gap in the energy band and therefore a decrease in the conductivity properties. In contrast, Tl(TCNQ) phase II adopts a homogeneous stacking motif with uniform distances between TCNQ radicals (3.22 (1) Å) and the Tl^{I} cations (3.79 (1) Å). As a consequence of the regular structure, the conductivity of Phase II is expected to be much higher than the first polymorph of Tl(TCNQ). Indeed, the pressed-pellet data revealed that Phase I exhibits a nearly insulating room-temperature conductivity of 2.4×10^{-4} $S\cdot cm^{-1}$, whereas Phase II exhibits a much higher room-temperature conductivity of 5.4×10^{-1} $S\cdot cm^{-1}$.

Crystals of 1, 3 and 4 were subjected to single-crystal conductivity measurements by the two-probe method. The temperature dependent conductivity data plotted in Figure 3.7 clearly indicate that all three compounds are semiconductors. The room temperature conductivities of 1 and 3 are very similar (9.3×10^{-3} $S\cdot cm^{-1}$ and 2.1×10^{-3} $S\cdot cm^{-1}$), which is not surprising given their structural similarity. Compound 4 exhibits a slightly higher room temperature conductivity at 2.9×10^{-2} $S\cdot cm^{-1}$. The energy gaps were obtained by fitting the curves to an Arrhenius expression and are 172 meV, 85 meV and 160 meV for 1, 3 and 4 respectively.

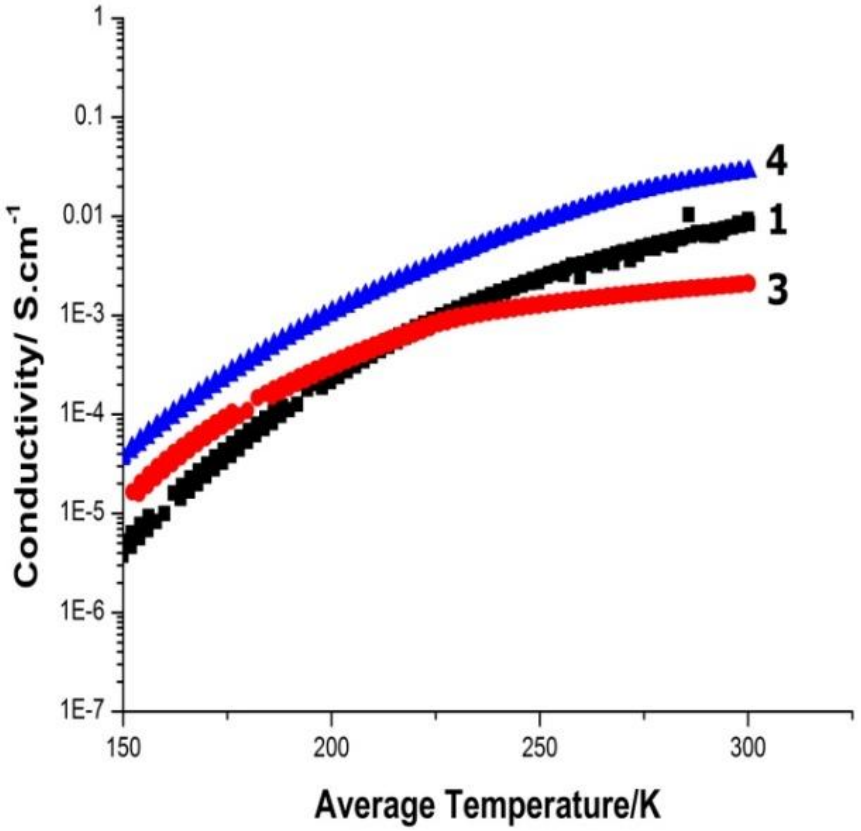

Figure 3.7. Temperature dependent conductivity data obtained on single crystals of $Tl(TCNQCl_2)$ Phase I (1), $Tl(TCNQBr_2)$ (3) and $Tl(TCNQI_2)$ (4).

Table 3.3 Selected structural and conductivity data for the series $Tl(TCNQX_2)$ (X = H, Cl. Br, I).

	Tl-Tl distance / Å	TCNQ-TCNQ distance/ Å	σ (RT) $S \cdot cm^{-1}$
Tl(TCNQ) Phase I	3.45/3.63	3.16/3.35	2.4×10^{-4}
Tl(TCNQ) Phase II	3.79	3.22	5.4×10^{-1}
Tl(TCNQ) Phase III(5)	3.39/3.61	3.13/3.29	2.8×10^{-4}
$Tl(TCNQCl_2)$ Phase I (1)	3.42	3.30*	9.3×10^{-3}
$Tl(TCNQBr_2)$ (3)	3.41	3.28*	2.1×10^{-3}
$Tl(TCNQI_2)$ (4)	4.10	3.28	2.9×10^{-2}

* Average distance, see structural description section**.** Powder pressed pellets were used for Tl(TCNQ) phase I, II and III and single crystals for **1**, **3** and **4**.

Table 3.3 contains a compilation of structural parameters and properties for all of the $Tl(TCNQX_2)$ (X=H, Cl, Br, I) phases. Except for Tl(TCNQ) phase I, the compounds adopt a stacking model with a uniform stacking distance between TCNQ moieties with no dimerization of TCNQ radicals and they exhibit higher conductivities. If one compares Tl(TCNQ) phase II to the halogen derivatives 1, 3, and 4, it is reasonable to expect longer distances between adjacent TCNQ radicals to result in more poor overlap of the frontier orbitals hence lower conductivities than for Tl(TCNQ) phase II. Indeed, the trend in the stacking distances is Tl(TCNQ) phase II < $Tl(TCNQI_2)$ (4) ≈ $Tl(TCNQBr_2)$ (3) < $Tl(TCNQCl_2)$ (1), and the observed conductivities are actually Tl(TCNQ) phase II> $Tl(TCNQI_2)$ (4) > $Tl(TCNQCl_2)$ (1)> $Tl(TCNQBr_2)$ (3).

Band Structure Calculations

Given that the valence shell electrons of the Tl^I metal ion are 6s electrons, the relativistically contracted valence shell is well known as being an inert lone pair, and expected to lead to much weaker interactions than 3d transition metal ions,[69] *e.g.* Cu^I with organocyanide acceptors,[23,53,70] nevertheless spin-density transfer from the ligand to the Tl^I ion has been reported in the case of $Tl(DM\text{-}DCNQI)_2$.[57] Since the Tl^I compounds are similar to potassium, the alkali metal TCNQ salts are more suitable as a theoretical model for a band structure study than are transition metal analogs for the series $Tl(TCNQX_2)$ (X = H, Cl, Br, I). In this manner, as a "first principles" approach, these materials can be treated as "radical only" charge carriers, which implies that the contributions to the conductivity can be described solely as an extended Hückel model of TCNQ columns of charge carriers.[71]

The approach of our simulation was to initially treat the Tl(TCNQ) species as a "TCNQ only" semiconductor, *i.e.*, to neglect the contribution of the 6s orbitals of Tl^{I} cation to evaluate the interaction between adjacent radicals. The 6s orbital contribution was then introduced in the next phase of the calculation as a perturbation on the major 1-D conducting feature. In the first step, the intra-stack transfer integrals between adjacent TCNQ radicals were calculated to be to be t_c = 156 and 170 meV for compounds 1 and 3 respectively (Figure 3.8a). These values are in agreement with the reported estimations of transfer integrals in TCNQ chains. The value for 4 was similarly evaluated to be 145 meV (Figure 3.8b). The largest inter-chain transfer integrals are less than 4 meV which implies that these compounds are highly one-dimensional. Indeed, the calculated bandwidths of TCNQ stacks are 0.62, 0.68, and 0.58 eV for 1, 3, and 4, respectively. The "organic-only" band structures and Fermi surfaces of them are displayed in Figure 3.9.

The second step was to take the effect of Tl(I) cations into the consideration. The transfers between the TCNQ LUMO and Tl 6s orbitals were evaluated and the values t_1-t_4 are listed in captions in Figure 3.10. The metal-organic transfers are approximately half (50-70 meV) of those within the TCNQ radical stacks. These values are approximately the same as the reported p-d-interactions (53.8 meV) for $Cu(DMDCNQI)_2$ (DMDCNQI: *N*,*N*'-dimethyldicyano- quinonediimine).[69] By adopting these transfer integrals, the tight-binding energy band shown in Figure 3.11 was obtained for 1, and the energy band of 3 is practically the same. Figure 3.12 displays a 3-D model of the Fermi surfaces of 1 and 3. The large dispersion on ΓZ at the right end of Figure 3.11 comes from the 1-D

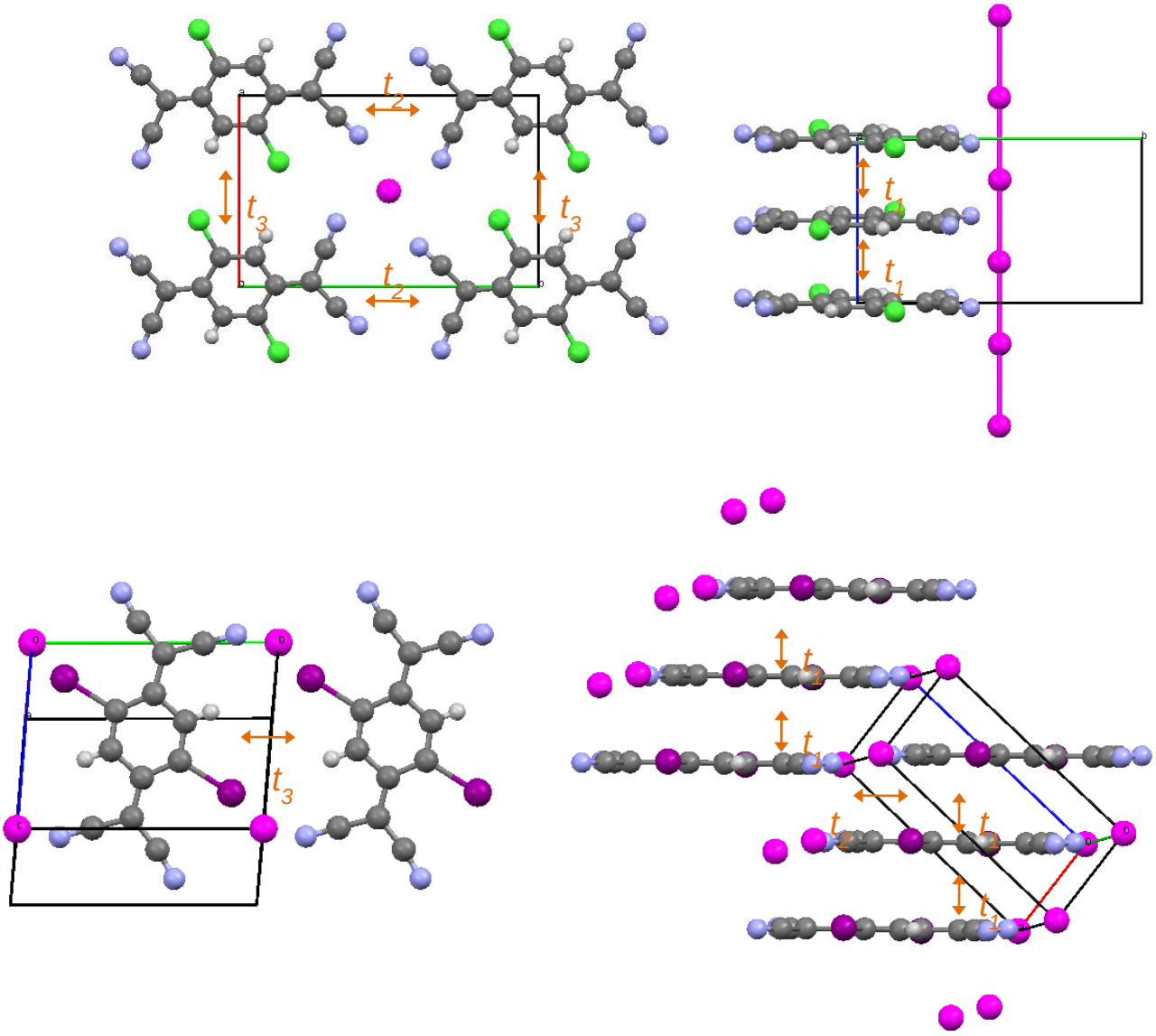

Figure 3.8. The transfer integral diagram of $Tl(TCNQCl_2)$ (1), $Tl(TCNQBr_2)$ (3) and $Tl(TCNQI_2)$ (4) in the case of ignoring the effect of the Tl(I) cations. (a) for 1, t_1=156meV, t_2=0meV, t_3=1meV; for 3, t_1=170meV, t_2=0meV, t_3=2meV; (b) for 4, t_1=145meV, t_2=1meV, t_3=4meV.

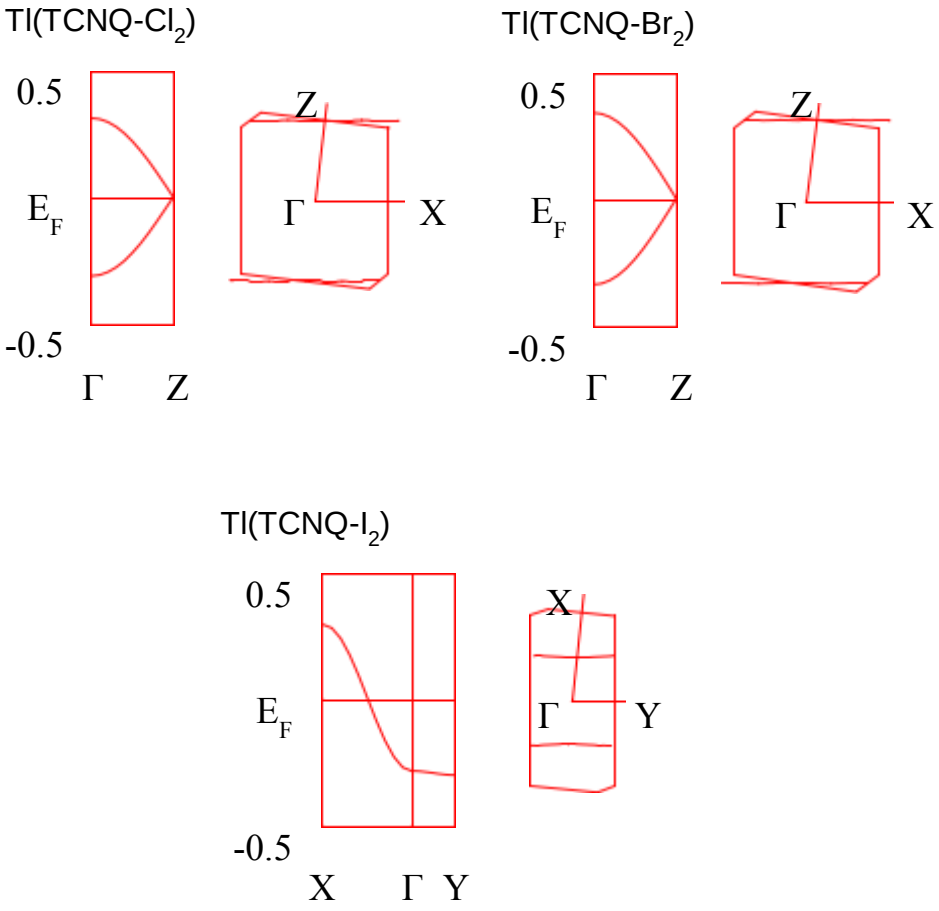

Figure 3.9. Energy band structures and Fermi surfaces of $Tl(TCNQCl_2)$ (1), $Tl(TCNQBr_2)$ (3) and $Tl(TCNQI_2)$ (4). 1 and 3 are two-fold due to the restrictions of crystal symmetry.

(a)

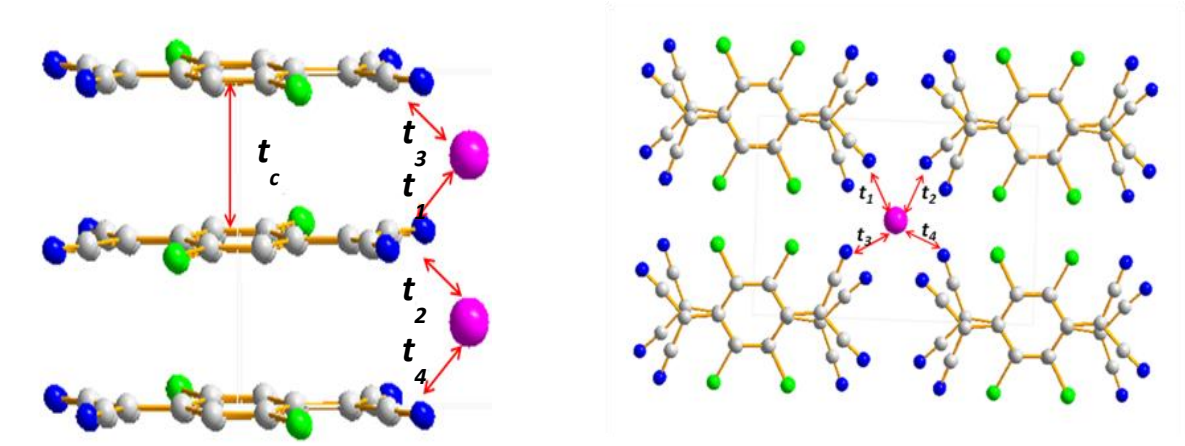

(b)

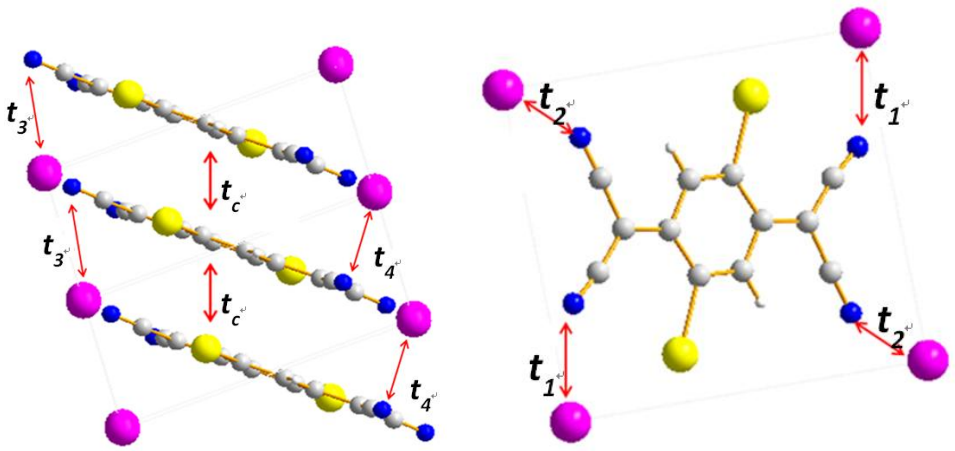

Figure 3.10. The transfer integral diagram between Tl(I) and TCNQ radicals of $Tl(TCNQCl_2)$ (1), $Tl(TCNQBr_2)$ (3) and $Tl(TCNQI_2)$ (4). (a) transfer integral diagram of 1 (3 adopts the same diagram). The t_c value represents the intra-stack transfer integral between adjacent TCNQ molecules, and is t_c=156 meV for 1 and 170 meV for 3. The $t_{1\text{-}4}$ number represents the transfer integrals between the Tl 6s orbital and LUMO of TCNQ molecule, and is $t_{1\text{-}4}$=-48, 71, -70, and 88 meV for 1 and -87, 70, -71, and 39 meV for 3, respectively. The types of transfers are restricted by the symmetry of the crystal structure. (b) transfer integral diagram of 4, where t_c=145meV and $t_{1\text{-}4}$=-7, 26, 57, and -69meV, respectively.

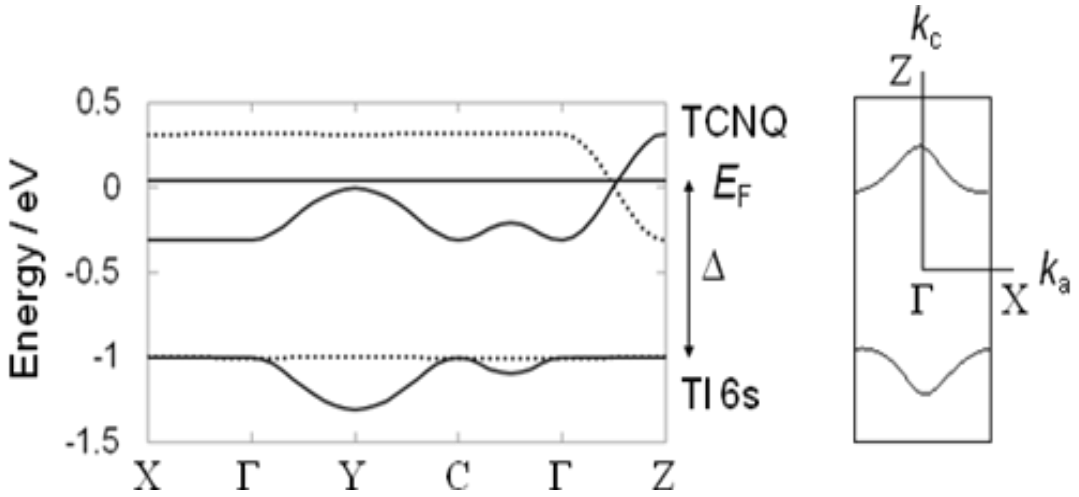

Figure 3.11 Tight-binding energy band (left) and Fermi Surface modulation (right) of $Tl(TCNQCl_2)$ including the TCNQ LUMO and the Tl 6s orbitals. The transfer integrals are taken from the caption of Figure 3.8. Solid and dashed curves represent the band dispersions with and without the consideration of Tl 6s orbitals, respectively. C represents the position, (π/a, π/b, k_c).

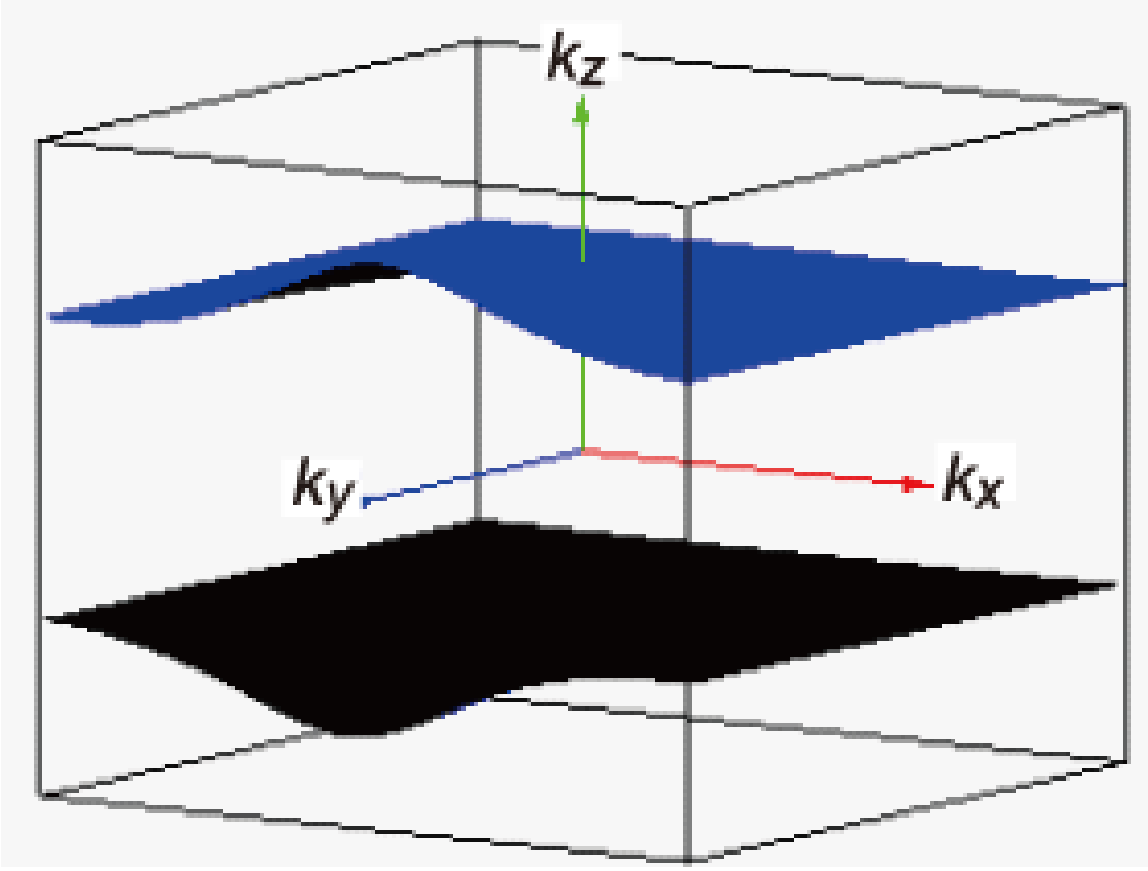

Figure 3.12 3D view of the Fermi surface modulation of $Tl(TCNQCl_2)(1)$ at $\Delta = 1.0$ eV. Compound 3 adopts the same model.

TCNQ band. We have assumed that the nearly flat Tl 6s band is located at Δ = 1 eV below the TCNQ band. Although the TCNQ chain is composed of two molecules in the repeat unit of the column (Figure 3.8), the stacking is uniform owing to the *c*-glide symmetry. As a consequence, the energy bands are degenerate at the k_c = p/2*c* point, namely the midpoint of Γ and Z in Figure 3.11. We can represent it as the solid curve in the extended-zone scheme, but the dashed curve crosses the solid curve at k_c = p/2*c* owing to this degeneracy. The dashed curve does not show any dispersion in the k_x and k_y directions as indicated in the left part of Figure 3.11, whereas the solid curve shows considerable dispersion on the ΓYC line. The dispersion is a mirror image of the Tl 6s band, indicating that this dispersion is mediated by the Tl 6s orbitals. Since the metal-organic interactions bridge the TCNQ molecules along the *x* and *y* axes (Figure 8), the dispersion appears in these directions. However, the Fermi surface is considerably modulated as depicted in Figure 3.11. Since even $Tl(DM\text{-}DCNQI)_2$ undergoes a Peierls-like transition, the metal orbital hybridization of Tl is expected to be less than that of Cu. Accordingly, the actual Δ is expected to be slightly larger than this value, and the Tl 6s hybridization is not so significant as to destroy the 1-D character of the TCNQ chain. Nonetheless, the Tl 6s mediates the interchain interaction to some extent, and this is probably responsible for the uniform chain arrangement in the Tl salts. If there is no hidden or diffuse dimerization, these energy bands lead to the Mott insulating states owing to the half-filled nature. We can attribute the comparatively high conductivities of the present compounds (10^{-3} to 10^{-2} $S \cdot cm^{-1}$) to the Mott insulating state.

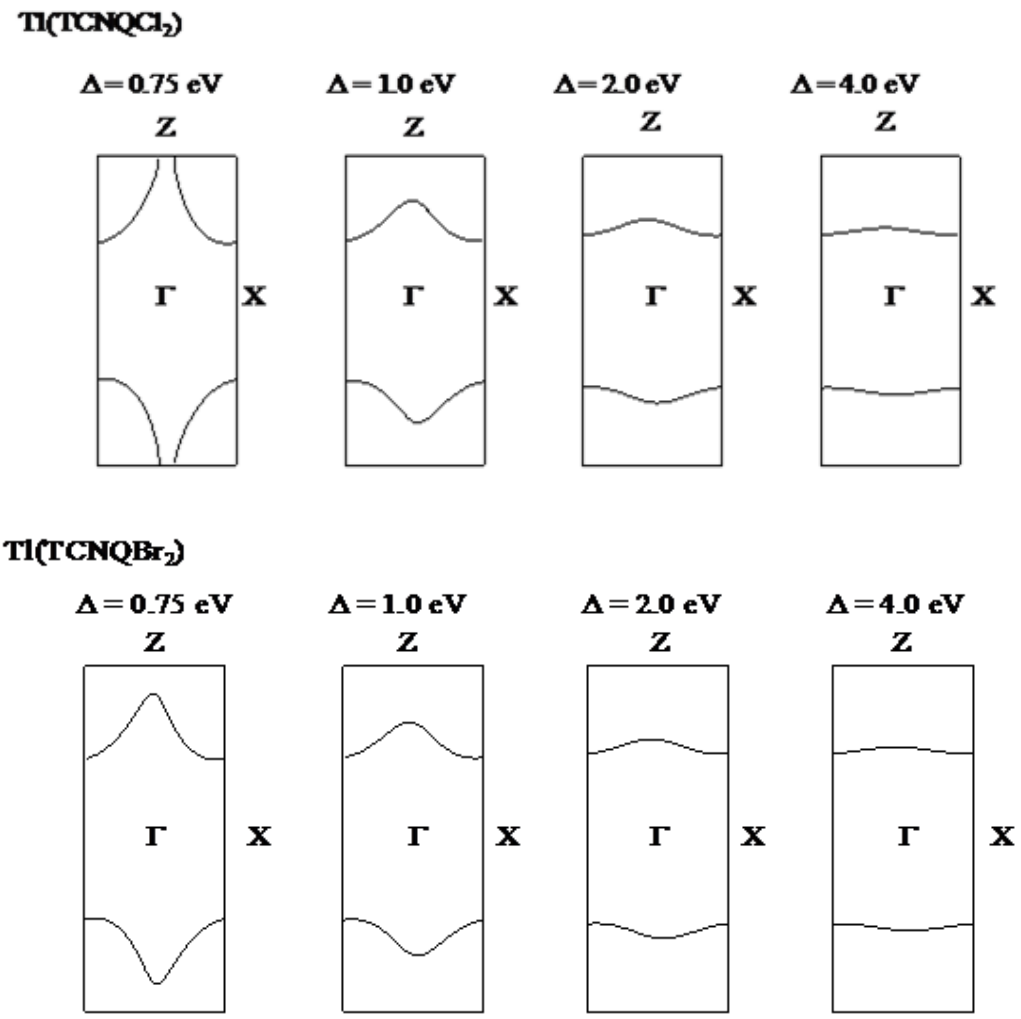

Figure 3. 13 The Fermi surface at $k_b = \pi/c$ for various Δ values.

This finding in in contrast to examples with obvious dimerization observed in such materials as Ag(TCNQ) phase I and Tl(TCNQ) phase I (10^{-4} $S \cdot cm^{-1}$). From the calculations, one can expect that the modulation degree of band structure is actually affected by the relative position of Tl 6s orbital. As discussed in the aforementioned section, the calculation is based on the assumption that the Tl 6s band is located at Δ= 1 eV below the TCNQ band. By alternating the value of Δ, the modulation degree of the band structure will be manipulated as illustrated in Figure 3.13. From Figure 3.13, it can be concluded that a smaller Δ value will lead to a higher degree of modulation. Although the real value of Δ may be even larger than 1 eV as the 1-D band structures of 1, 3 and 4 are consistent with the measurements. The result did suggest that the valence orbitals of metal cation may potentially perturb the 1-D band structure which arises TCNQ columns.

Figure 3.14 depicts the LUMO components of the $TCNQX_2$ radicals and illustrates the contribution of the halogen substituents. In addition to the stacking arrangement, the electron-withdrawing effect of different halogen groups affects the conductivity of materials as well through involvement of the LUMO of the radical which alters the energy gap. As mentioned earlier, compounds 1 and 3 exhibit analogous stacking patterns with 3.30 Å and 3.28 Å separations respectively. Since the LUMO of 1 has a bigger component from Cl atomic orbitals (Mulliken charge = 0.0280) than does 3 with Br atomic orbitals (Mulliken charge = 0.0258), the electron-withdrawing halogen groups in 1 lead to a higher electron-accepting LUMO hence an increased room temperature conductivity.

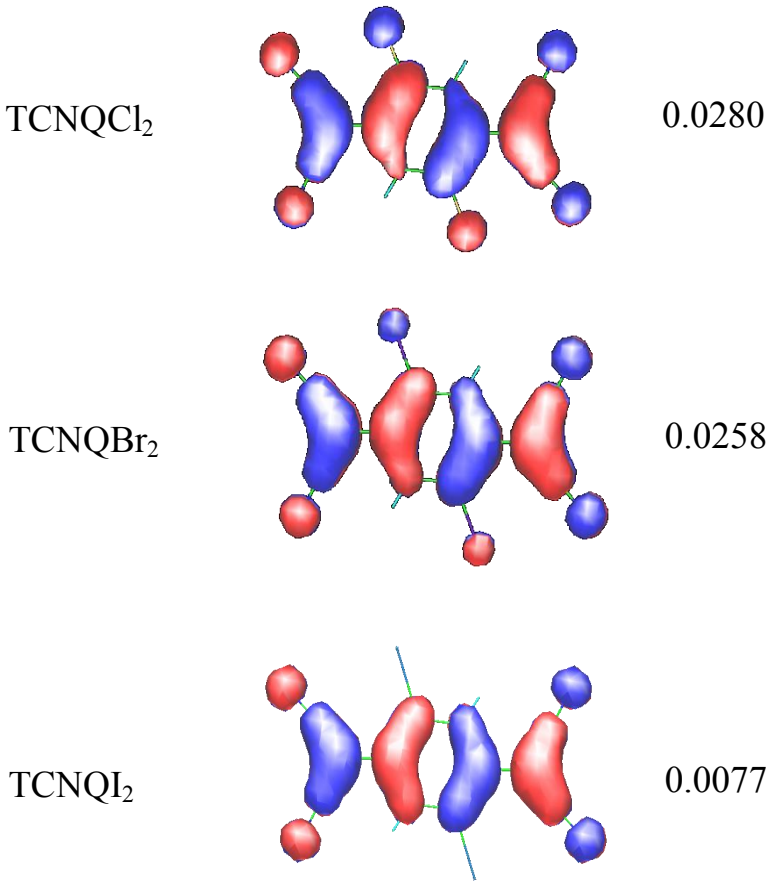

Figure 3.14 LUMO diagrams of $TCNQX_2^-$ radicals with the indicated Mulliken charges on the halogen atom.

Details of the Theoretical Simulations. For the transfer integral between adjacent TCNQ radical in the columnar stackings, the LUMOs of TCNQ radicals are treated as infinite 1-D chain model and the energy can be derived from the following calculations:

$$\Sigma(H_{ij}- \varepsilon_i S_{ij})C_i=0. \qquad \textbf{Equation 3.1}$$

(Here S_{ij}=1 when i=j, 0 for other case. H_{ij}=α when i=j, β when i=j+1 or j-1, 0 for other case.).

Here we set α = 0, and β represents t (transfer intergral) in the physical meaning. By solving the equation we obtained:

$$\varepsilon(k)=2t\cos(kc), \qquad \textbf{Equation 3.2}$$

k is the space vector, and c is the unit cell parameter. The t is obtained by $t = ES$ (S is the overlapping constant between adjacent TCNQ, and E is assumed to be –10 eV as the energy of the molecular orbital) By the equation we can derive the band-structure vs k-vectors.

After the 1-D model, we attempted to introduce the Tl orbitals. Tl^+ has the valence electronic configuration $6s^2 6p^0$, so the fully occupied 6s level should be located below the Fermi level, and the empty 6p level above the Fermi level. The isotropic 6s orbital is much more easily accounted for than the anisotropic 6p orbitals for the calculations. The energy band structure is determined by the following secular equation; here the energy difference (Δ) represents the energy gap between Tl 6s orbital and LUMO of TCNQ radicals. The energy band is calculated based on different Δ value assumptions.

$$\begin{vmatrix} \mathrm{TCNQ-TCNQ} & \mathrm{TCNQ-Tl} \\ \mathrm{Tl-TCNQ} & \mathrm{Tl-Tl} \end{vmatrix} = \begin{vmatrix} 2t_c \cos k\mathbf{r} - E & \sum_i 2t_i \cos k\mathbf{r}_i \\ \sum_i 2t_i \cos k\mathbf{r}_i & -\Delta - E \end{vmatrix} \qquad \textbf{Equation 3.3}$$

Here, sigma is a sum of four metal-organic interactions. This quadratic equation is easily solved to give the following:

$$E = \frac{-\Delta + 2t_c \cos k\mathbf{r} \pm \sqrt{(\Delta + 2t_c \cos k\mathbf{r})^2 + 4(\sum_i 2t_i \cos k\mathbf{r}_i)^2}}{2} \qquad \textbf{Equation 3.4}$$

The energy bands are analytically calculated by substituting the actual calculated numerical values of t_c, t_1-t_4, and Δ in it.

Conclusions

A new family of main group molecule-based semiconductors $Tl(TCNQX_2)$ (X = H, Cl, Br, I) has been obtained and subjected to a comprehensive treatment of their structures and properties. Single crystal conductivity measurements revealed that the derivatives exhibit room temperature conductivities in the range $\sim 10^{-2} \sim 10^{-3}$ $S \cdot cm^{-1}$ which falls into normal range of semiconductors. A comparison between the metrical parameters of the structures and the conductivities leads to predictions based on the stacking model and the separation distances of TCNQ radicals as supported by band structure simulations. These new results add to the relatively small database of structure/property correlations documented for TCNQ binary conductors and, importantly, introduces the first examples with main group element materials, an entirely unexplored area of hybrid inorganic-organic donor-acceptor solids.

CHAPTER IV

DEVELOPMENT OF HIGHLY CONDUCTING MATERIALS WITH SWITCHING BEHAVIOR WITH SILVER(I) CATIONS AND TCNQ DERIVATIVES

Background

Resistance-based bistability in materials is highly relevant to the future development of electronic devices in which a high resistance "OFF" state rapidly switches to a low resistance "ON" state as a result of external stimulation. The use of different stimuli to trigger the switching process has unearthed a variety of phenomena including magnetoresistivity (response to an external magnetic field)[72] piezoresistivity (response to mechanical pressure),[73] photoresistivity (response to light),[74] and direct non-linear resistance (response to the strength of electric field).[75] Given that the timescale of switching is very fast, materials in these categories are being sought for incorporation into new types of electronic devices. The interest in these materials stems from the fact that they are not just merely stimuli-responsive sensors; their properties reflect an interplay between the external field and the electric response which has promise in fast data processing for random access memory applications (RAM). The memory effect arises from the "ON" and "OFF" states which are able to represent "0" and "1" in data processing and storage. RAMs are differentiated into two categories based on whether the data can be maintained after the external stimulus is removed. Dynamic RAM (DRAM) refers to volatile memory which is lost when the power supply is removed, but its fast write/erase speed and high circular write/erase numbers makes it ideal for temporary storage (main memory) for the central processing unit (CPU).

Non-volatile RAM (NVRAM) maintains a memory effect without the power supply which translates to permanent information storage. Advances in technologies involving computation and data storage continue to rely heavily on the development of DRAM and NVRAM.[76]

With the requirement of reduction in device size and enhancement of processing speeds for vastly improved information technology, there is an intense effort to realize ever-increasing density for memory storage and fast processing speeds.[2] Most traditional RAM devices are based on solid-state semiconductors such as silicon chips[77] and metal oxides,[78] whose size limits are determined by the limitations of fabrication. Molecule-based resistive switching materials are attracting more attention in recent years because they can respond to the aforementioned stimuli but have much smaller domain sizes of a molecule and offer greater ease of manipulation and fabrication. Excellent examples of such materials are organic ferroelectrics which can be used for non-volatile memory because of their long retention times.[79] A recent advance in this area is the report of Donor-Acceptor (D-A) charge transfer salts containing pyromellitic diimide-based acceptors.[80] These organic materials exhibit ferroelectric behavior at room temperature, a fact that renders them ideal candidate for modern ferroelectric RAM (FeRAM) which is being used in devices to replace traditional flash memory.[81]

Apart from purely organic materials, another important category of compounds vis-à-vis resistive switching behavior is metal-organic hybrid materials. To date, the most extensively studied examples are the binary phases Cu(TCNQ) and Ag(TCNQ) (TCNQ = 7,7,8,8-tetracyanoquinodimethane), a family of compounds formed by spontaneous redox reactions of the group 11 metal with neutral TCNQ molecules. It was discovered in 1979

that thin films of these materials exhibit a remarkable transition in their electrical properties with the application of an electric field or upon irradiation.[23a,23b,25.] In the case of Cu(TCNQ) a sandwich device composed of Cu/Cu(TCNQ)/Al was prepared by growing the film on a Cu electrode by spontaneous electrolysis which exhibits a sharp resistance state change from nearly insulating (2MΩ) to a low resistance state (200Ω) at a field strength of $4\times10^{3}V\cdot cm^{-1}$; full recovery to the high resistance state was observed upon application of an electric field in the opposite direction. The devices based on these materials are highly compatible for the application of new generation NVRAM due to the fast switching behavior and the convenience and low cost preparation by a self-assembly process. The dicovery of the remarkable properties exhibited by these materials spawned a large number of studies directed at the fabrication of device-friendly structures including nanowires, nanoribbons and nanosize fabricated micro-devices.[82]

Throughout the decades of research on Cu(TCNQ) and related materials, a great deal of research has been directed at understanding the mechanism of the non-linear response of the external voltage and switching properties of M(TCNQ) materials. Techniques that proved to be useful at providing details include *in situ* Raman spectroscopy, X-ray photoelectron spectroscopy (XPS) and ultrafast electron microscopy, the collective results of which point to the fact that the material undergoes partial decomposition and that the presence of metal atoms/islands are responsible for the switching behavior. (Equation 4.1)[83] In the case of Cu(TCNQ), the transition from the "OFF" state to the "ON" state is proposed to lead to the production of Cu(0) and $TCNQ^{0}$ as a result of an electric field induced ligand-to-metal charge transfer (LMCT). In this scenario, the presence of Cu metal in the material would drastically enhance the

conductivity and lead to a low resistance state. Although the presence of Cu^0 and $TCNQ^0$ has been detected by different methods, the actual mechanism still remains debatable as real time observation under electric field has never been reported.

$$Cu(TCNQ) \xrightarrow[\text{or } h\nu]{\text{electric field}} Cu^0{}_x + TCNQ^0{}_x + \{Cu(TCNQ)\}_{1-x} \qquad \textbf{Equation 4.1}$$

Equation 4.1 The proposed mechanism for Cu(TCNQ) switching. Ag(TCNQ) is thought to a similar mechanism.

One of the issues with the switching behavior of the originally prepared Cu(TCNQ) material is polymorphism which exerts a profound effect on the reproducibility of the devices. The Cu/Cu(TCNQ) film/Al sandwich devices have been found to exhibit a sharp switching response under an applied voltage, but the resistivity behavior highly depends on the conditions of film preparation.[12b,13c,15] The difficulty of separating and characterizing pure crystalline phases of these distinct polymorphs has been a major obstacle to understanding their physical properties. In 1999, our group successfully obtained the first samples of single crystals of Cu(TCNQ), albeit very small, and found that there are two distinct polymorphs with completely different resistivity behavior.[24] The highly conducting polymorph (Phase I) adopts a perpendicular arrangement of adjacent TCNQ columns and is responsible for the switching behavior in the device, whereas Phase II is nearly insulating at room temperature.

Another main subject of scrutiny vis-à-vis its switching behavior is the related material Ag(TCNQ) whose structure was first reported by Shields.[28] The material is also suspected to be polymorphic based on infrared spectroscopy and slight differences in the powder XRD patterns but this has never been verified by single crystal X-ray data.[29] Clearly, structural characterization of these molecule-based materials is critical for a deep

understanding of the physical behavior but it is notoriously difficult to obtain single crystals.

In contrast to the numerous studies conducted over the years on the TCNQ-based materials, corresponding derivatives of TCNQ are essentially unknown in terms of their solid-state properties. Many substituted derivatives of TCNQ are known,[84] with tunable electronic and steric properties, but their tedious preparation, low yields, thermal decomposition and air or solvent sensitivity has hampered extensive research on the use of TCNQ derivatives. In recent years, our group has focused on 2,5-dihalogen substituted TCNQ derivatives, namely $TCNQX_2$ (X=Cl, Br). By incorporating the radical form of these ligands into network solids with the Cu(I) cation, two unprecedented semi-conducting materials, $Cu(TCNQCl_2)$ and $Cu(TCNQBr_2)$ were prepared in 2010[32] which exhibited enhanced conductivity. As compared to the original Cu(TCNQ) material, the room temperature conductivities are 1.15 and 0.27 $S \cdot cm^{-1}$, respectively, with the former value being the highest among the family of 1:1 M^+: $TCNQ^{\bullet -}$ salts. In this chapter, I report two crystalline materials $Ag(TCNQCl_2)$, (**1**), and $Ag(TCNQBr_2)$, (**2**) synthesized by electrocrystallization using a silver electrode in contact with an acetonitrile solution of $TCNQX_2$. Compound **1** exhibits a room temperature conductivity of 0.25 $S \cdot cm^{-1}$ and a current-induced switching behavior at room temperature whereas compound **2** is nearly insulating.

Experimental Section

Syntheses. $TCNQCl_2$ and $TCNQBr_2$: The preparative methods involve a procedure similar to that of $TCNQCF_3$ which was described in a preliminary report.[85] The starting

materials, 1,4-dichloro-2,5-diiodobenzene and 1,4-dibromo-2,5-diiodobenzene were obtained from the iodination of benzene.

$Ag(TCNQCl_2)$: An electrocrystallization cell with two compartments separated by a medium porosity frit was outfitted with a Ag anode and a Pt cathode electrode. The anode side was filled with 5 mL of MeCN and 2.5 mL of MeOH, and the cathode side was filled with 7.5 mL of MeCN with 54 mg (0.2 mmol) of a suspension of $TCNQCl_2$. The applied current was gradually adjusted from 2.5 μA to 3.0 μA to obtain samples with the best crystallinity. After 2 days, a dark greenish crystalline film was observed on both electrodes.

$Ag(TCNQBr_2)$: The cell set-up is the same as the aforementioned case. The anode side was filled with 5 mL of MeCN and 2.5 mL of MeOH and the cathode side was filled with 7.5 mL of MeCN and 72 mg (0.2mmol) of a suspension of $TCNQBr_2$. The applied current was gradually adjusted from 1.5 μA to 2.3 μA which led to the formation of the highest quality crystals. After 2 days, a dark purple crystalline film was present on both electrodes.

Thin film preparation of $Ag(TCNQX_2)(X=Cl, Br)$. A section of 1 cm^2 Ag foil was pre-cleaned with 1M HNO_3 for 30 minutes, rinsed with water followed by ethanol, and finally dried in *vacuo*. The clean foil was immersed in 20 mL of MeCN containing 0.05 mmol of $TCNQX_2$ which led to instantaneous formation of a dark purple film. The foil was fully immersed for a total of 30 minutes after which time it was removed from the solution, rinsed with acetonitrile and dried in *vacuo.*

Single crystal data collection and Refinement. Single crystal diffraction data were collected at the ChemMatCars beamline at the Advanced Photon Source (APS), Argonne

National Lab at 110K. The data collection strategy consisted of obtaining two ω-scans with one full-sphere and one half-sphere for a total 1080 frames with a 0.5º width. Integration was performed with the Bruker-APEXII software package, and the absorption correction (SADABS) was based on fitting a function to the empirical transmission surface as sampled by multiple equivalent measurements. A large correction was adopted considering the presence of the heavy atoms Br and Ag. Solution and refinement of the crystal structure was performed with the SHELX programs[86] and the graphical interface X-SEED. All non-hydrogen atoms were assigned in the difference Fourier maps after several rounds of least square refinements. The hydrogen atoms were placed in calculated positions.

Conductivity measurements. Temperature dependent conductivity measurements were performed by attaching two gold wires (15 μm diameter) to each side of a piece of rectangular shaped crystalline film obtained from electrocrystallization. The film was found to be composed of 4-5 domains of single crystals by X-ray diffraction and is a better candidate for measuring the intrinsic properties than pressed pellets. A Quantum Design model MPMS SQUID magnetometer with an attachment of a voltmeter and current source was used to collect the voltage changes with temperature. A square-wave current of 1.0 μA was applied for the measurement to avoid the non-linear current response and thermal resistance from the contact between gold wire and film.

EPR measurements. The data were obtained on an JEOL JES-FA200 X-band EPR instrument**.** A pressed powder pellet of 1 was used to avoid the potential of complications caused by twinned crystals. The pellet was placed parallel to the direction of the magnetic

field and a DC current source was used. A 30 second measurement interval was used to avoid heating effects with the application of current.

Structure Analysis

The structure of 1 (Figure 4.1) is a three-dimensional network with Ag(I) ions coordinated to four adjacent $TCNQCl_2^{\bullet-}$ radicals in a highly distorted tetrahedral environment with N-Ag-N angles of 97.75º, 103.77º, 126.53º and 131.04º. The columns of stacked $TCNQCl_2^{\bullet-}$ radicals are oriented along the *b* axis with a homogenous separation of 3.23 Å which is similar to the distance of 3.24 Å found in the Cu(TCNQ) phase; adjacent columns exhibit a dihedral angle of 135.3º.

The structure of compound **2** (Figure 4.2) is also that of a 3D network and is best described as a stack of slightly distorted 2-D layers in which Ag(I) cations are coordinated in an unprecedented arrangement to six $TCNQBr_2^{\bullet-}$ radicals with four in-plane Ag-N bonds of 2.197, 2.226,2.572 and 3.082Å, and two inter-layer Ag-N bonds of 2.616 and 2.675 Å. The adjacent columns of $TCNQBr_2^{\bullet-}$ radicals, which are oriented in a parallel manner, do not perfectly overlap along the *a* axis. The alternating separation distance of TCNQ radicals along the column (3.23 and 3.03 Å) indicates a high degree of dimerization of radicals in the stacks. In both **1** and **2**, the separation distances between adjacent TCNQ molecules are much shorter than the sum of van der Waals radii of the halogen atoms (3.60 Å for Cl-Cl and 3.80 Å for Br-Br), which further supports the fact that there are strong interactions between the neighboring radicals in the stacks. Crystallographic data for **1** and **2** are listed in Table 4.1.

Infrared Spectral Analysis

Infrared spectral data are very useful for diagnosing the charge and coordination strength of the TCNQ radicals. For both **1** and **2**, two strong $\nu_{C\equiv N}$ modes are observed (2189cm^{-1} and 2165cm^{-1} for **1**, 2187cm^{-1} and 2160cm^{-1} for **2**) which are indicative of coordinated TCNQ radicals. For comparison sake, the neutral compounds exhibit $\nu_{C\equiv N}$ stretches as 2224 cm^{-1} for $TCNQCl_2$ and 2218 cm^{-1} for $TCNQBr_2$. The out-of-plane bending mode, $\delta_{C\text{-}H}$, for TCNQ is also quite sensitive to the oxidation state of the TCNQ ring; the values for **1** and **2** are 830 cm^{-1} and 866 cm^{-1} respectively as compared to neutral $TCNQCl_2$ and $TCNQBr_2$ (848 cm^{-1} and 874 cm^{-1}) which reflect the reduced state of the molecules.

Preparation of Thin Films

Thin films of **1** and **2** were prepared from spontaneous corrosive electrolysis by immersing a section of pre-cleaned silver foil into acetonitrile solutions of $TCNQCl_2$ and $TCNQBr_2$ for 30 minutes at room temperature. A comparison of the experimental powder X-ray diffraction pattern with simulations obtained from the single crystal structures confirms the presence of **1** and **2** in the films (Figure 4.3). The SEM photos (Figure 4.4), reveal micrometer-sized rod-shaped crystals that grow epitaxially along the propagating axis of TCNQ stacks much like the growth of nanoribbons and nanowires reported for Cu(TCNQ) phase I and Ag(TCNQ) [83] which bodes well for preparing similar nanodevices of **1** and **2** by the same strategies.

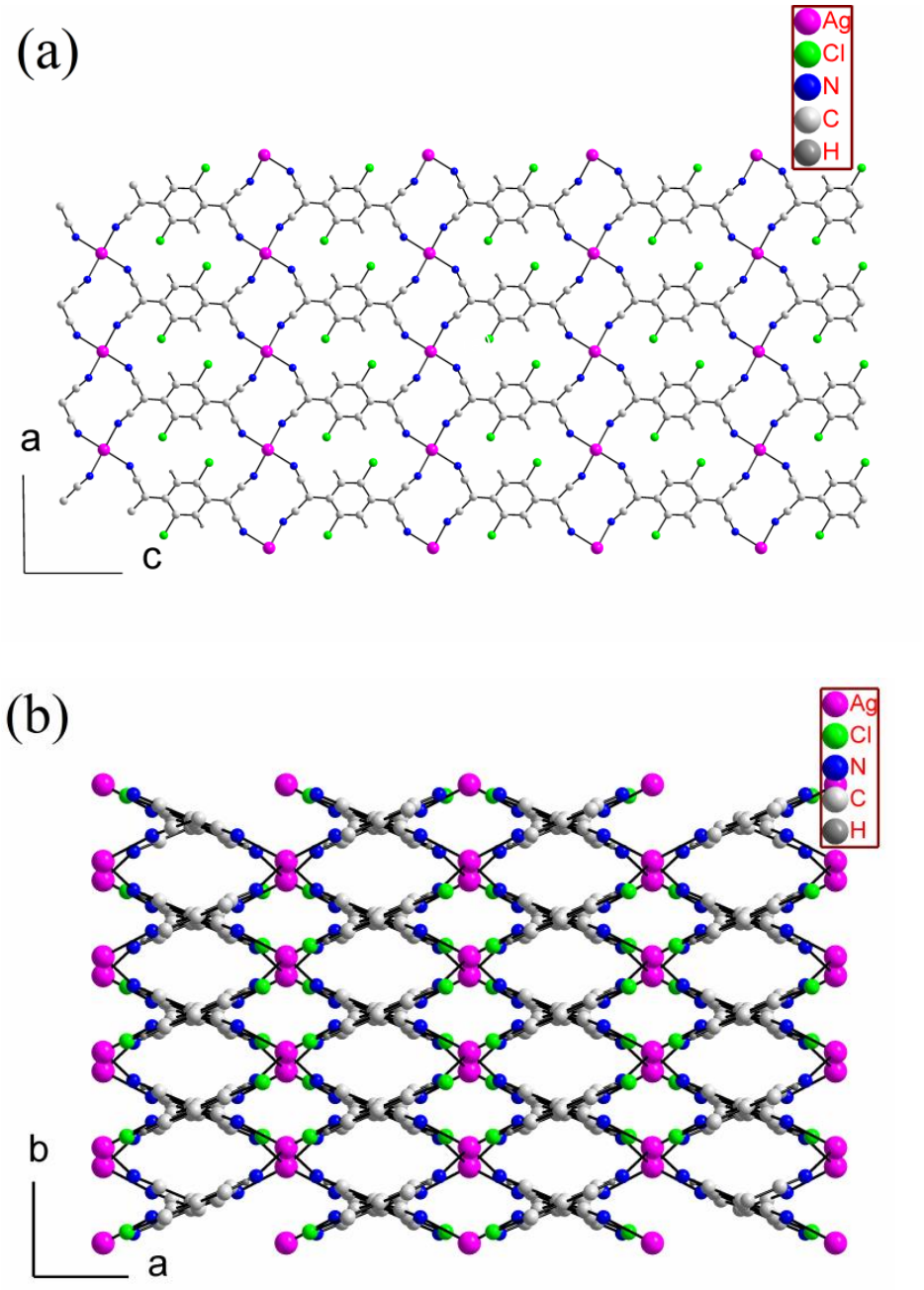

Figure 4.1. The structure of $Ag(TCNQCl_2)$, (1) (a) viewed in the *ac* plane and (b) in the *ab* plane.

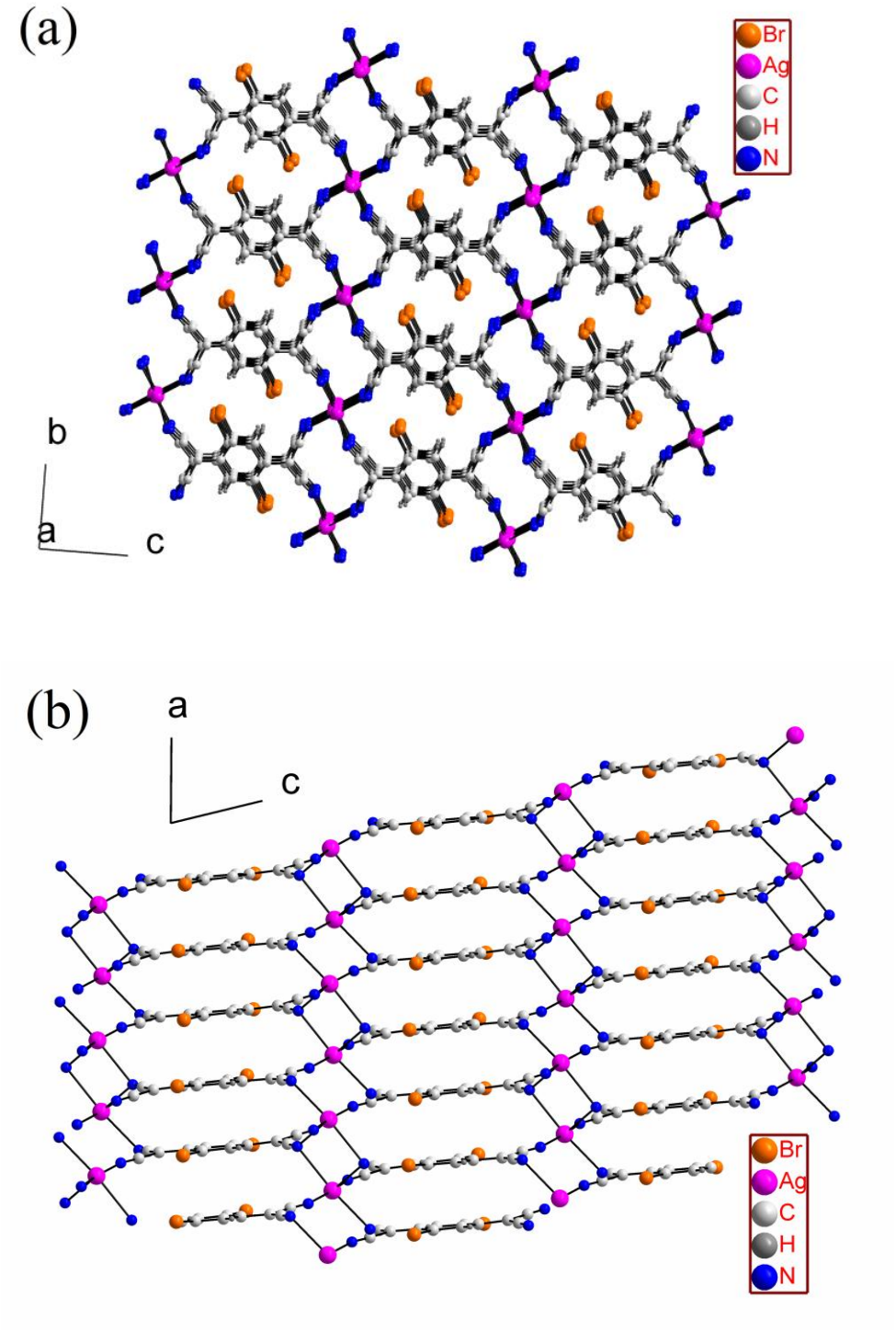

Figure 4.2. The structure of Ag(TCNQBr$_2$), (2) (a) viewed in the *bc* plane and (b) the *ac* plane.

Table 4.1 Crystallographic data for $Ag(TCNQCl_2)$ (1) and $Ag(TCNQBr_2)$ (2). The CIF files are available from the CCDC database, under the numbers 924677 and 924678.

Compound	1	2
Formula	$C_{12}H_2N_4Cl_2Ag$	$C_{12}H_2N_4Br_2Ag$
F_w [g mol^{-1}]	380.95	469.87
Crystal size [mm^3]	0.02 x 0.008 x 0.005	0.04x 0.02 x 0.01
Crystal system	Monoclinic	Triclinic
Space group	P2/c	P-1
a [Å]	6.7867(14)	7.2540(15)
b [Å]	3.5336(7)	7.7900(16)
c [Å]	22.719(4)	11.640(2)
α [°]	90	84.02(3)
β [°]	90.69(3)	74.69(3)
γ [°]	90	65.01(3)
V [$Å^3$]	544.80(18)	575.0(2)
Z	2	2
ρ_{calc} [g cm^{-3}]	2.322	2.714
μ (Synchrotron) [mm^{-1}]	0.413	0.413
Reflections collected	8855	5294
Unique reflections	811	5294
Reflections with I >2σ(I)	980	3467
Parameters	47	173
R(int)	0.0497	0.0358(based on data of the twinning domain that is used for structure resolving)
$R1$[a]	0.0392	0.0643
$wR2$[b]	0.0906	0.1502
GOF	1.396	1.024

[a] $R1 = \Sigma||F_o| - |F_c||\Sigma|F_o|$. [b] $wR2 = [\Sigma[w(F_o^2 - F_c^2)^2]/\Sigma[w(F_o^2)^2]]^{1/2}$.

Linear Conductivity Measurement

Temperature-dependent conductivity measurements were performed on rectangular-shaped crystalline film samples of **1** and **2** obtained by electrocrystallization. Two-probe methods were used due to the small size of the crystallites. The conductivity data revealed that **1** exhibits good semiconducting behavior with a room temperature conductivity of 0.25 S/cm (Figure 4.5) and an activation energy of 0.065 eV. In sharp contrast, compound **2** exhibits no recordable voltage signal with an applied current as low as 5 nA (the responding voltage is much higher than the limit of voltmeter), which is indicative of an insulator with a roomtemperature conductivity less than 1×10^{-7} S/cm. These observations are consistent with the fact that there are regularly stacked TCNQ radicals in **1** but alternating short and long distances in **2**. The conductivity of **1** is essentially the same as that found for Cu(TCNQ) and is $\sim10^{3}$ times higher than the originally reported Ag(TCNQ) material ($3.6\times10^{-4}S\cdot cm^{-1}$).[28] The strong antiferromagnetic interactions between the dimerized radicals in compound **2** is expected to greatly decrease the electron mobility along the stack, resulting in an insulating behavior.

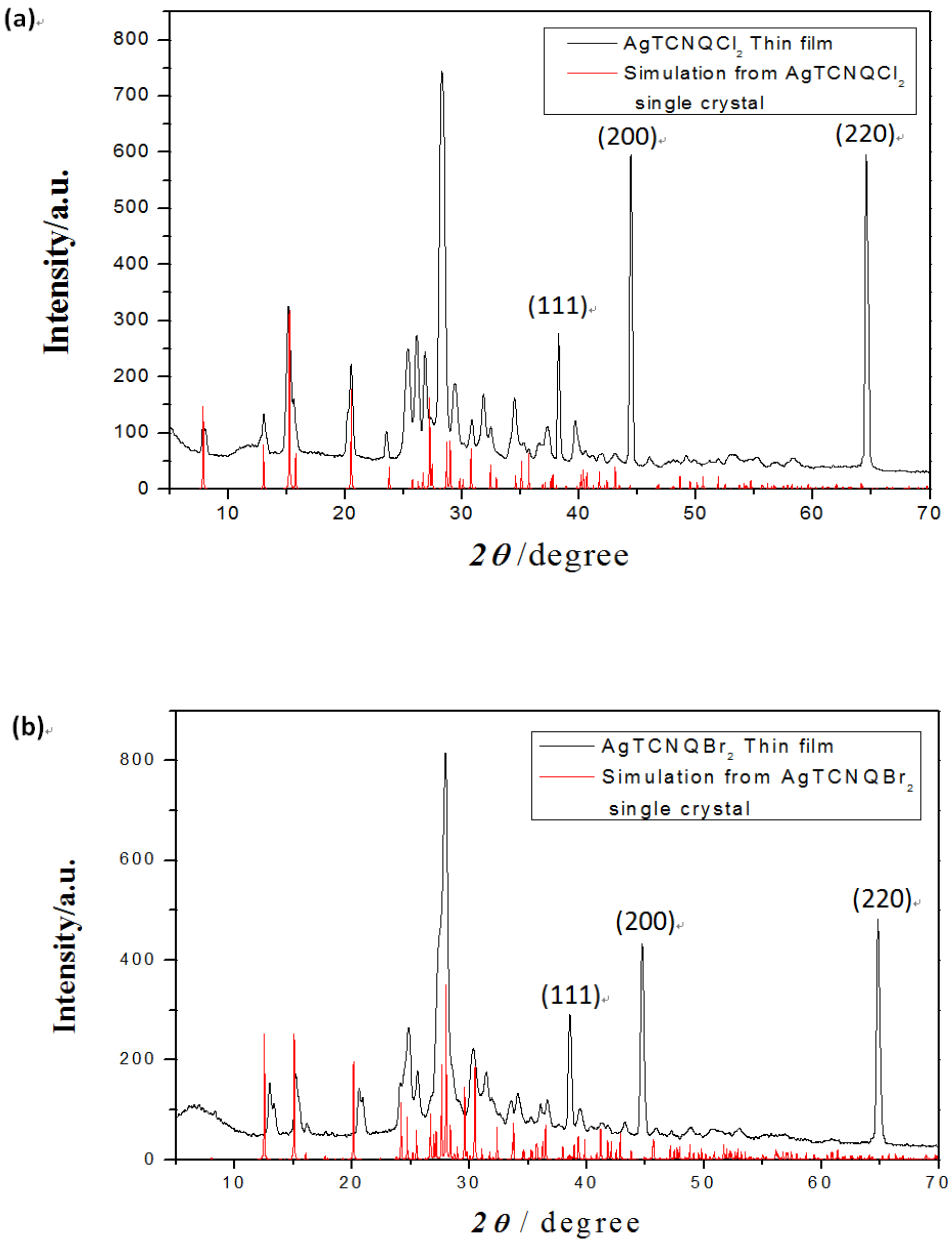

Figure 4.3. A comparison of the powder diffraction pattern for a thin film and single crystal simulation of (a) $AgTCNQCl_2$ (1) and (b) $AgTCNQBr_2$ (2). The diffraction peaks of silver are marked in both figures.

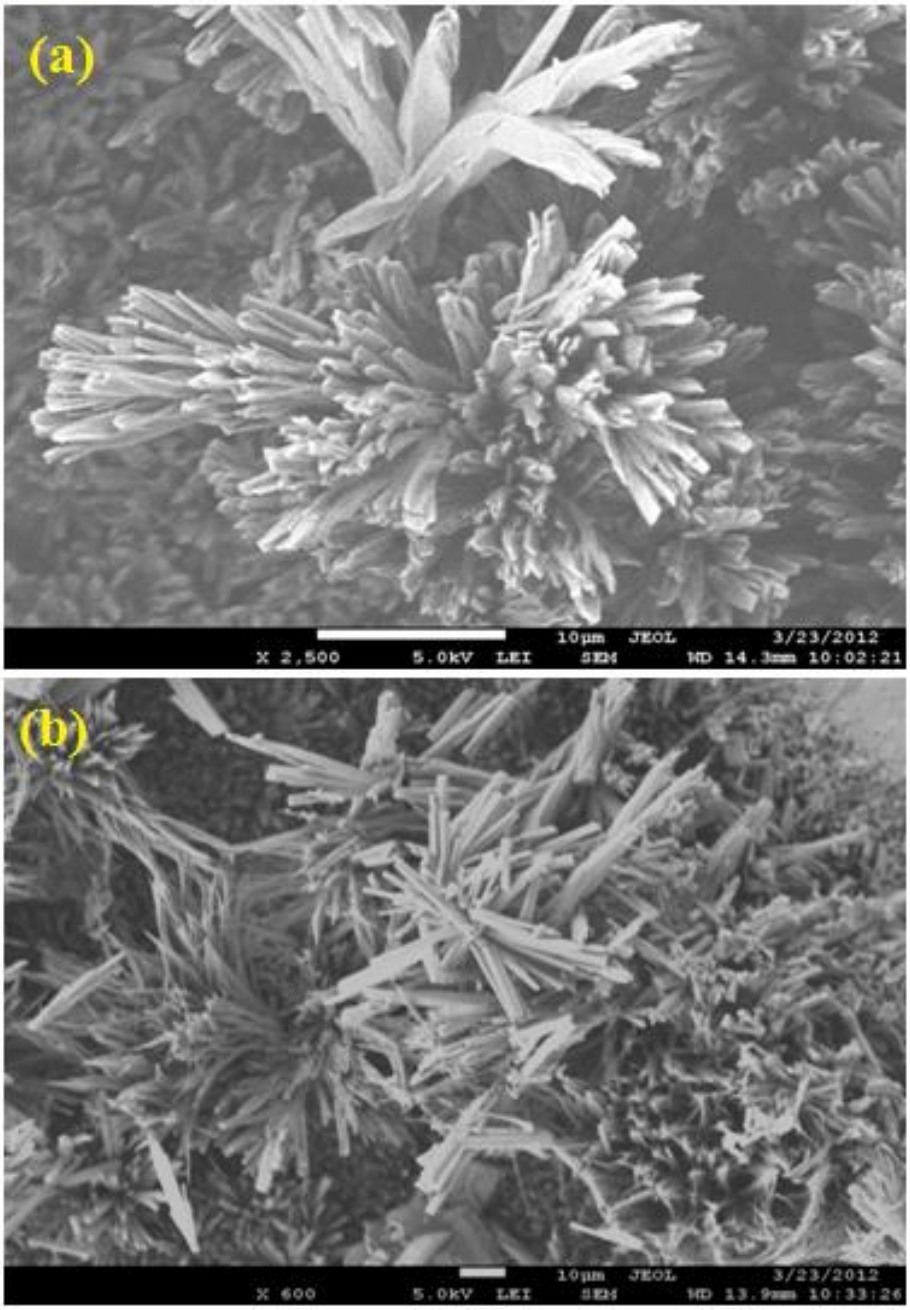

Figure 4.4. SEM images for thin film of $AgTCNQCl_2$ (1) (a) and $AgTCNQBr_2$ (2) (b).

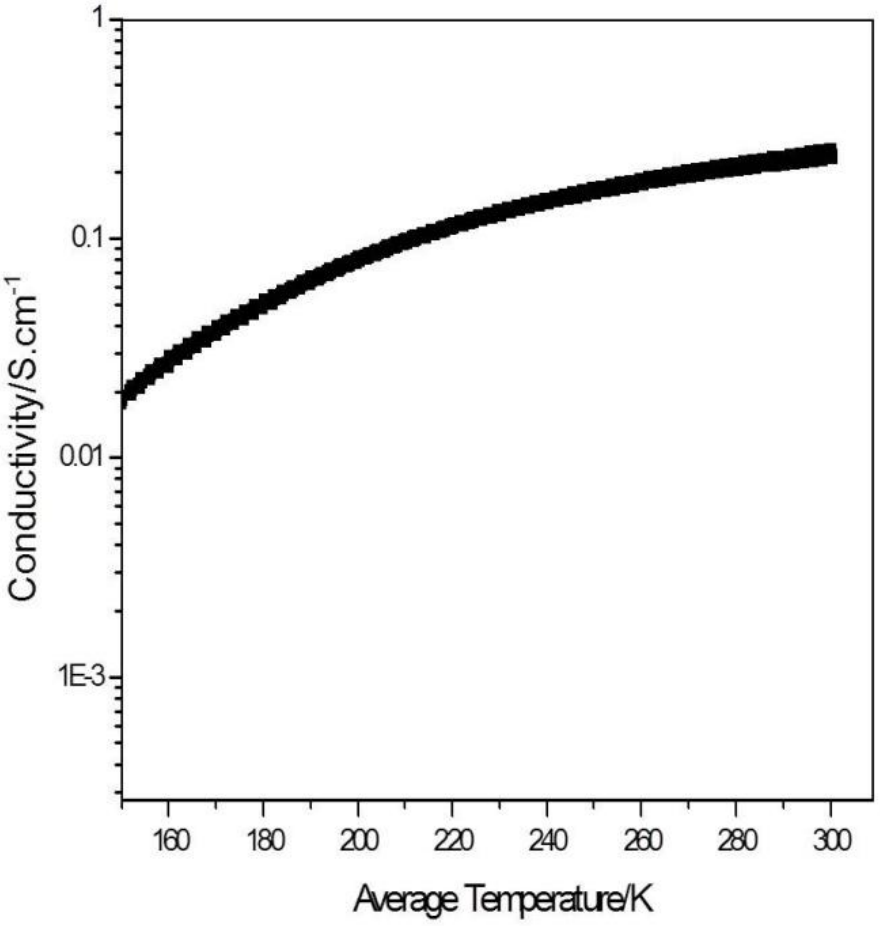

Figure 4.5. Temperature dependent conductivity data for $AgTCNQCl_2$ (1).

Non-linear Conductivity Measurements

Evidence for switching behavior was obtained by recording the non-linear I-V behavior of crystalline films that were used for the typical conductivity measurements at room temperature. The strategy is to vary applied current in order to avoid the risk of melting or decomposing the sample during the measurement. Given that **2** is insulating, only data of compound **1** were recorded. A negative differential resistance was observed at about 50 V with a current sweep of opposite directions (0 → 300 μA → -300 μA → 0 for 2 times, Figure 4.6a). A hysteresis loop was observed between 20-50 V. These results are in accord with a conducting state transition from a low resistance state to high resistance state which is clear evidence of switching behavior. The symmetrical shape of the I-V curve in the sweeping cycle indicates the full reversibility of this state transition. By plotting the resistance change with time, one can see that **1** exhibits as an intrinsic oscillation of resistance, which suggests the potential for being an intrinsic thyristor (Figure 4.6b). The current sweep in one direction was performed for two cycles (0 to 1000 μA to 0, Figure 4.7a) and it was found that the state transition appears at much lower voltages during the second cycle, specifically at 35 V as compared to 44 V for the first one. The resistance versus time plot (Figure 4.7b) indicates a clear state transition between the on and off states. The shape of the curve appears to be reaching a plateau at the on state, which indicates the saturation of the state transition. The continuous feature of the curve indicates that the resistance of the 2nd cycle starts at approximately one half of the 1st cycle, which could potentially arise from the uncompensated state transition under the high applied voltage without the erasing of the current from the opposite direction.

An I-V measurement with a sweep of voltage was also performed. (Figure 4.8) Non-linear behavior for **1** was observed in the voltage sweep experiment but it is more challenging to control the current and protect the sample with the voltage sweep method. As a result, it is difficult to observe hysteresis behavior. The sample exhibits a sharp increase in conductivity with an applied voltage of ~60 V, but then decomposes. The distinctive orange-yellow color of neutral $TCNQCl_2$ was observed by inspecting the sample under a microscope. (Figure 4.9).

Investigation of Mechanism of Switching: EPR Study with A Load of Current

In an effort to probe the mechanism of the observed switching behavior, a current-dependent electron paramagnetic resonance (EPR) spectrum of **1** was recorded (Figure 4.10a.) A g-factor shift was observed with amplification of the applied current. Interestingly, the degree of g-factor shifting is proportional to the logarithm value of the current. (Figure 4.10b) This special behavior can be understood by adopting an p-n diode model between the stack of Ag(I) cations and $TCNQCl_2^-$ radicals. The column of TCNQ radicals can be treated as a stack of all singly occupied radicals which is known as an intrinsic Mott-insulator type semiconductor. In this case the Ag 5s orbital is empty. The potential gap between the stack of TCNQ radicals and Ag(I) cations is attributed to the difference in their electrochemical potential, which is positive, given that the reaction between Ag(0) and $TCNQCl_2$ is spontaneous. In this case, the electrons will reside in the stack of TCNQ radicals. Under an applied current, the partial charge transfer occurs, which converts the TCNQ radical stack into a p-type semiconducting stack, and the string of Ag(I) cations into a n-type of stack. Therefore the system can be viewed as a sum of micro p-n diodes.(Figure 4.11) From the law of diodes, we have:

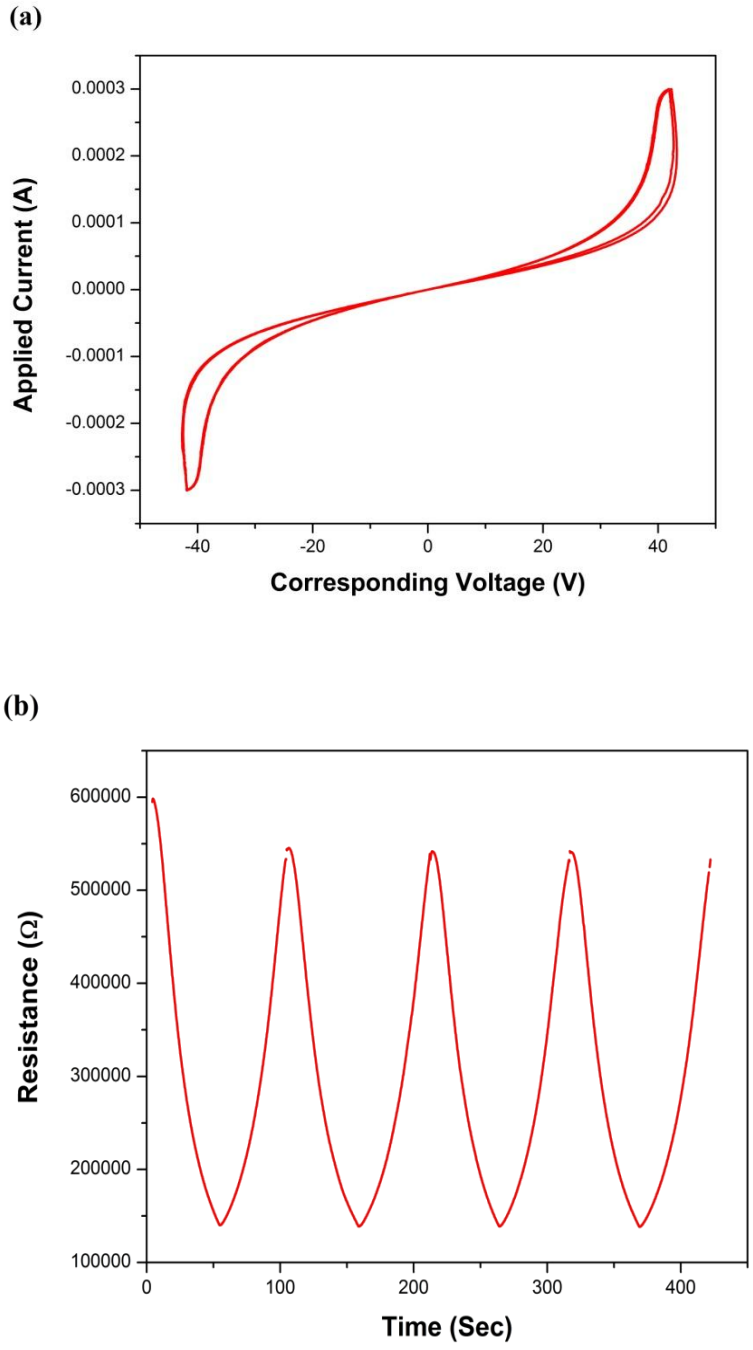

Figure 4.6. Two-direction sweeping non-linear conductivity measurements on $Ag(TCNQCl_2)$ (1): (a) I-V plot (b) resistance vs sweeping time plot.

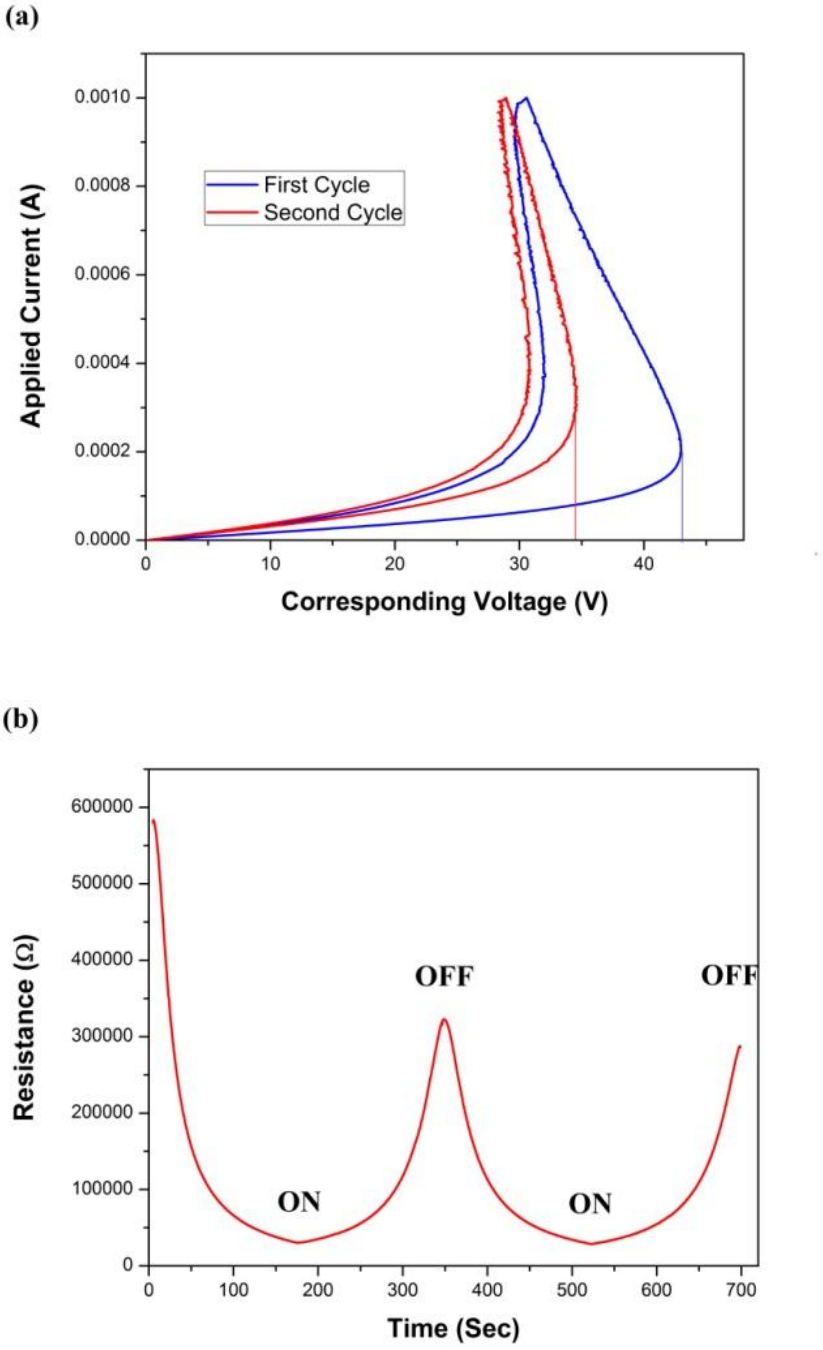

Figure 4.7. One-direction sweeping non-linear conductivity measurement on $Ag(TCNQCl_2)$ (1): (a) I-V curve and (b) resistance vs sweep time plot. The lines in (a) are placed at the transition voltages (~44 V for the first cycle and ~35 V for the second cycle).

(a)

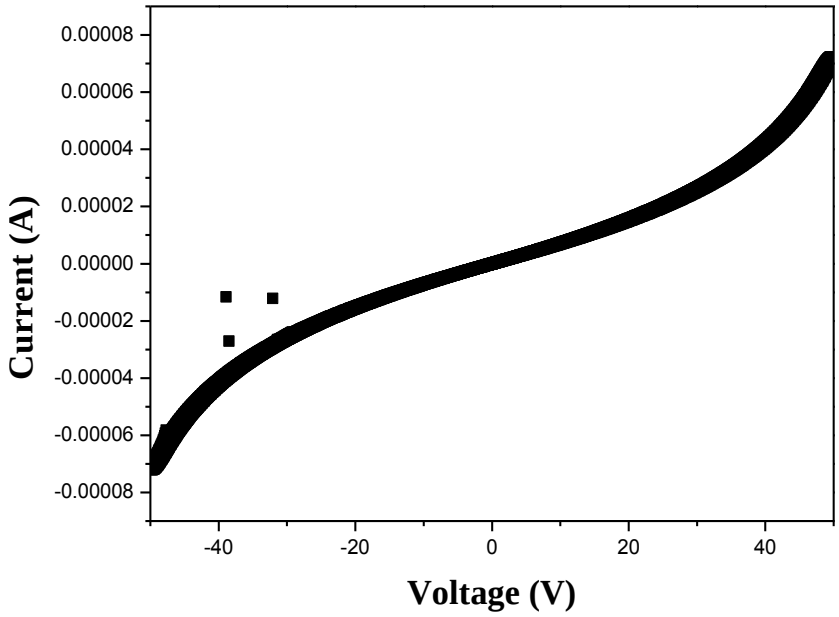

(b)

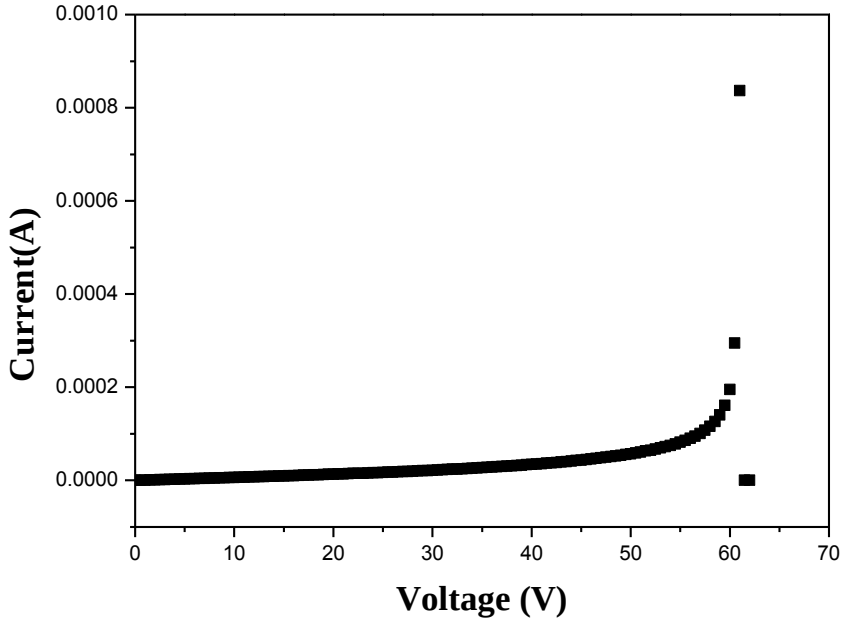

Figure 4.8. Voltage sweep I-V curve for $Ag(TCNQCl_2)$ (1): (a) -50V to 50V, five segments and (b) 0 to 70V, one segment.

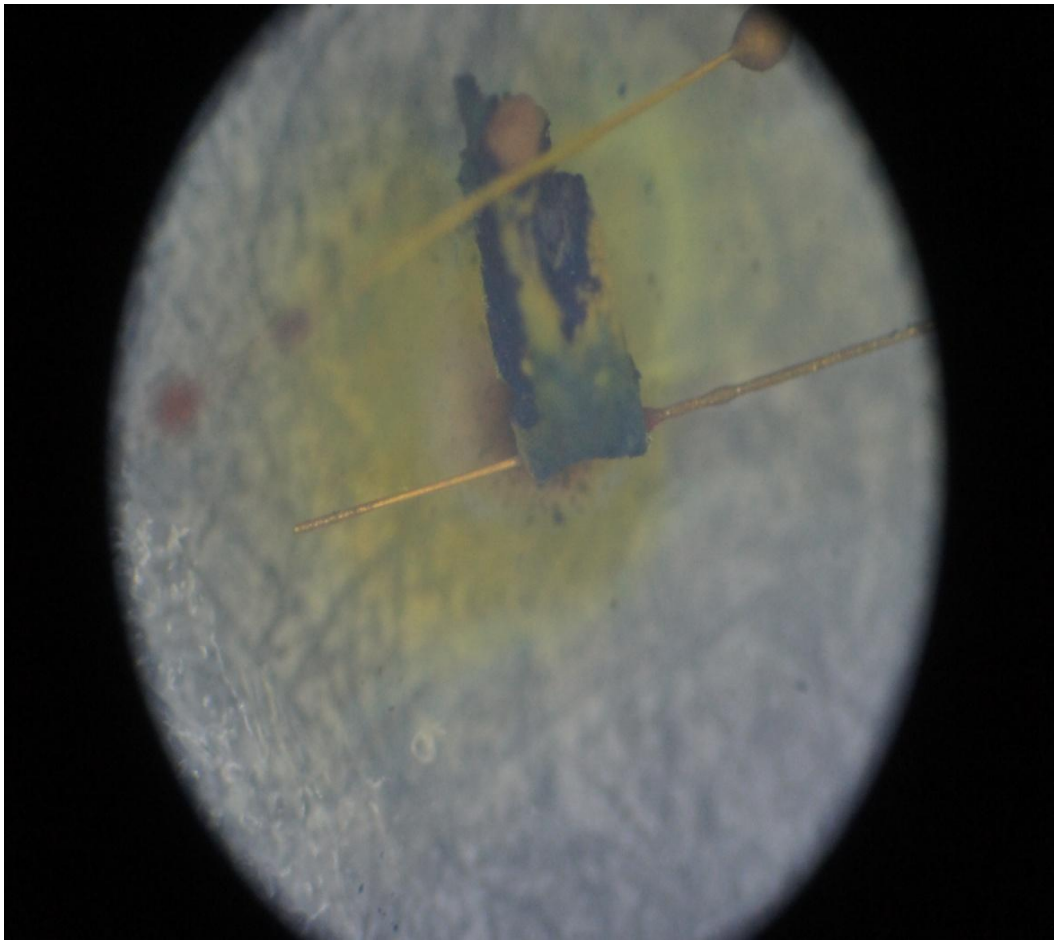

Figure 4.9. The decomposition of $Ag(TCNQCl_2)$. Yellow areas are neutral $TCNQCl_2$ whereas the dark regions indicate the presence of the radical form.

$$I = I_s(\exp(\Delta V/V_T) - 1)$$ **Equation 4.2**

In which I is the applied current, I_s refers to the reverse saturation current, ΔV is the voltage across the diode, and $V_T=k_BT/q$, is the thermal voltage which is a constant at a given temperature.

From the formula, we can see that the logarithm of current is proportional to ΔV, which is the voltage gap between the TCNQ stack and the Ag(I) stack. Furthermore, ΔV is proportional to the concentration of existing Ag(0) atoms and neutral $TCNQCl_2$ molecules in the stack (in other words the degree of charge transfer).

From the experimental data, the logarithm value of current is proportional to the shift of the g-factor. The g-factor of the reference compound $Li(TCNQCl_2)$ is 1.99669, which is smaller than the zero-current g-factor for $Ag(TCNQCl_2)$ (2.00478), from which it can be concluded that the hybridization between the Ag 5s orbital and HOMO of $TCNQCl_2$ will lead to a larger $g_\perp$ value. The increase in the $g_\perp$ value is expected to be proportional to the degree of hybridization. Since the hybridization interaction must communicate through the CN-Ag coordination bond, the ligand metal charge transfer (LMCT) induced by current will lead to elongation and dissociation of CN-Ag bonds, thereby generating Ag(0) in the structure and decreasing the hybridization degree. (Figure 4.12) This suggests that the charge transfer degree is also proportional to the $g_\perp$ value shift. The relationship can be discribed as below:

$$g = g_a\chi_a/(\chi_a+\chi_b) + g_b\chi_b/(\chi_a+\chi_b)$$ **Equation 4.3**

Here g_a is the g-tensor for a coordinated TCNQ radical, and g_b is the g-tensor for a free TCNQ molecule. Although the free TCNQ molecules should possess a close shell

frontier orbital, it will still share the spin density with other TCNQ radicals as the electrons are highly delocalized as charge carriers in the stack of TCNQ. The χ_a, χ_b values are the susceptibility of coordinated and ”free” TCNQ and are proportional to their concentration in the structure. As a result, g-tensor shift is proportional to the charge transfer degree.Given the fact that the logarithmic value of current is proportional to the shift of g-factor, it is suggested that the logarithm value of current is proportional to the charge transfer degree, which corresponds to the model mentioned above.

Conclusions

To summarize the findings, the tool of electrocrystallization was used to prepare materials containing the radical form of $TCNQCl_2$ and $TCNQBr_2$ co-assembled with Ag(I) cations. The new compounds are the semiconducting crystalline material $Ag(TCNQCl_2)$ and the insulator $Ag(TCNQBr_2)$. The presence of the chlorine substituents on the 2,5 positions of TCNQ leads to a highly enhanced room temperature conductivity for $Ag(TCNQCl_2)$ which is three orders of magnitude greater than the original Ag(TCNQ) material. Nevertheless, intrinsic switching behavior with a memory effect is observed at room temperature. Importantly, variable current EPR data have provided, for the first time, direct, real time evidence for the mechanism of switching behavior as being due to hybridization of Ag 5s orbitals into the conduction band. The ease of manipulation and fabrication of this material opens up the opportunity for the development of new generations of $Ag(TCNQCl_2)$ nanodevices with useful potential applications for fast processing memory devices.

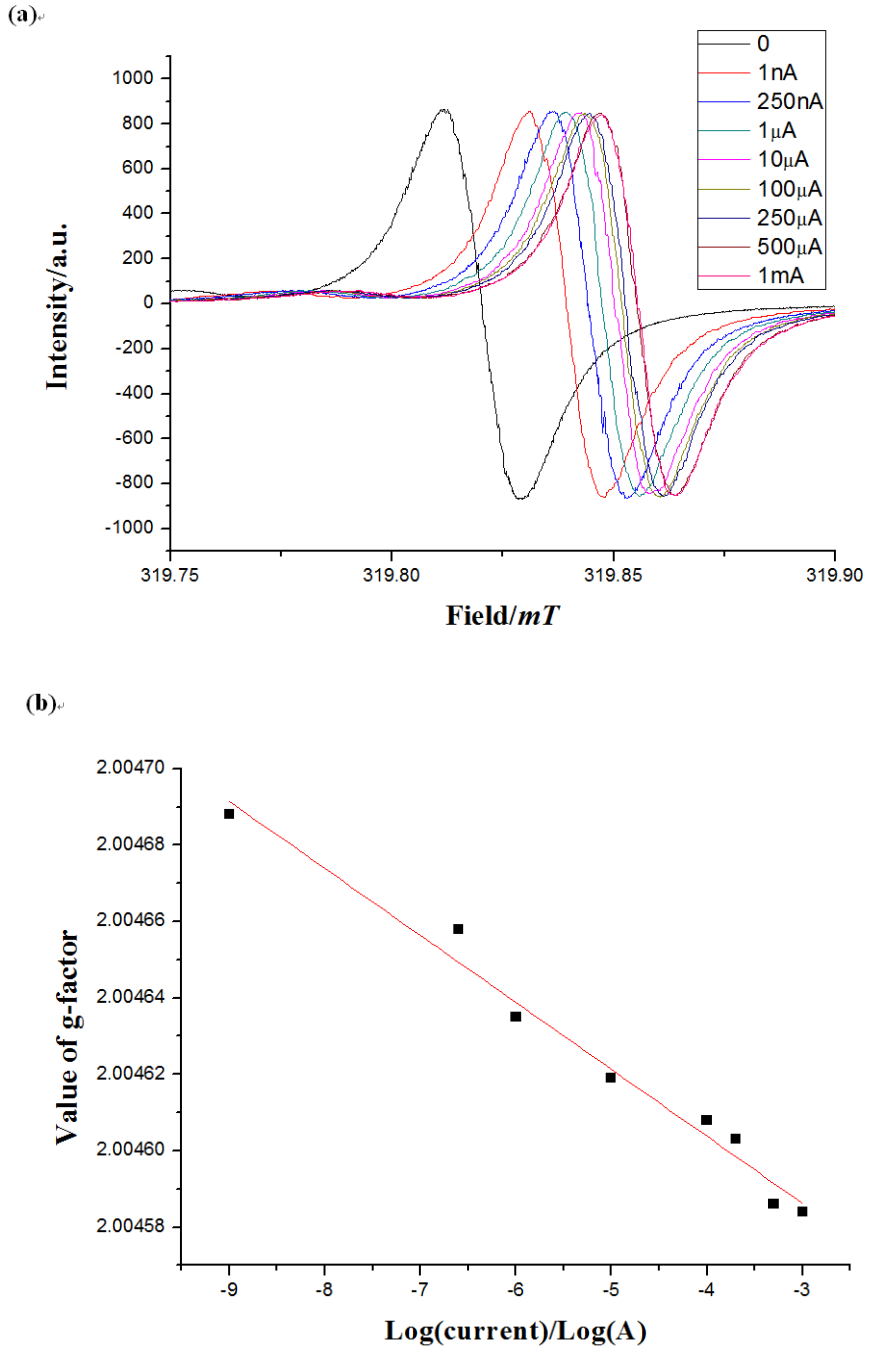

Figure 4.10. EPR spectrum of $Ag(TCNQCl_2)$ (a) under different current loading and (b) the linear fit of the g-factor values and the logarithm of the applied current. (R = 0.9770)

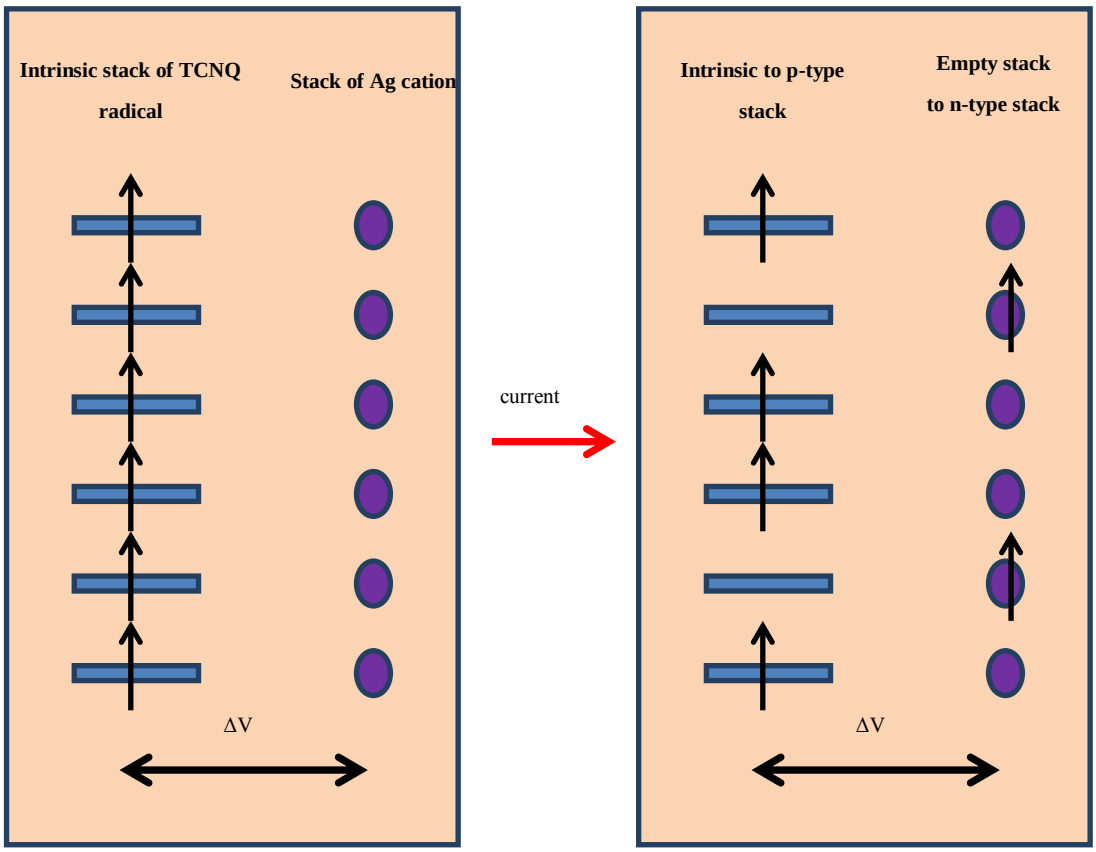

Figure 4.11. A micro p-n diode model of current induced charge transfer in $Ag(TCNQCl_2)$.

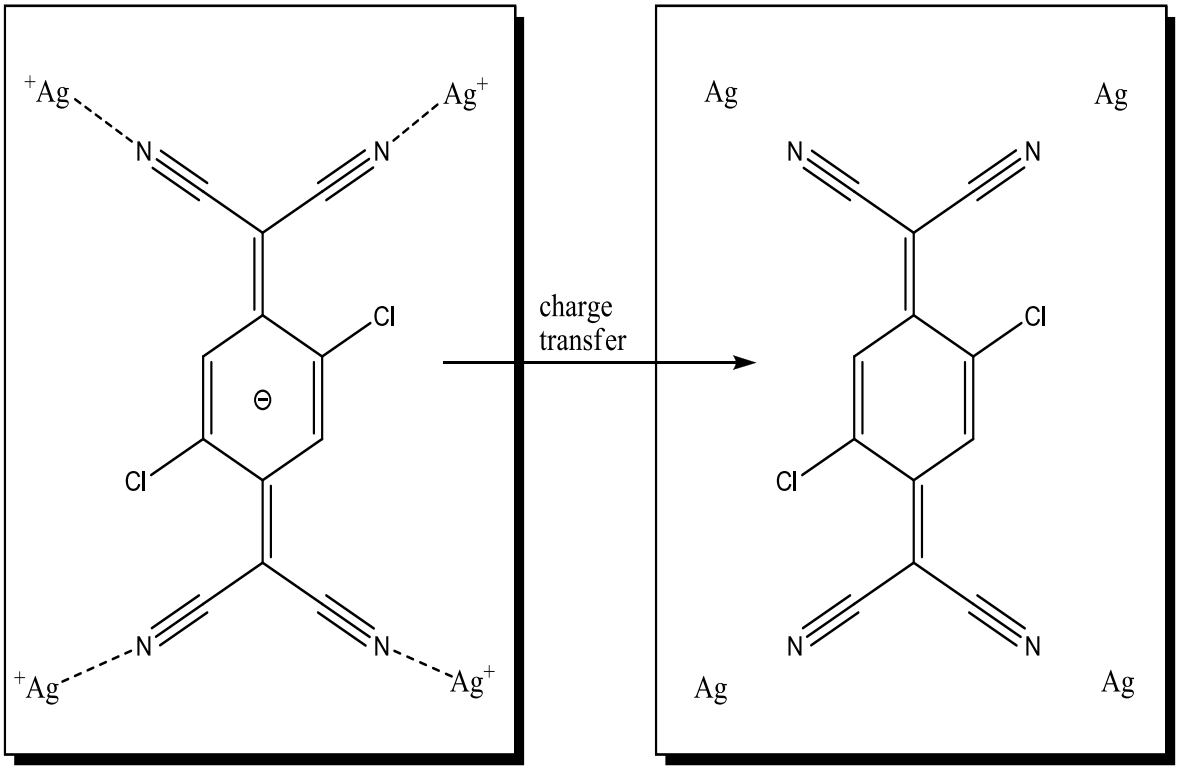

5s orbitals of Ag^+ are hybridized with HOMO through C-N---Ag bond, g-factor will be increased.

After charge transfer, the bonds are broken and a non-hybridized HOMO orbital is produced in the $TCNQCl_2$ band, average g-factor will decrease.

Figure 4.12. The hybridization-decomposition model of g-value shifting.

CHAPTER V

TUNING THE CONDUCITIVY OF METAL-TCNQ FRAMEWORKS WITH SOLVENT MOLECULES

Background

Advances in modern computer technology require improved electronic and memory devices with smaller domain sizes, faster operation speeds and control of property by the external stimuli.[2,52] Among the promising approaches is the study of molecular conductors including those that exhibit conductivity properties comparable to a metal. The first metallic conductor based solely on organic molecules is the charge transfer material TTF-TCNQ (TTF = tetrathiafulvalene, TCNQ = 7,7,8,8-tetracyanoquinodimethane), discovered in 1973. The structure of TTF-TCNQ consists of segregated stacks of TTF and TCNQ molecules; the partial degree of charge between this Donor-Acceptor pair (D-A) is 0.59 which leads to a hole-doping state in the conducting pathway. [9,10] This work inspired a great deal of research into materials based on TCNQ which continues to this day.

The TCNQ molecule is an excellent electron acceptor and can be singly reduced to form the radical anion, $TCNQ^{-}$, which coordinates to cations to form metal-TCNQ coordination compounds, the structures of which typically contain columnar stacks of TCNQ radicals. The application of an external electric field promotes transfer of electrons from one radical to another and transport along the stack occurs which results in conducting behavior of these compounds. [20,21]

Understanding structure-property relationships in the chemistry of TCNQ-based conductors is critical for improving the performance of these materials. An excellent illustration of this statement is the material Cu(TCNQ) [23a,23b] whose thin film properties have fascinated researchers for over three decades, interest that has been fueled further by the discovery by the our group that there are two distinct polymorphs of Cu(TCNQ).[24] The first phase (Phase I) exhibits a room-temperature conductivity of 0.25 S/cm and is responsible for the switching properties. The second phase, however, formed by soaking Phase I in acetonitrile, is essentially an insulator at room temperature. The problems with reproducibility was found to arise from the different proportions of the two polymorphs present in a given Cu(TCNQ) thin film because of the preparative conditions.

In recent years, we have demonstrated that substitution of TCNQ with various derivatives of TCNQ lead to profound changes in the structure of framework as well as the conducting behavior. Specifically, for TCNQ radicals with dihalogen-derivatives, an enhancement of the conductivity was found with $Cu(TCNQCl_2)$ which has a room temperature conductivity of 1.15 S/cm-a record for 1:1 metal-TCNQ binary compounds.[32] From this perspective, one can expect that an additional steric effect of the substituent groups on the TCNQ radicals will modulate the packing mode of the TCNQ stacks and potentially generate cavities or channels in the structure and/or free coordination sites and allow for solvent molecules to coordinated to the metal cations. In this chapter, the effect of solvent molecules on the structures and conductivity of the metal-TCNQ frameworks is probed. The investigation is based on two compounds that were prepared by Dr. Nazario Lopez, namely $Cu(TCNQBr_2)(MeCN)$ (**1**), $Cu(TCNQI_2)(MeCN)_2$ (**2**) along with the four new compounds, namely

$Cu_2(TCNQBr_2)(MeCN)_2$, (**3**), $Cu_2(TCNQBr_2)(MeCN)_4$, (**4**), $Cu(TCNQI_2)(MeCN)$, (**5**), and $Ag(TCNQI_2)(MeCN)$, (**6**). The synthesis of **1** and **2** will not be covered but their full characterization and physical properties will be reported since they were not previously carried out or described.

Experimental Section

General Considerations. All reactions and manipulations were conducted under a dry nitrogen atmosphere. Acetonitrile was dried over 3 Å molecular sieves and distilled under an atmosphere of nitrogen prior to use. The TCNQ starting material was purchased from TCI and CuI was purchased from Aldrich. The derivatives $TCNQX_2$ (X= Cl, Br, I) and their Li^+ and $[Bu_4N]^+$ salts were synthesized according to literature methods.[64] The Cu foil and silver electrodes were pre-treated with dilute nitric acid to remove metal oxides on the surface. Thermal Gravimetric Analysis was performed on a SHIMAZU-TGA-60 thermogravimetric analyzer with a heating rate of 5 ºC /min. Elemental analyses were performed by Atlantic Microlab, Inc. on bulk prepared powders. Variable temperature conductivity measurements over the range 150 K - 300 K were obtained on a Quantum Design model MPMS SQUID magnetometer by using gold paste to connect four 50 μm diameter gold wires evenly to a rectangular shaped fine powder pressed pellet. Infrared spectra were recorded as Nujol mulls between KBr plates using a Nicolet IR/42 FT-IR spectrometer.

Syntheses. $Cu_2(TCNQBr_2)(MeCN)_2$ (3): The bulk product of **3** was obtained by the following method: compound **1** (0.015g, 0.03mmol) was placed in a vial and 10 mL of acetonitrile was added. Five pieces of clean Cu foil (~1mm thick and $1cm^2$) were immersed in the solution. The vial was capped and left to stand undisturbed for 2 days

during which time a beige-white crystalline material appeared on the surface of the Cu foil which was carefully scraped free and rinsed with acetonitrile. Yield: 0.007g, 55.2%. Single crystals of **3** was obtained electrocrystallization method: compound **1** (0.015g, 0.03mmol) was placed in the cathode side of an H-shaped, 25 mL electrocrystallization cell separated by a coarse frit glass (pore size: 40-60 μm in diameter). The cell was filled with a mixture of 12 mL of acetonitrile and 4 mL of MeOH. A copper electrode was used as the anode and an inert platinum electrode was used as the cathode. A current of 3.50 μA was applied and the voltage across the cell was ~1.5 V. Pale-yellow needle crystals appeared on the cathode after ~2-3 days.

$Cu_2(TCNQBr_2)(MeCN)_4$ (4): Single crystals of **4** were obtained by taking 10 mg of **1** and suspending it in 10 mL of acetonitrile along with 5 pieces of clean Cu foil pieces (5 cm ×l cm ×1 mm). The vial was capped and the solution was left to stand undisturbed for 8 weeks. Pale-yellow needle crystals slowly formed on the surface of the Cu foil.

$Cu(TCNQI_2)(MeCN)$ (5): Both crystals and microcrystalline powder of **5** were obtained by slow diffusion methods: CuI (0.053g, 0.28mmol) was placed on one side of an H-shaped, 25 mL electrocrystallization cell separated by a coarse glass frit (pore size: 40-60 μm in diameter) and a quantity of $TCNQI_2$ (0.007g, 0.015mmol) was placed on the other side with 10 mL of acetonitrile in each compartment. The cell was placed in the dark for 2-3 days, which leads to the formation of green platelet crystals along with green microcrystals. The material was carefully transferred to a small vial and rinsed with acetonitrile (3x 10 mL) to remove residual $TCNQI_2$ and then dried *in vacuo*. Yield: 0.007g, 82.3%.

$Ag(TCNQI_2)(MeCN)$ (6): A quantity of $TCNQI_2$ (0.091g, 0.2 mmol) was added to the cathode compartment of an electrocrystallization cell as mentioned above for the synthesis of **5** and the cell was filled with 20 mL of dry acetonitrile. A silver electrode was used as the anode and a platinum electrode was used as the cathode. A current of 10 μA was then applied and the voltage was measured as being ~1.2 V. Green, shiny chunks of aggregated microcrystalline particles appeared after 2-3 days on the cathode side that contained the unconsumed $TCNQI_2$ starting material. The materials were transferred into a 20 mL glass vial and rinsed with acetonitrile until no red crystals of $TCNQI_2$ were observed under the microscope. Yield: 0.018g, 15%. Elemental Analysis: Calcd%: C: 27.80, H: 0.83, I: 41.96, N: 11.58; Anal%: C: 27.09, H: 0.80, N: 11:14. Note: the acetonitrile turns light yellow even after the removal of $TCNQI_2$ as $AgTCNQI_2(MeCN)$ is slightly soluble in acetonitrile, so the color of the acetonitrile rinse cannot be used as a indicator of the endpoint of the purification procedure.

Single Crystal Synchrotron Radiation Diffraction Studies: Single crystal X-ray diffraction data of **4** were obtained on a Bruker-GADDS diffractometer at Texas A&M University. The synchrotron radiation diffraction data for **3, 5** and **6** were collected at ChemMatCars beamline at the Advanced Photon Source (APS), Argonne National Lab. Data collection strategies consisting of two ω-scans with one full sphere and one half sphere for a total of 1080 frames with 0.5º widths. The integration was performed with the Bruker-APEXII software package. Absorption corrections (SADABS) were based on fitting a function to the empirical transmission surface as sampled by multiple equivalent measurements and a strong correction was adopted considering the existence of heavy atoms (Br, Ag, I). Solution and refinement of the crystal structure was performed with

SHELX programs[88] and the graphical interface X-SEED. All non-hydrogen atoms were assigned in difference Fourier maps after several rounds of least square refinements. Positions of hydrogen atoms were located by calculation.

Structure Description and Analysis

The structures of **3-6** will be described here but since compound **1** and **2** were first prepared by Dr. Nazario Lopez, their structures will not be included. The structures of both **3** and **4** consist of a 1-D chain structure. In a single chain, two linear arrays of Cu(I) cations are connected by μ_4-bridging $(TCNQBr_2)^{2-}$ anions with one and two coordinating acetonitrile molecules, respectively. A view along the *a* axis of **3** reveals a columnar stacked nature of 1-D chains, with $(TCNQBr_2)^{2-}$ ligands in the adjacent chain along the stack being perpendicular. When viewed along the *a* axis, the packing diagram of **4** reveals that the chains form columns with a dihedral angle between aromatic rings of $(TCNQBr_2)^{2-}$ in two adjacent columns of 78.4(5)º. The Cu(I) cations in compound **3** adopt a trigonal coordination environment with Cu-N bond distances of 1.912(9) Å, 1.920(8) Å and 1.926(8) Å, and N-Cu-N angles of 118.6(3) º, 118.2(3) º and 122 º. Interestingly, two weak interactions between the Cu(I) and nitrogen atom in the adjacent layer, and Cu(I) and Br atom in the adjacent layer are observed and evidenced by their contact distances of Cu---N of 2.720(9) Å and Cu---Br of 3.149(2) Å. Both distances are slightly shorter than the sum of the van der Waals radii for Cu-N and Cu-Br which are 2.90 Å and 3.24 Å. These two distacnes can be interpreted as weak interactions in the axial positions of the Cu(I) ions, as they are nearly perpendicular to the plane of the three equatorial nitrogen atoms. Given that no π-π stacking interactions can be noted in the structure (the $TCNQBr_2$ dianions are located above the coordinated acetonitrile), the

weak Cu---N and Cu---Br interactions may be responsible for the columnar packing. In the structure of **4**, Cu(I) cations adopt a slightly less distorted tetrahedral coordination environment as compared to **1**, with Cu-N bonds of 1.961(7)Å, 1.966 (7) Å, 1.985(8) Å, and 2.050(9) Å, and N-Cu-N angles of 107.7(3) º, 114.8(3) º, 107.5(3) º, 114.0 (3) º, 110.2 (3) º, 102.2 (3) º. Interplanar distances between $TCNQBr_2$ anions in the chain are 7.322(2) Å, which is much longer than the sum of Br---Br van der Waals radii (3.80 Å). This long separation distance supports an absence of interactions between the frontier orbitals of $TCNQBr_2$ anions.

Compound **5** and **6** adopt very similar structures with slight differences in the space group, namely $P2_1/c$ versus $P2_1/m$. and are best described as an aggregation of one-dimensional polymers with columnar π-stacking of the $TCNQI_2$ radicals which serve to link the Cu(I) and Ag(I) cations by acting as a μ_2-ligand. With a coordinated acetonitrile molecule, both Cu(I) and Ag(I) centers adopt an unprecedented 3-coordinate, trigonal geometry with N-Cu-N angles of 138.57(1) º,122.53(1) º and 163.87(1) º, and N-Ag-N angles of 136(1)º, 92(1)º, and 131(1)º respectively. Iodine groups are shifted from an eclipsed position due to steric effects (Figure 4). The separation of adjacent layers is 3.223(2) Å and 3.23 (1) Å correspondingly. Both distances are similar to Cu(TCNQ) phase I and shorter than the TCNQ separation distances found in $Tl(TCNQX_2)$ (X=Cl, Br, I). The structures of **3**, **4**, **5** and **6** are displayed in Figure 5.1-5.3. Pertinent crystallographic data of **3**, **4, 5** and **6** are listed in Table 5.1 and selected bond distances and angles are provides in Table 5.2.

Thermal Gravimetric Analyses

Thermal Gravimetric Analysis (TGA) measurements were performed on **1** and **6** on 3-5 mg of sample at a heating rate of 5 ºC/min, since **2** and **5** are very difficult to purify. Also **3** and **4** can only be obtained as single crystals in very low yields. From the TGA analysis of compound **1** (Figure 5.4a), the acetonitrile molecules are lost at ~ 40 ºC. The weight loss remains constant until 140 ºC where an ~6 % loss occurs without a plateau until 273 ºC with a total 8.90% weight loss followed by decomposition of the sample. The weight loss percentage corresponds well to the liberation of the acetonitrile (calc. to be 8.85%). The lack of a plateau during the process suggests that intermediates are formed during the solvent loss process. TGA studies of **6** reveal that the compound undergoes a weight loss of 6.58% when heated from 120-150 ºC, which correlates well with the expected percentage for the removal of one coordinated acetonitrile molecule (6.77%). A plateau between 150-175 ºC indicates a stable desolvated $Ag(TCNQI_2)$ intermediate which subsequently decomposes at temperatures above 175 ºC (Figure 5.4b).

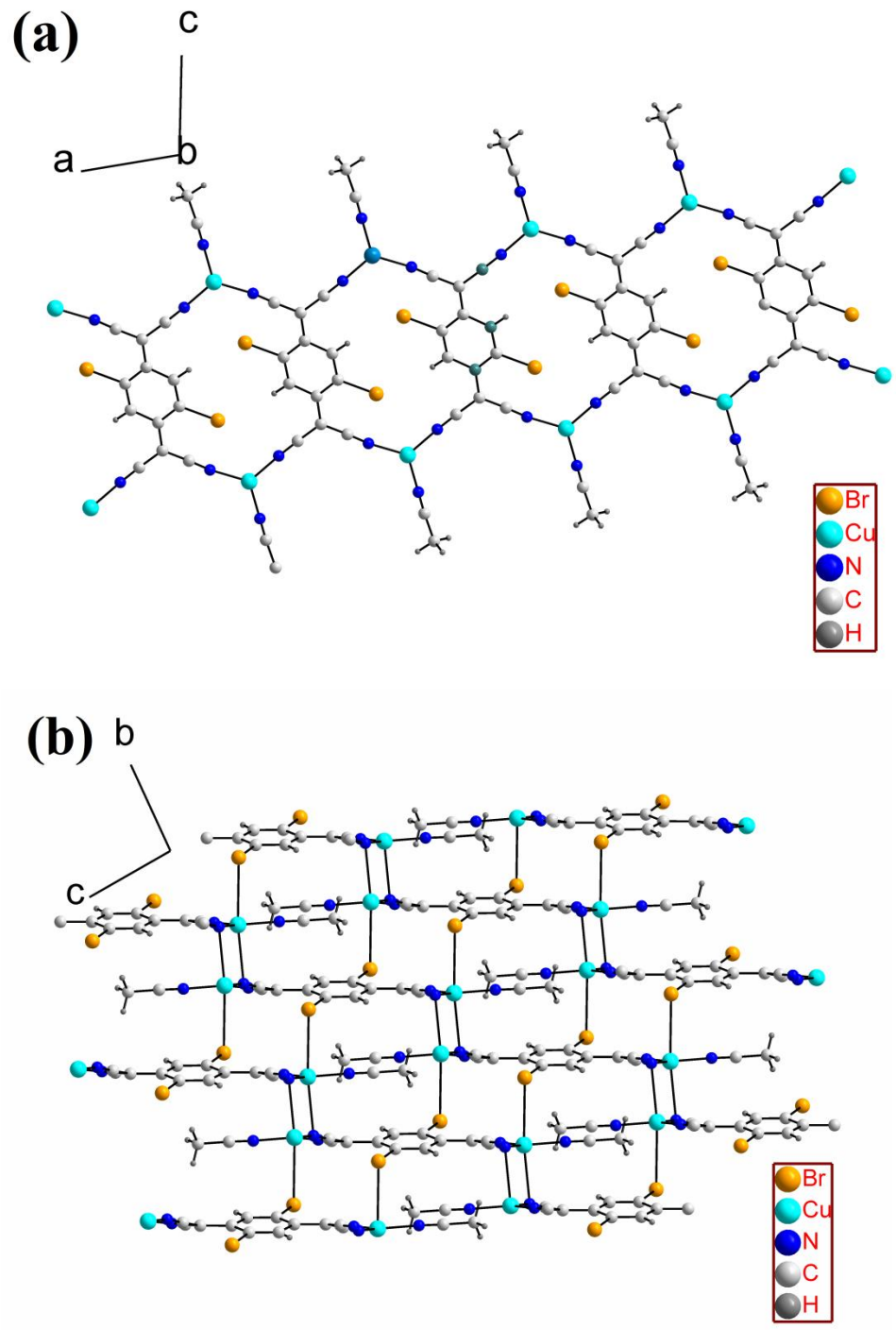

Figure 5.1 Structure of (a) a single chain and (b) packing diagram along the *a* axis of $Cu_2(TCNQBr_2)(MeCN)_2$ (3).

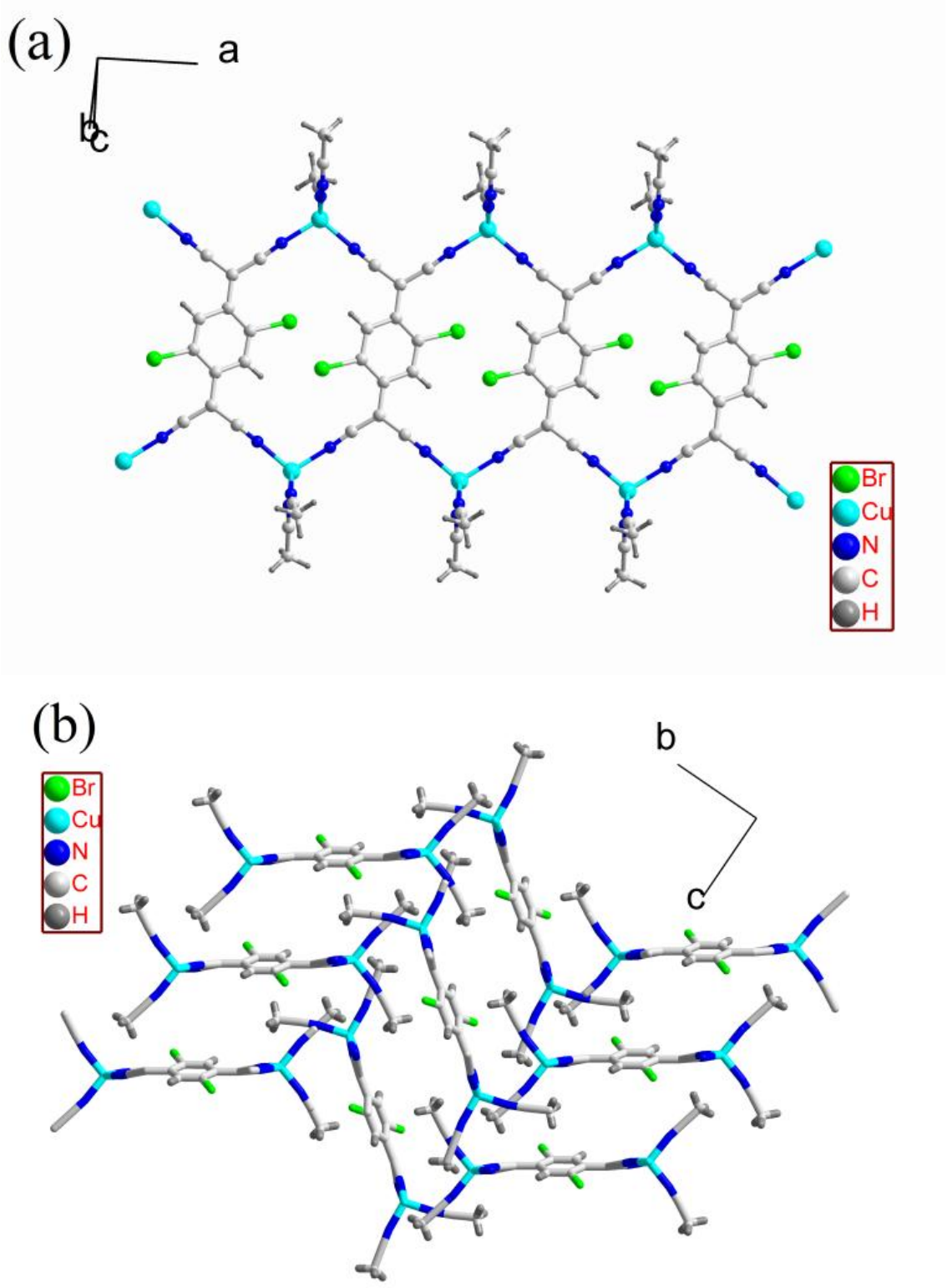

Figure 5.2 Structure of (a) a single chain and (b) packing diagram along the *a* axis of $Cu_2(TCNQBr_2)(MeCN)_4$ (4)..

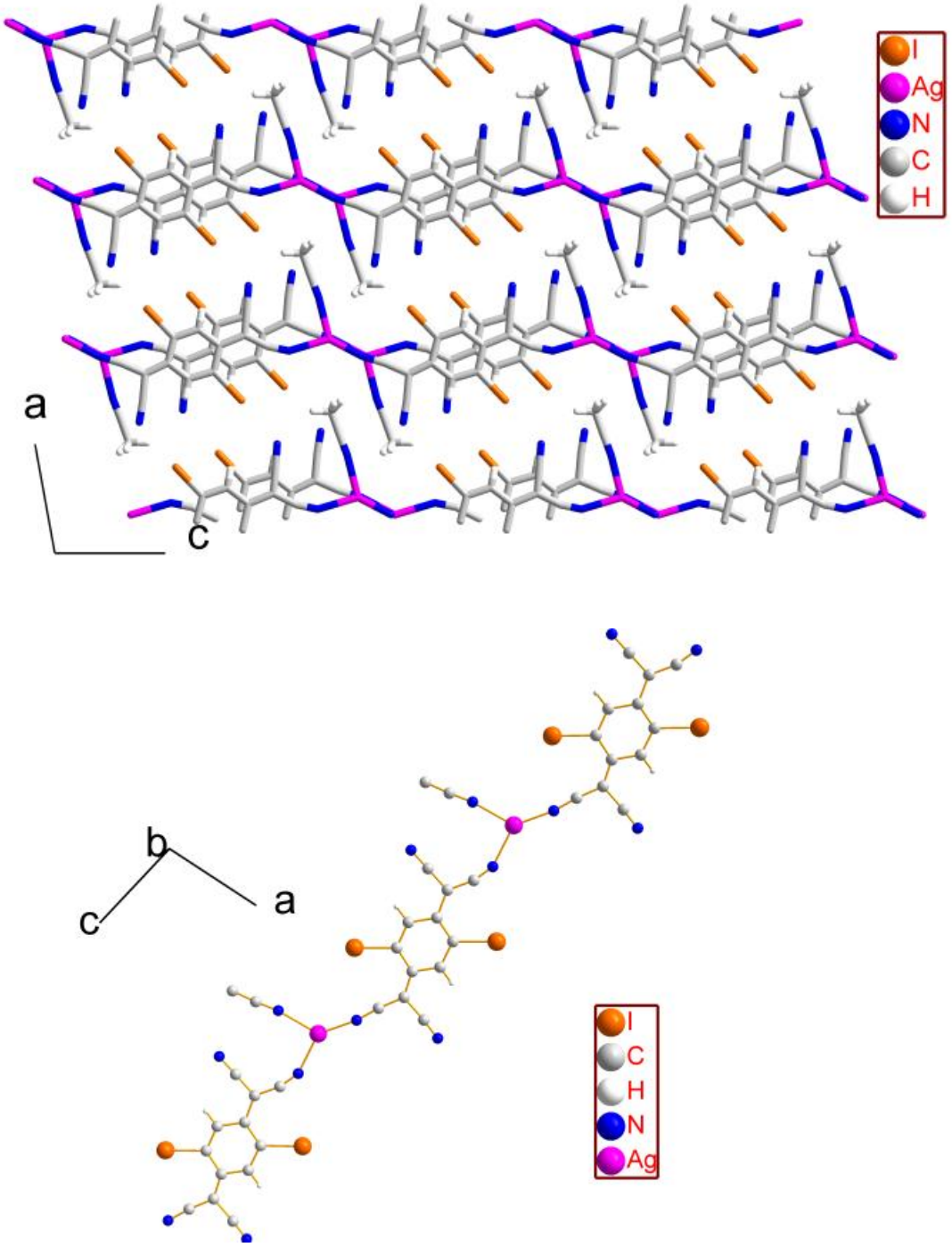

Figure 5.3 The *ac* plane view of $Ag(TCNQI_2)(MeCN)$ (6) packing diagram (upper) and a single chain of $Ag(TCNQI_2)(MeCN)$ (6) (lower). $Cu(TCNQI_2)(MeCN)$ (5**)** adopts the same structure.

Table 5.1. Pertinent crystallographic data and refinement parameters for $Cu_2(TCNQBr_2)(MeCN)_2$ (3), $Cu_2(TCNQBr_2)(MeCN)_4$ (4), $Cu(TCNQI_2)(MeCN)$ (5) and $Ag(TCNQI_2)(MeCN)$ (6).

Compound	3	4	5	6
Formula	$C_{16}H_8Br_2Cu_2N_6$	$C_{20}H_{14}Br_2N_8Cu_2$	$C_{14}H_5CuI_2N_5$	$C_{14}H_5N_5I_2Ag$
F_w [g mol^{-1}]	571.18	653.29	560.57	604.90
Crystal size	0.03 x 0.02 x0.004mm^3	0.08 x0.06 x 0.01mm^3	0.06x 0.05 0.003mm^3	0.02 x 0.01 x 0.003mm^3
Crystal system	Triclinic, *P*-1	Monoclinic, $P2_1/n$	Monoclinic, $P2_1/c$	Monoclinic, $P2_1/m$
a [Å]	7.5021(15)	7.3225(15)	8.5503(17)	8.509(2)
b [Å]	7.6995(15)	22.465(5)	6.4448(13)	6.463(2)
c [Å]	7.9024(16)	8.1495(16)	27.304(6)	14.007(3)
α [°]	94.65(3)	90	90	90
β [°]	100.65(3)	92.35(3)	98.82(3)	100.33(3)
γ [°]	91.37(3)	90	90	90
V [Å^3]	446.77(15)	1339.5(5)	1486.8(5)	757.8(3)
Z	1	2	4	2
ρ_{calc} [g cm^{-3}]	2.123	1.620	2.504	2.651
λ (Mo/Kα or Synchrotron) [Å]	0.41328	0.71073	0.41328	0.41328
Reflns collectged	4452	9903	28847	10344
Unique Reflns	4452	1891	4502	2261
Reflns with I >2σ(I)	2745	1623	1103	1812
Parameters	80	147	115	77
R(int)	0.1150	0.0535	0.0594	0.0662
$R1$[a]	0.0956	0.0603	0.0457	0.1255
$wR2$[b]	0.2142	0.2041	0.1119	0.2940
GOF	1.083	1.092	1.219	1.178

[a] $R1 = \Sigma||F_o| - |F_c||\Sigma|F_o|$. [b] $wR2 = [\Sigma[w(F_o^2 - F_c^2)^2]/\Sigma[w(F_o^2)^2]]^{1/2}$.

Table 5.2. Selected bond distances and angles for $Cu_2(TCNQBr_2)(MeCN)_2$ (3), $Cu_2(TCNQBr_2)(MeCN)_4$ (4), $Cu(TCNQI_2)(MeCN)$ (5) and $Ag(TCNQI_2)(MeCN)$ (6).

Compound **3**:

Bond Distance (Å)					
Cu1-N1	1.920(8)	Cu1-N2	1.926(8)	Cu1-N3	1.912(9)
Cu1-N2'	2.720(7)				
Br1-C5	1.925(8)	Br1'-Cu1	3.149(2)		
C1-N1	1.116(1)	C3-N2	1.154(1)	C5-N3	1.177(1)
Bond Angles(º)					
N1-Cu1-N3		118.67(1)	N2-Cu1-N3		118.28(2)
N1-Cu1-N2		122.80(2)	N2-Cu1-N3'		95.34(2)
N1-Cu1-N2'		88.93(2)	N2-Cu1-N2'		90.80(2)

Compound **4**:

Bond Distance (Å)					
Cu1-N1	1.960(7)	Cu1-N2	1.966(7)	Cu1-N3	1.985(8)
Cu1-N4	2.050(9)				
Br1-C5	1.915(8)				
C1-N1	1.16(1)	C6-N2	1.15(1)	C7-N3	1.133(1)
C9-N4	1.15(1)				
Bond Angles(º)					
N1-Cu1-N2		107.7(2)	N1-Cu1-N3		114.8(3)
N1-Cu1-N4		107.5(3)	N2-Cu1-N3		114.0(3)
N2-Cu1-N4		110.2(3)	N3-Cu1-N4		102.2(3)

Compound **5**

Bond Distance (Å)					
Cu1-N1	1.9877(4)	Cu1-N2	1.8760(5)	Cu1-N5	1.9311(5)
I1-C5	2.0968(5)				
I1-I2	4.1168(6)				
C1-N2	1.1539(3)	C2-N1	1.1274(2)	C4-N3	1.1431(3)
C13-N4	1.1626(3)	C14-N5	1.1615(2)		
Bond Angles(º)					
N2-Cu1-N5		138.57(1)	N1-Cu1-N2		122.53(1)
N1-Cu1-N5		98.86(1)			

Compound **6**:

Bond Distance (Å)					
Ag1-N1	2.22(2)	Ag1-N3	1.99(5)	Ag1-N5	2.28(5)
Ag1-Ag2'	4.01(3)				
I1-C5	2.11(3)	I2-C8	2.08(3)		
I1-I2'	3.87(3)				
C1-N1	1.15(3)	C3-N2	1.21(4)	C12-N3	1.29(6)
C11-N4	1.12(5)	C13-N5	1.18(8)		
Bond Angles(º)					
N3-Ag1-N1		136(1)	N3-Ag1-N5		131(1)
N1-Ag1-N5		92(1)			

Infrared Spectra

A comparison of the infrared spectra of fresh and heated samples of **1** after heating to 270℃ as in the TGA experiment, revealed that a weak absorption at 2266 cm^{-1} corresponding to the $\nu_{C\equiv N}$ for coordinated disappears in the spectrum after heating (Figure 5.5a). Sharp absorptions at 2191 and 2131cm^{-1} and a shoulder at 2158 cm^{-1} in the spectrum of a fresh sample suggests the presence of $TCNQBr_2^-$ radicals; these features for the radical form appear at 2191, 2158 and 2147 cm^{-1} in the spectrum of the heated sample indicating different coordination environments. The three latter features match well with the $\nu_{C\equiv N}$ stretches of $TCNQBr_2^-$ radicals observed for $Cu(TCNQBr_2)$.[32] A TGA analysis of **6** shows a plateau between 150-175℃ which indicates a stable intermediate therefore a bulk sample of **6** was subjected to solvent loss by heating at 130 ºC *in vacuo* for 2 hours. A comparison of the infrared spectrum of the sample before and after heating clearly indicates the loss of the acetonitrile ligand. From the spectra, one can see that the two absorptions at 2295 and 2267 cm^{-1} which represent the $\nu_{C\equiv N}$ mode of the coordinated CH_3CN disappear; meanwhile the other two ν_{CN} stretches assigned to $TCNQI_2^-$, namely 2178 and 2153 cm^{-1} remain after heating. These two latter features are in accord with the radical form of $TCNQI_2^-$.[87] The desolvated sample remains dark green, another indication that the $Ag(TCNQI_2)$ compound has not decomposed with heating (Figure 5.5b).

Owing to the low yields and the polymorphism problem it was difficult to collect sufficient sample amounts for **2**, **3**, **4** and **5** for TGA analyses. The IR data, however, indicate the presence of $\nu_{C\equiv N}$ modes for TCNQ and acetonitrile ligands. The ν_{CN} stretches of coordinated acetonitrile molecules for compounds **2** and **5** appear at 2298;

2269 cm^{-1} and 2296; 2267 cm^{-1} respectively whereas the $\nu_{C\equiv N}$ stretches of the TCNQ moiety appear at 2191; 2149 cm^{-1} and 2194; 2185; 2143; 2135(sh) cm^{-1} for **2** and **5** respectively. The $\nu_{C\equiv N}$ stretches clearly indicate the radical form of $TCNQI_2^{\cdot}$ in compounds **2** and **5**.[87] although **2** and **5** are very similar, the more complicated features of the $\nu_{C\equiv N}$ stretches in **5** reflect the lower symmetry of the crystal structure ($P2_1/c$ vs $C2/c$). For compounds **3** and **4**, the dianionic form of $(TCNQBr_2)^{2-}$ is evidenced by $\nu_{C\equiv N}$ stretches that appear at 2195, 2141, 2131cm^{-1} and 2193, 2142 cm^{-1} respectively.[32] Finally, the weak $\nu_{C\equiv N}$ stretches that appears at 2289, 2266 cm^{-1} and 2293, 2267 cm^{-1} are attributed to coordinated acetonitrile respectively. Given that the local symmetry of the $(TCNQBr_2)^{2-}$ dianions are nearly identical in compounds **3** and **4**, and the ν_{CN} stretches of coordinated acetonitrile are relatively weak and broad, the striking similarities in the infrared spectra is not surprising.

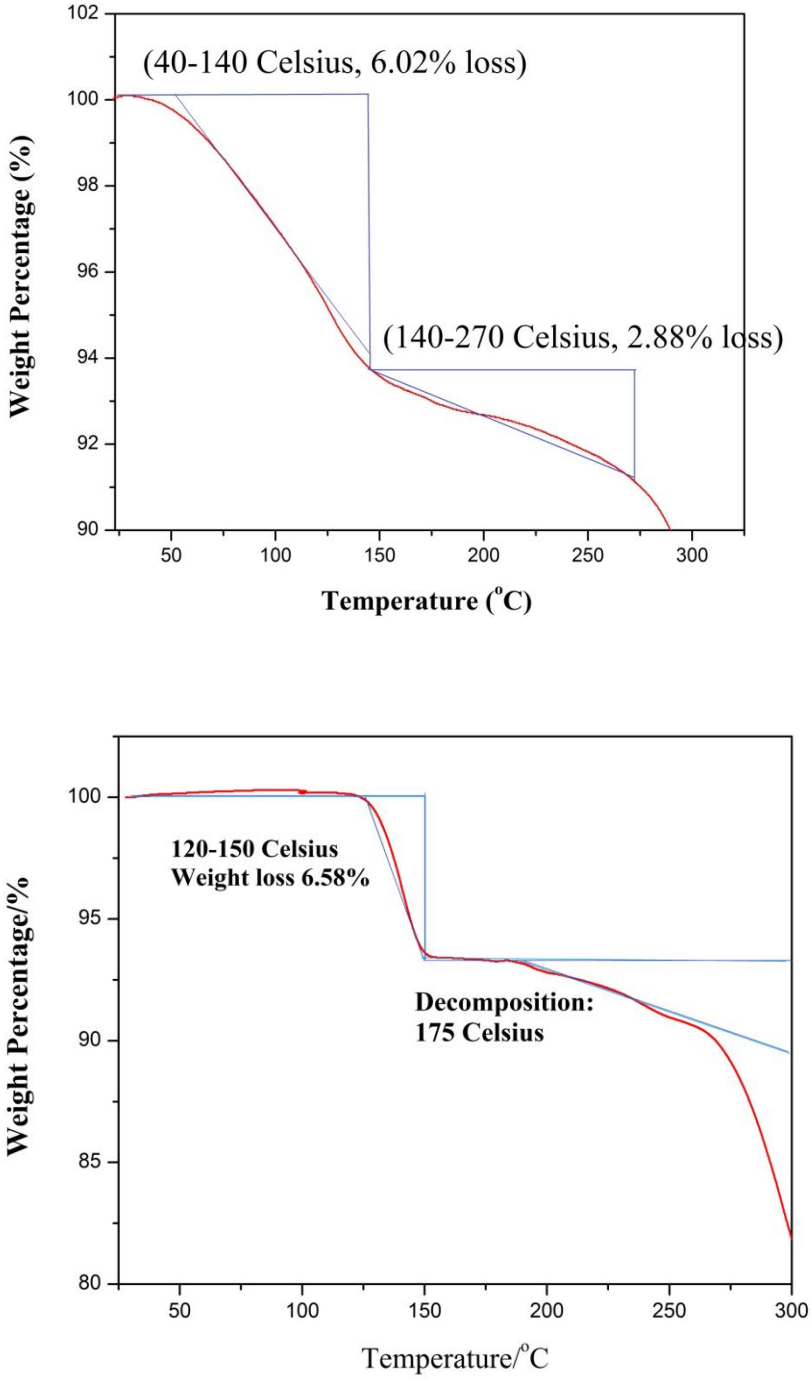

Figure 5.4 TGA analysis of $Cu(TCNQBr_2)(MeCN)$ (1**)** (on a 4.1 mg sample) and $Ag(TCNQI_2)(MeCN)$ (6**)** (on a 2.3 mg sample) at a heating rate of 5℃ /min.

(a)

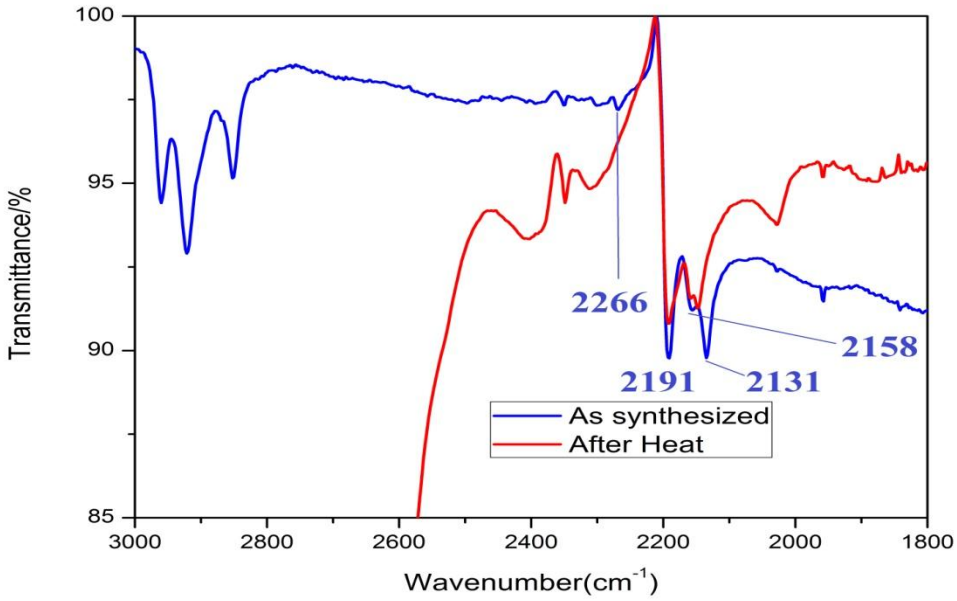

(b)

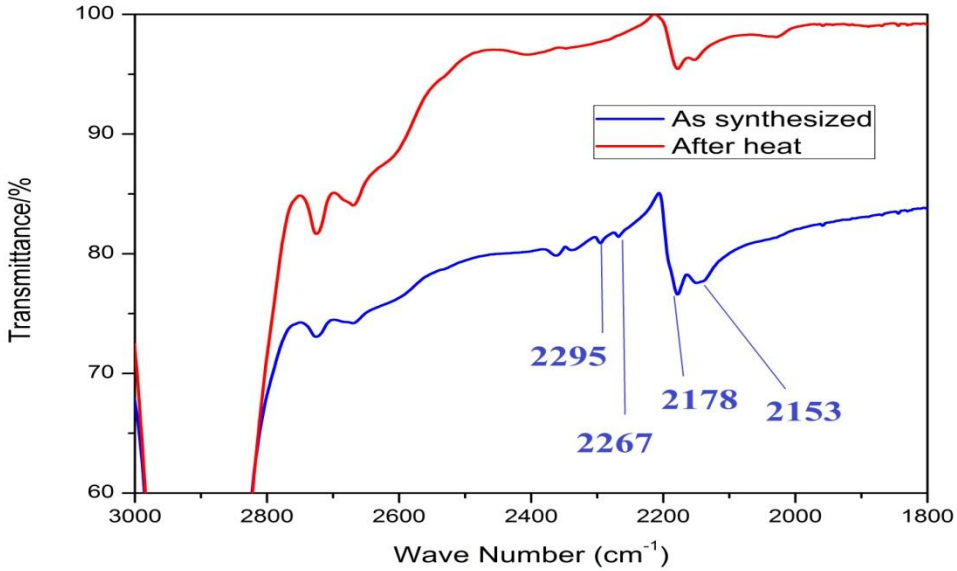

Figure 5.5 Comparison of the infrared spectra of an "as-synthesized sample" and a sample after heating for (a) $Cu(TCNQBr_2)(MeCN)$ (1) and (b) $Ag(TCNQI_2)(MeCN)$ (6).

Powder X-ray Diffraction Studies

Powder X-ray diffraction studies are useful for probing subtle changes in the structures of samples prepared by different methods. By comparing the powder diffraction pattern of a bulk product to the simulated pattern from a single crystal structure, one can ascertain if the powder and the single crystal have the same structure and assess the purity of the bulk product. A comparison of the powder diffraction pattern of "as-synthesized" **1** with the PXRD data for a sample that has been heated to 270 ℃ (Figure 5.6 reveals that the pattern of the as-synthesized sample of **1** matches well with the simulation from single crystal structures of **1** which is not the case for the heated sample which is a close match to the simulation data taken from the single crystal structure of our previously reported compound, $Cu(TCNQBr_2)$.[32] Given that **1** was obtained from $Cu(TCNQBr_2)$ in acetonitrile, it can be concluded that the transformation of $Cu(TCNQBr_2)$ and $Cu(TCNQBr_2)(MeCN)$ is reversible.

$$Cu(TCNQBr_2) \underset{\text{Heat}}{\overset{\text{MeCN}}{\rightleftharpoons}} Cu(TCNQBr_2)(MeCN)$$

Equation 5.1

Powder X-ray diffraction results collected on a freshly obtained sample of **6** and a sample that had been desolvated *in vacuo* at 130 ºC for 2 hours revealed that the solvent-free framework remains crystalline but that the unit cell is altered which may be a resulted of collapse caused by the flexibility of the chain structure. This hypothesis is supported by the results of soaking the desolvated sample in acetonitrile for 2 days.

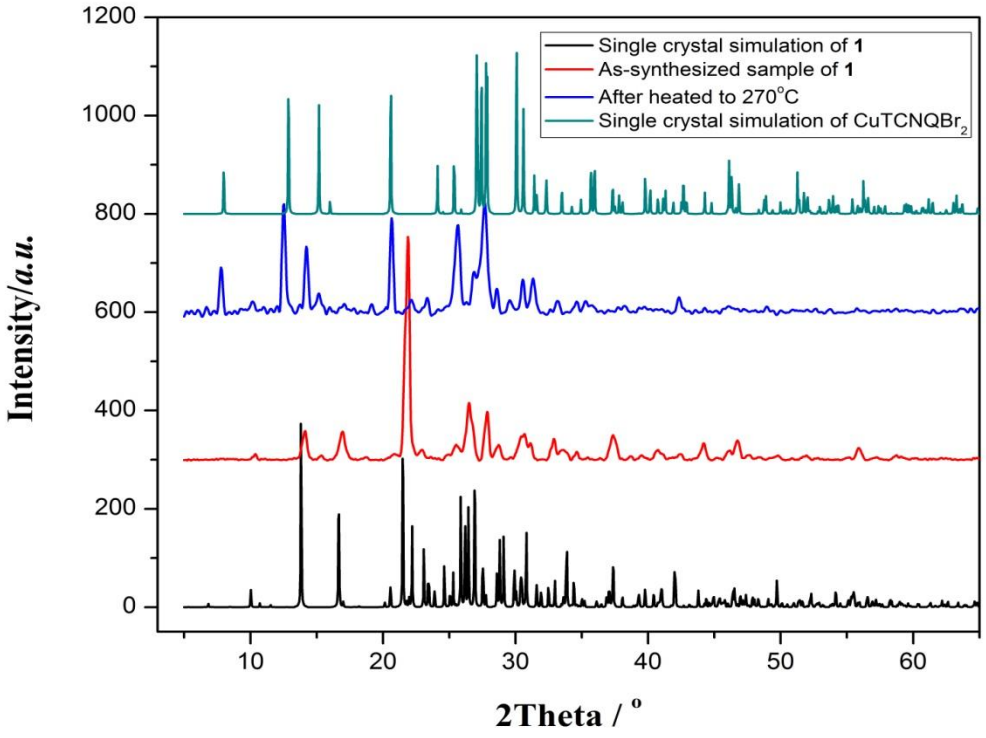

Figure 5.6. Simulated powder X-ray diffraction data obtained from the single crystal structure of $Cu(TCNQBr_2)(MeCN)$ (1), the "as-synthesized" sample of $Cu(TCNQBr_2)(MeCN)$ (1) , a sample that has been heated to 270 ºC, and a simulation from the single crystal data for $Cu(TCNQBr_2)$.

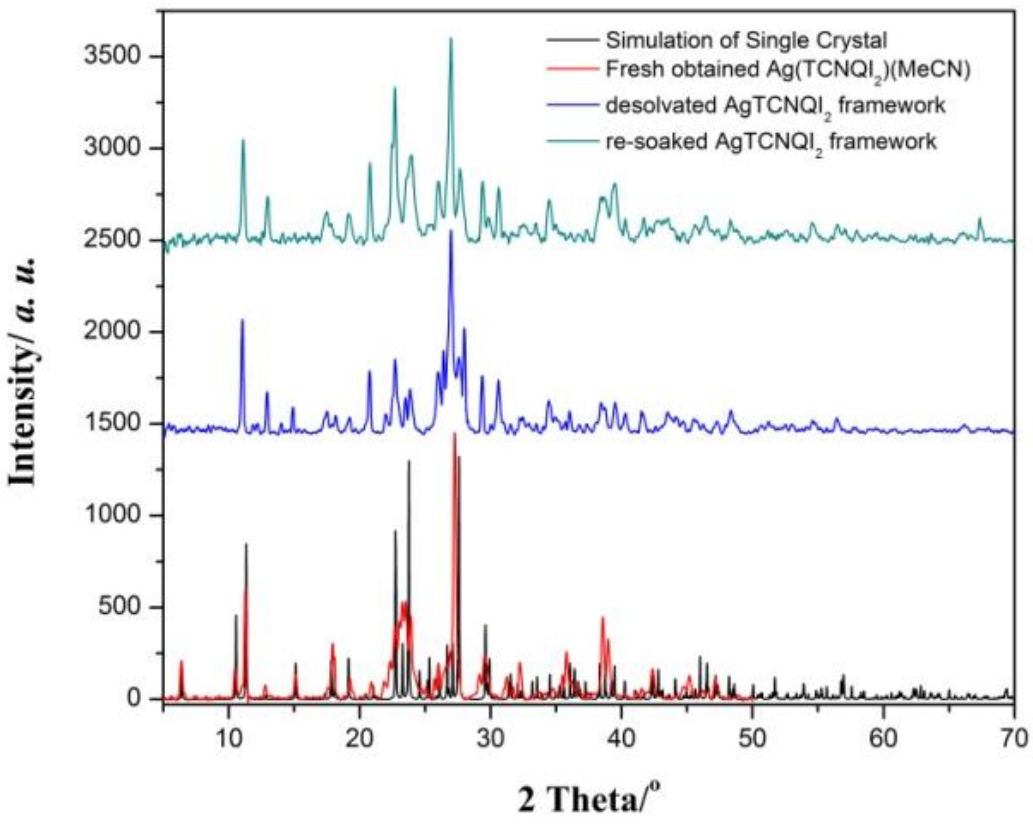

Figure 5.7. Powder X-ray Diffraction patterns of a freshly obtained sample, a desolvated sample, a re-soaked sample and a simulated pattern from the single crystal structure of $Ag(TCNQI_2)(MeCN)$, (6).

Powder X-ray diffraction studies of the soaked sample exhibit no obvious differences from the desolvated framework other than a slight loss of crystallinity (Figure 5.7). Continued refluxing of the desolvated framework in acetonitrile decomposes the sample and leads to an amorphous powder. These results are a clear indication that **6** undergoes an irreversible structural transition with solvent loss.

Powder X-ray diffraction patterns of **2**, **3**, **4** and **5** were simulated from the single crystal structures and compared to the PXRD of the microcrystalline bulk products. Since the same slow diffusion reaction can lead to both products **2** and **5**, likewise for **3** and **4**, a comparison was made of **2** and **5** with a bulk product of CuI and $TCNQI_2$, as well as **3** and **4** with a bulk product of **1** with copper foil. (Figure 5.8). The results indicate that the bulk product of CuI and $TCNQI_2$ contains mostly compound **5**; the small differencse between the bulk product and the simulation data for **5** may be due to a small amount of an unknown polymorph impurity. On the other hand, the bulk reaction product of **1** with copper foil exhibits a powder diffraction pattern that matches with the simulation of **3**. These observations imply that **3** and **5** are possibly kinetic products of the bulk reaction and that with prolonged exposure to acetonitrile, a slow solvation occurs with subsequent formation of crystals of **2** and **4**, which are the thermodynamic products under these reaction conditions.

Conductivity Measurements

Four-probe variable temperature conductivity data were collected on the compounds in this study. It was necessary to use pressed-pellet samples because the largest dimensions of the crystals are less than 0.1 mm. For compounds **1** and **6**, it was also essential to measure the conductivity of sample after the solvent loss in order to

investigate the effect on the physical properties. Figure 5.9 depicts the temperature-dependent conductivities of **1** and $Cu(TCNQBr_2)$. The room temperature value of **1** (4.5×10^{-2} $S\cdot cm^{-1}$) is slightly lower than $Cu(TCNQBr_2)$ (2.7×10^{-1} $S\cdot cm^{-1}$). By fitting the data to an Arrhenius law ($\sigma = \sigma_0 exp(-E_g/k_BT)$, E_g = energy gap of semiconductor, k_B = Boltzmann constant, and T = average temperature), the activation energy of **1** (0.140 eV) was found to be much higher than $Cu(TCNQBr_2)$ which is 0.036 eV. The result is not surprising, as the density of TCNQ stacks in the structure of **1** is decreased by the presence of the coordinated acetonitrile molecules as compared to the binary compound $Cu(TCNQBr_2)$. Meanwhile, since it was demonstrated[30] that the Cu 3d orbitals are involved in the conduction band (which decreases the effective activation energy and promotes higher conductivity), loss of Cu-TCNQ coordination bonds in **1** in favor of coordinated acetonitrile molecules also decreases the component of Cu 3d orbitals which is expected to lead to a lower conductivity.

As expected, compound **3** and **4** are insulators due to the closed shell nature of the dianionic $TCNQBr_2^{2-}$ ligand in the structure. Variable temperature conductivity measurements on **5** (Figure 5.10) revealed that the r.t. value is 6.5×10^{-3} $S\cdot cm^{-1}$ with an activation energy of 0.193eV. The large separation distances between TCNQ radicals (3.76Å) caused by the steric effect of the iodine substituents are responsible for the low conductivity and high activation energy. As already mentioned, the two acetonitrile ligands serve to decrease the involvement of Cu 3d orbitals as compared to the binary compounds which should also lead to a lower conductivity.[30]

Variable temperature conductivity measurements were performed on a pressed pellet of the "as-synthesized" sample of **6** and a desolvated sample (Figure 5.11). The

room temperature conductivities were determined to be 4.9×10^{-5} S/cm and 2.1×10^{-4} S/cm, respectively. The variable temperature behavior indicates that both phases are semiconductors and undergo semiconductor-to-insulator transitions at ~181 K and 168 K respectively. By fitting the semiconducting region to an Arrhenius Law, the activation energies are 0.249 eV and 0.250 eV respectively for fresh and desolvated samples respectively. Given that the conductivity behavior of metal-TCNQ compounds can be considered as being quasi 1-D and the band structure is mainly decided by the stacking distance of TCNQ radicals, the essentially identical energy gaps suggest that the stacking models and separation distances between TCNQ radicals in the fresh and desolvated sample are essentially the same.[89] The enhancement of conductivity by desolvation is likely a result of collapse of the cavities previously occupied by the coordinated acetonitrile molecules leading to improved conducting pathways through space.

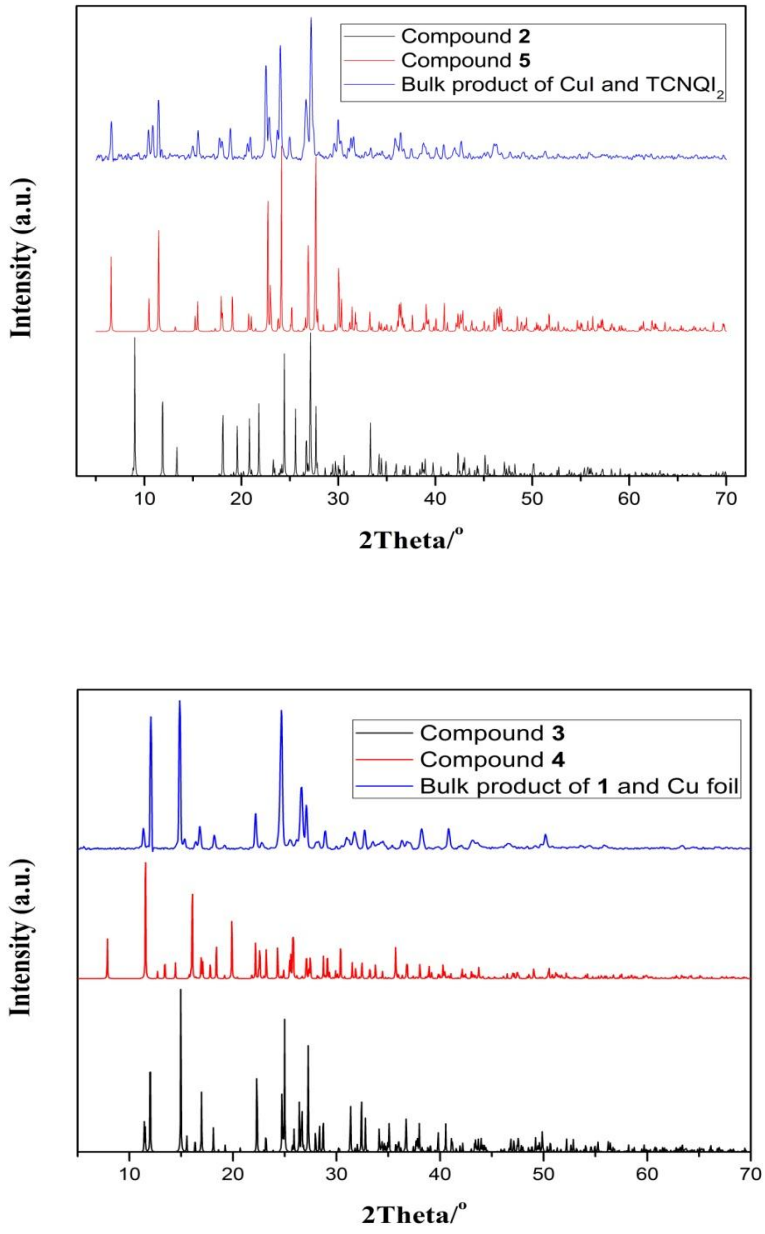

Figure 5.8. Comparison of the simulated powder diffraction from the single crystal (black and red trace) and experimental data from a bulk product (blue trace) for $Cu(TCNQI_2)(MeCN)_2$ (2) and $Cu(TCNQI_2)(MeCN)$ (5) (upper) and $Cu_2(TCNQBr_2)(MeCN)_4$ (3) and $Cu_2(TCNQBr_2)(MeCN)_2$ (4) (lower). The comparison indicates that 3 and 5 are the kinetic products whereas 2 and 4 are thermodynamic products.

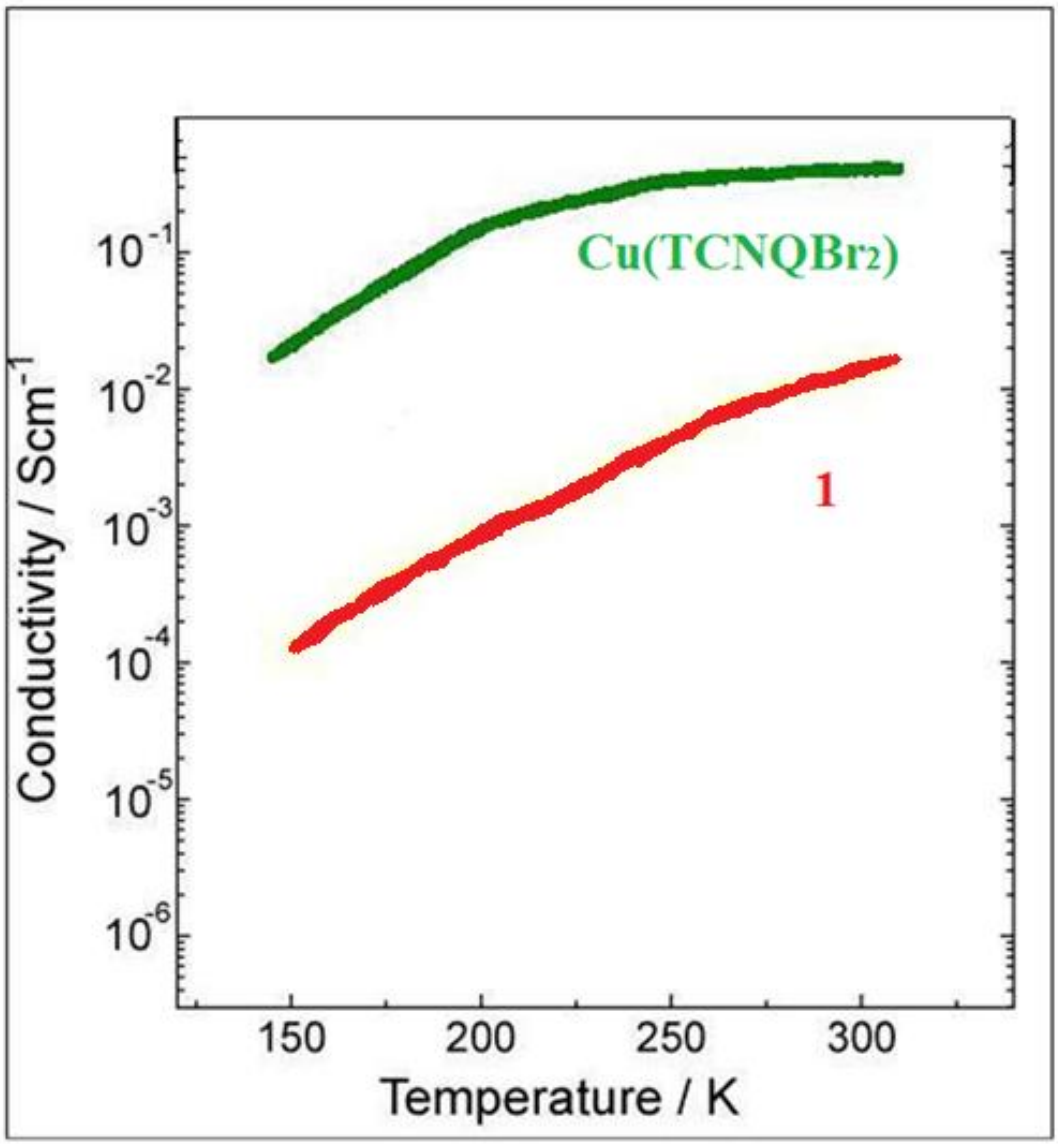

Figure 5.9. Variable temperature conductivity data for the reported compound $Cu(TCNQBr_2)$ and $Cu(TCNQBr_2)(MeCN)$ (1).

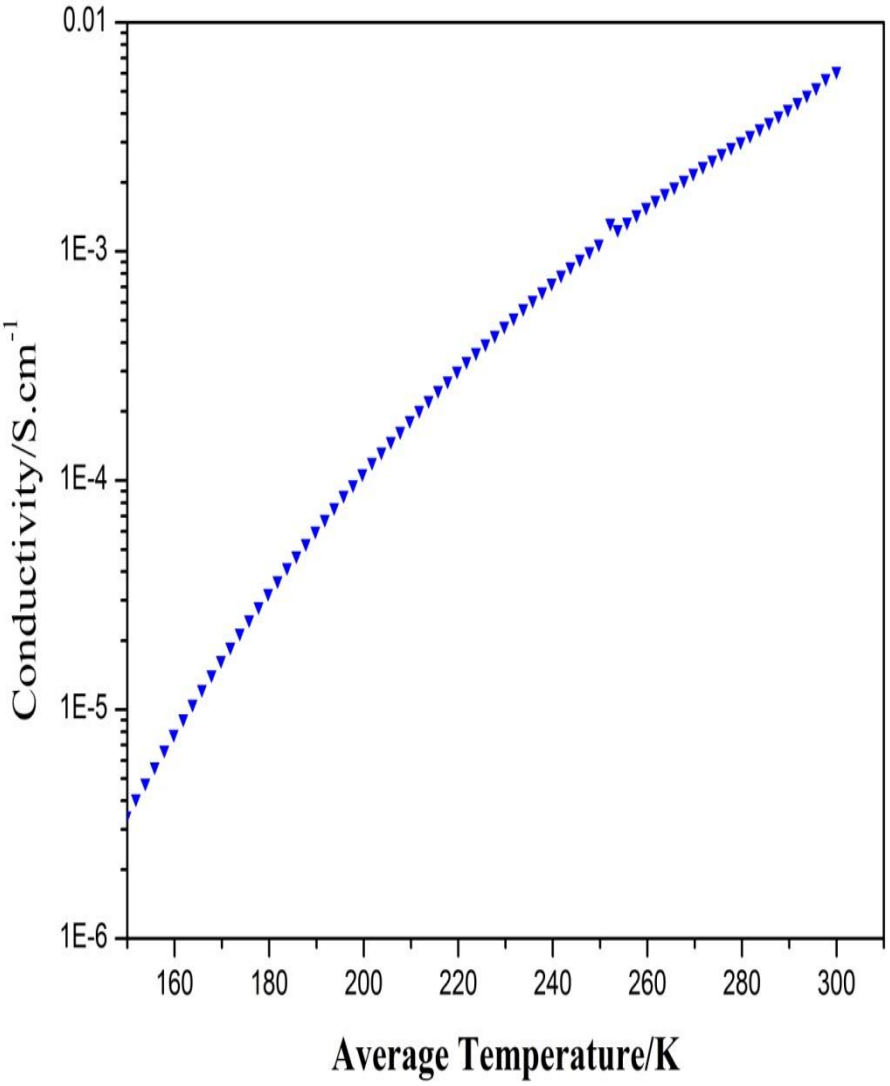

Figure 5.10. Variable temperature conductivity data for $Cu(TCNQI_2)(MeCN)$ (5).

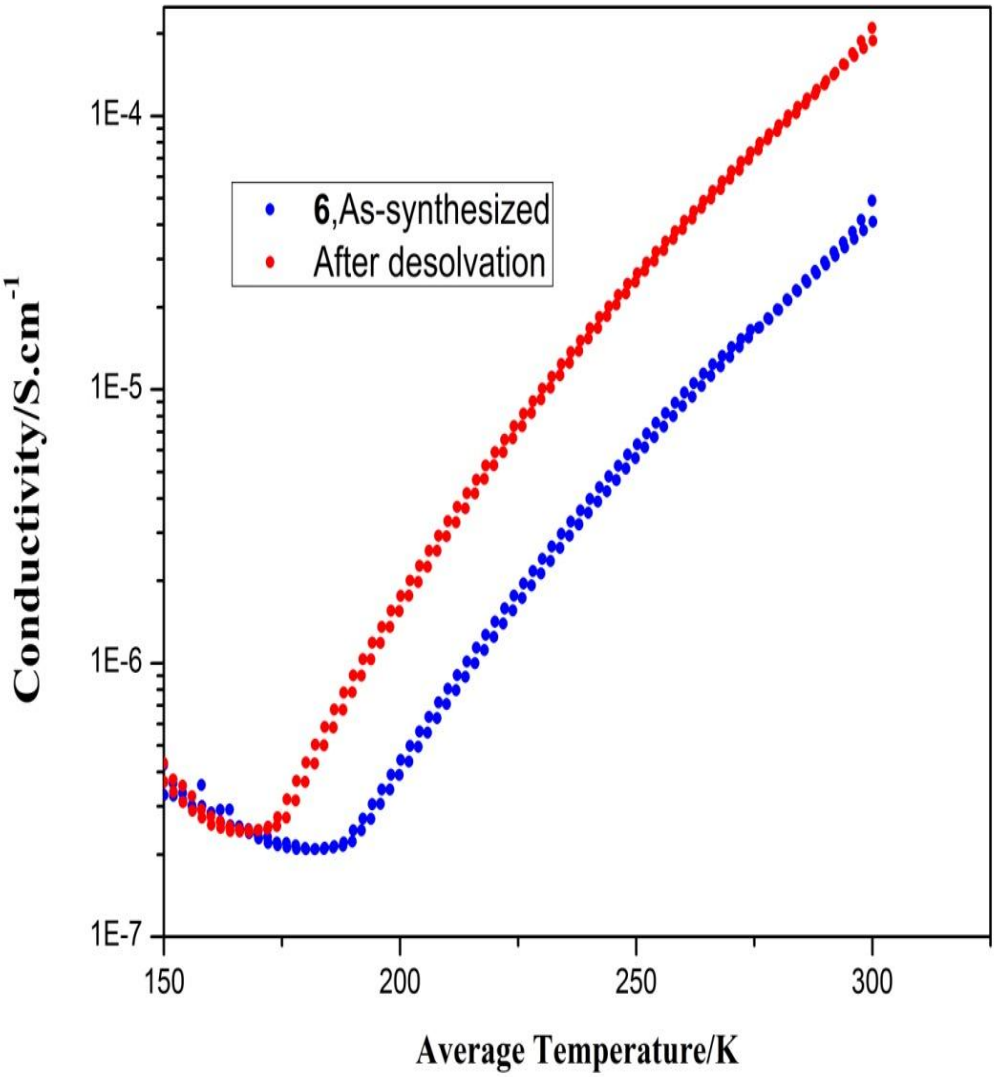

Figure 5.11. Variable temperature conductivity measurements of an "as-synthesized sample" (blue circles) and desolvated sample (red circles) of $Ag(TCNQI_2)(MeCN)$ (**6**).

Conclusions

The introduction of bulky Br and I halogen substituent groups into the metal-TCNQ framework of Cu(I) and Ag(I) ions produces one- and two-dimensional structures that contain coordinated acetonitrile ligands. As compared to the binary metal-TCNQ phases, the lower density of conducting pathways and decreased number of metal-TCNQ coordination bonds leads to relatively lower conductivities and an increase in the activation energy of these semiconductors. The interconversion of these materials with $TCNQX_2$ derivatives and solvent molecules hints at a much more flexible framework for these molecular conductors than was previously thought which allows for tuning of their physical properties.

CHAPTER VI

SUMMARY

The research in this dissertation focused on the application of TCNQ and its derivatives in order to tune the structure and conductivity of these materials, with the overarching goal being to understand the mechanism of conductivity. The first chapter provides a brief review to the history and ongoing research of the field of molecular conductors. Chapter II reports the details of the first main-group TCNQ binary compound, Tl(TCNQ). Two distinct polymorphs have been discovered and a remarkable water-induced phase transition from one to the other was observed. With different modes of TCNQ stacking (alternating or homogenous distances), the two polymorphs exhibit very different conductivities, namely 2.4×10^{-4}S/cm and 5.4×10^{-1}S/cm. Chapter III reports a series of semiconductors, $Tl(TCNQX_2)$ (X =Cl, Br, I), which was prepared and structurally characterized. The steric effect of the halogen substituents leads to a variety of structures and a band structure simulation has suggested a clear structure-property relationship that involves perturbation of the Tl 6s orbital into the conduction band. Chapter IV reports two semiconducting frameworks, $Ag(TCNQCl_2)$ and $Ag(TCNQBr_2)$, which were prepared by electrocrystallization methods. Importantly, the former material exhibits a high room temperature conductivity of 0.25 S/cm and an unusual room temperature negative differential resistance (NDR) which is the source of intrinsic switching behaviors. The effect of solvent on the structure of these binary phases was also investigated and discussed in chapter V. The series $M(TCNQX_2)(MeCN)_n$ (M = Cu, Ag; X = Br, I; n =1, 2) was discovered and the interconversion of these solvated phases

was studied. The effect of coordinated solvent molecules decreases the density of conducting stacks, consequently leading to a decrease of conductivity.

REFERENCES

1. International Technology Roadmap For Semiconductors (ITRS), 2011 Edition Executive Summary. http://www.itrs.net/Links/2011ITRS/2011Chapters/2011ExecSum.pdf.
2. Meijer, G. I.; *Science* **2008**, *319*, 1625-1626.
3. Heath, J. R. ; *Annu. Rev. Mater. Res.* **2009**, *39*, 1–23.
4. McGimpsey, W. G.; "Molecular Electronics, Past, Present, Future?" Lecture Slides.
5. Del Nero, J.; de Souza, F. M.; Capaz, R. B.; *J. Comput. Theor. Nanosci.* **2010**, *7*, 1-14.
6. McCoy, H. N.; Moore, W. C.; *J. Am. Chem. Soc.*, **1911**, *33*, 273–292.
7. Akamatu, H.; Inokuchi, H.; Matsunaga, Y.; *Nature* **1954**, *173*, 168-169.
8. Kepler, R. G.; Bierstedt, P. E.; Merrifield, R. E.; *Phys. Rev. Lett.* **1960**, *5*, 503-504.
9. Ferraris, J.; Cowan, D. O.; Walatka, V.; Perlstein, J. H.; *J. Am. Chem. Soc.* **1973**, *95*, 948-949.
10. Ishiguro, T.; Yamaji, K.; Saito, G.; "*Organic Superconductors*", Second Edition , **1998**, Springer-Verlag.
11. Mott, N. F.; Peierls, R.; *Proc. Phys. Soc.* **1937**, *49*, 72-73.
12. Ishiguro, T.; Sumi, H.; Kagoshima, S.; Kajimura, K.; Anzai, H.; *J. Phys. Soc. Jpn.* **1980**, *48*, 456-463.
13. Berlinsky, A. J.; Carolan, J. F.; Weiler, L.; *Solid State Commun.* **1974**, *15*, 75-801.
14. Coleman, L. B.; Cohen, M. J.; Sandman, D. J.; Yamagishi, F. G.; Garito, A. F.; Heeger, A. J.; *Solid State Commun.* **1973**, *12*, 1125-1132.

15. Jérome, D.; Mazaud, A.; Ribault, M.; Bechgaard, K.; *J. Physique Lett.* **1980**, *41*, L95-98.

16. Yagubskii, E. B.; Shchegolev, I. F.; Laukhin, V. N.; Kononovich, P. A.; Kartsovnic, M. V.; Zvarykina, A.V.; Bubarov, L. I.; *JETP Lett.* **1984**, *39*, 12-15.

17. Murata, K.; Tokumoto, M.; Anzai, H.; Bando, H.; Saito, G.; Kajimura, K.; Ishiguro, T.; *J. Phys.Soc. Jpn.* **1985**, *54*, 1236-1239.

18. Vegter, J. G.; Hibma, T.; Kommandeur, J.; *Chem. Phys. Lett.* **1969**, *3*, 427-429.

19. Sakai, N.; Shirotani, I.; Minomura, S.; *Bull. Chem. Soc. Jpn.* **1972**, *45*, 3321-3328.

20. (a) Konno, M.; Saito, Y.; *Acta. Cryst.* **1975**, *B31*, 2007-2012. (b) Konno, M.; Ishii, T.; Saito, Y.; **1977**, *B33*, 763-770. (c) Hoekstra, A.; Spoelder, T.; Vos, A.; *Acta. Cryst.* **1972**, *B28*, 14-25. (d) Shirotani, I.; Kobayashi, H.; *Bull. Chem. Soc. Jpn.* **1973**, *46*, 2595-2596. (e) van Bodegom, B.; De Boer, J. L.; Vos, A.; Acta Cryst. **1977**. *B33*, 602-604.

21. (a) Potember, R. S.; Poehler, T. O.; Cowan, D. O.; *Appl. Phys. Lett*. **1979**, *34* , 405-407. (b) Potember, R. S.; Poehler, T. O.; Benson, R. C., *Appl. Phys. Lett*. **1982**, *41*, 548-550. (c) Hoagland, J. J.; Wang, X. D.; Hipps. K. W. *Chem. Mater.* **1993**, *5*, 54.; (d) Liu, S.; Liu, Y.; Wu, P.; Zhu. D., *Chem. Mater.* **1996,** *8,* 2779. (e) Gu, N.; Lu, W.; Pang, S.; Yuan, C.; Wei, Y., *Thin Solid Films* **1994**, *243* , 468-471. (f) Liu, S.; Liu, Y.; Zhu, D., *Thin Solid Films,* **1996,** *280*, 271-277. (g) Wakida, S.; Ujihira, Y., *Jpn. J. Appl. Phys.* **1988**, *27*, 1314-1316. (h) Hua, Z. Y.; Chen, G. R. *Vacuum* **1992**, *43*, 1019-1023.

22. Heintz, R. A.; Zhao, H.; Ouyang, X.; Grandinetti, G.; Cowen, J.; Dunbar, K. R.; *Inorg. Chem*. **1999**, *38*, 144-156.

23. (a) Potember, R. S.; Pohler, T. O.; Cowan, D. O.; Carter, F. L.; Brant, P. I.; "*Molecular electronic devices II.*" **1987**, Marcel Dekker. (b) Potember, R. S.; Pohler, T. O.; Hoffman, R. C.; Speck, K. R.; Benson, R. C.; "*Molecular electronic devices.*" **1982**, Marcel Dekker. (c) Kamitsos, E. I.; Risen, W. M. Jr.; *Solid State Commun.*, **1983**, *45*, 165-169. (d) Potember, R. S., Pohler, T. O., Cowan, D. O., Brant, P., Carter, F. L., Bloch, F. N., *Chem. Scr*., **1981**, *17*, 219-223. (e) Kamitsos, E. I., Risen, W. M. Jr., *Solid State Commun.* **1982**, *42*, 561-565.

24. Hefczyc , A.; Beckmann, L.; Becker, E.; Johannes, H.; Kowalsky, W. *Phys. Stat. Sol. (a)* **2008** , *205*, 647–655.

25. Potember, R. S.; Poehler, T. O.; Benson, R. C., *Appl. Phys. Lett*. **1982**, *41*, 548-550.

26. Shields, L., *J. Chem. Soc. Faraday Trans. 2,* **1985**, *81*, 1-9.

27. (a) O'Kane, S. A.; Clérac, R.; Zhao, H.; Ouyang, X.; Galán-Mascarós, J. R.; Heintz, R.; Dunbar, K. R., *J. Solid State Chem.* **2000**, *152*, 159-173. (b) Harris, A. R.; Nafady, A.; O'Mullane, A. P.; Bond, A. M.; *Chem. Mater.* **2007**, *19*, 5499-5509.

28. Mori, T.; Inokuchi, H.; Kobayashi, A.; Kato, R.; Kobayashi, H.; *Phys. Rev. B* **1988**, *38*, 5913-5923.

29. Kato, R.; Kobayashi, H.; Kobayashi, A.; *J. Am. Chem. Soc.* **1989**, *111*, 5224-5232.

30. Lopez, N.; Zhao, H.; Ota, A.; Prosvirin, A. V.; Reinheimer, E. W.; Dunbar, K. R.; *Adv. Mater.,* **2010**, *22*, 986-989.

31. (a) Iwasa, Y.; Koda, T.; Koshihara, S.; Tokura, Y.; Iwasawa, N.; Saito, G.; *Phys. Rev. B,* **1989**, *39*, 10441-10444. (b) Iwasa, Y.; Koda, T.; Tokura, Y.; Koshihara, S.;Iwasawa, N.; Saito, G.; *Appl. Phys. Lett.* **1989**, *55*, 2111-2113.

32. Mori, T.; Kawamoto, T.; *Annu. Rep. Prog. Chem., Sect. C,* **2007**, *103*, 134–172.

33. Kumai, R.; Okimoto, Y.; Tokura, Y.; *Science* **1999**, *284*, 1645-1646.

34. Gatteschi, D.; Sessoli, R.; Villain, J.; *Molecular Nanomagnets*, Oxford University Press, 2006.

35. *Single-Molecule Magnets and Related Phenomena, Structure and Bonding* ed. Winpenny, R., Springer, Berlin, Heidelberg, 2006, vol. 122.

36. (a) Coulon, C.; Miyasaka, H.; Clérac R.; *Single-Molecule Magnets and RelatedPhenomena, Structure and Bonding* ed. Winpenny, R., Springer, Berlin, Heidelberg, **2006**, *122*, 163-206. (b) Miyasaka, H.; Julve, M.; Yamashita, M.; Clérac, R.; *Inorg. Chem*. **2009**, *48*, 3420-3437.

37. Kobayashi, H.; Kobayashi, A.; Tajima, H.; *Chem. Asian J.* **2011**, *7*, 1688-1704.

38. Kurmoo, M.; Graham, A. W.; Day, P.; Coles, S. J.; Hursthouse, M. B.; Caulfield, J. M.; Singleton, J.; Ducasse, L.; Guionneau, P.; *J. Am.Chem. Soc.* **1995**, *117*, 12209-12217.

39. Ojima, E.; Fujiwara, H.; Kato, K.; Kobayashi, H.; Tanaka, H.; Kobayashi, A.; Tokumoto, M.; Cassoux, P.; *J. Am. Chem. Soc.* **1999**, *121*, 5581-5582.

40. Coronado, E.; Galán-Mascarós, J. R.; Gómez-Garcia, C. J.; Laukhin, V.; *Nature* **2000**, *408*, 447-449.

41. (a) Sessoli, R.; Tsai, H. T.; Schake, A. R.; Wang, S.; Vincent, J. B.; Folting, K.; Gatteschi, D.; Christou, G.; Hendrickson, D. N.; *J. Am. Chem. Soc.* **1993**, *115*, 1804-1816; (b) Sessoli, R.; Gatteschi, D.; Caneschi, A.; Novak, M. A.; *Nature* **1993**, *365*, 141-143.

42. Lecren, L.; Li, Y.; Wernsdorfer, W.; Roubeau, O.; Miyasaka, H.; Clérac, R.; *Inorg. Chem. Commun.* **2005**, *8*, 626-630.

43. (a) Ahmad, M. M.; Underhill, A. E.; *J. Chem. Soc., Dalton Trans*. **1982**, *6*,

1065–1068. (b) Kobayashi, A.; Mori, T.; Sasaki, Y.; Kobayashi, H.; Ahmad,M. M.; Underhill, A. E.; *Bull. Chem. Soc. Jpn.* **1984**, *57*, 3262–3268. (c) Kobayashi, A.; Sasaki, Y.; Kobayashi, H.; Underhill, A. E.; Ahmad, M. M.; *Chem. Lett.* **1984**, *13*, 305–308.(d) Ahmad, M. M.; Turner, D. J.; Underhill, A. E.; *Phys. Rev. B*, **1984**, *29*, 4796–4799.

44. Hiraga, H.; Miyaska, H.; Nakata, K.; Kajiwara, T.; Takaishi, S.; Oshima, Y.; Nojiri, H.; Yamashita, M.; *Inorg. Chem.* **2007**, *46*, 9661-9671.

45. Miyasaka, H.; Saitoh, A.; Abe, S.; *Coord. Chem. Rev.* **2007**, *251*, 2622-2664.

46. Hiraga, H.; Miyasaka, H.; Clérac, R.; Fourmigué, M.; Yamashita, M.; *Inorg. Chem.* **2009**, *48*, 2887-2898.

47. (a) Côté, A. P.; Benin, A. I.; Ockwig, N. W.; O'Keeffe, M.; Matzger, A. J.; Yaghi, O. M.; *Science* **2005**, *310*, 1166-1170. (b) Zhou, H. C.; Long, J. R.; Yaghi, O. M.; *Chem. Reviews* **2012**, *112*, 673-674.

48. Wiers, B. M.; Foo, M.; Balsara, N. P.; Long, J. R.; *J. Am. Chem. Soc.* **2011**, *133*, 14522-14525.

49. (a) Morikawa, S.; Yamada, T.; Kitagawa, H.; *Chem. Lett.* **2009**, *38*, 654-655. (b) Yamada, T.; Sadakiyo, M.; Kitagawa, H.; *J. Am. Chem. Soc.* **2009**, *131*, 3144-3145. (c) Sadakiyo, M.; Yamada, T.; Kitagawa, H.; *J. Am. Chem. Soc.* **2009**, *131*, 9906-9907. (d) Sadakiyo, M.; Okawa, H.; Shigematsu, A.; Ohba, M.; Yamada, T.; Kitagawa, H.; *J. Am. Chem. Soc.* **2012**, *134*, 5472-5475.(e) Sen, S.; Nair, N.; Yamada, T.; Kitagawa, H.; *J. Am. Chem. Soc.* **2012**, *134*, 19432-19437.

50. (a) Sato, O.; Tao, J.; Zhang, Y.; *Angew. Chem. Int. Ed.* **2007**, *46*, 2152-2187. (b) Sato, O.; Kawakami, T.; Kimura, M.; Hishiya, S.; Kubo, S.; Einaga, Y.; *J. Am. Chem. Soc.* **2004**, *126*, 13176-13177.

51. Kunkeler, P. J.; van Koningsbruggen, P. J.; Cornelissen, J. P.; van der Horst, A.N.; van der Kraan, A.M.; Spek, A.L.; Haasnoot, J. G.; Reedijk, J. *J. Am. Chem. Soc.* **1996**, *118*, 2190-2197.

52. (a) Tanaka, H.; Okano, Y.; Kobayashi, H.; Suzuki, W.; Kobayashi, A.; *Science*, **2001**, *291*, 285-287; (b) Kobayashi, A.; Fujiwara, E.; Kobayashi, H.; *Chem. Rev*., **2004**, *104*, 5243–5264. (c) Valade, L.; Legros, J.; Bousseau, M.; Cassoux, P.; *J. Chem. Soc. Dalton Trans.* **1985**, *4*, 783-794.

53. (a) Karutz, F. O.; von Schütz, J. U.; Wachtel, H.; Wolf, H. C.; *Phys. Rev. Lett.* **1998**, *81*, 140-143. (b) Schmitt, H.; von Schütz, J. U.; Wachtel, H.; Wolf, H. C.; *Synth. Met.* **1997**, *86*, 2257-2258. (c) von Schütz, J. U.; Bauer, D.; Wachtel, H.; Wolf, H. C.; *Synth. Met.* **1995**, *71,* 2089-2090. (d) von Schütz, J. U.; Gomez, D.; Wachtel, H.; Wolf, H. C.; *Synth. Met.* **1997**, *86,* 2095-2096. (e) von Schütz, J. U.; Gomez, D.; Wachtel, H.; Wolf, H. C.; *J. Chem. Phys.* **1996**, *105,* 6538-6546.

54. (a) Ota, A.; Yamochi, H.; Saito, G.; *J. Mater. Chem.* **2002**, *12*, 2600-2602. (b) Chollet, M.; Guerin, L.; Uchida, N.; Fukaya, S.; Shimoda, H.; Ishikawa, T.; Matsuda, K.; Hasegawa, T.; Ota, A.; Yamochi, H.; Saito, G.; Tazaki, R.; Adachi, S.; Koshihara, S.; *Science* **2005**, *307*, 86-89.

55. (a)McGuire, M. A.; Reynolds, T. K.; DiSalvo, F. J.; *Chem. Mater.* **2005**, *17*, 2875-2884. (b) Akhbari, K.; Morsali, A. *Coord. Chem. Rev.* **2010**, *254*, 1977-2006.

56. Bouhadir, G.; Bourissou, D.; *Chem. Soc. Rev.* **2004**, *33*, 210-217.

57. Hünig, S.; Meixner, H.; Metzenthin, T.; Langohr, U.; von Schütz, J. U.; Wolf, H. C.; Tillmans, E.; *Adv. Mater.* **1990**, *8*, 361-363.

58. Janczak, J.; Kubiak, R.; *J. Alloys Compd.* **1993**, *2diff02*, 69-72.

59. (a) Cornelissen, J. P.; van Diemen, J. H.; Groeneveld, L. R.; Haasnoot, J. G.; Spek, A. L.; Reedijk, J. *Inorg. Chem.* **1992**, *31*, 198-202. (b) Kaim, W.; Moscherosch, M. *Coord. Chem. Rev.* **1994,** *129*,157. (c) Lunelli, B.; Pecile, C. *J. Chem. Phys.* **1970**, *52*, 2375. (d) Van Dyne, R. P.; Suchanski, M. R.; Lakovits, J. M.; Siedle, A. R.; Parks, K. D.; Cotton, T. M. *J. Am. Chem. Soc.* **1979**, *101*, 2832. (e) Chappell, J. S.; Bloch, A. N.; Bryden, W. A.; Maxfield, M.; Poehler, T. O.; Cowan, D. O. *J. Am. Chem. Soc.* **1981**, *103*, 2442. (f) Moscherosch, M.; Waldör, E.; Binder, H.; Kaim, W.; Fiedler, J. *Inorg. Chem.* **1995**, *34*, 4326.

60. (a) Inoue, M.; Inoue, M. B.; *J. Chem. Soc. Faraday Trans. 2* **1985**, *81*, 539-547. (b) Inoue, M.; Inoue, M. B. *Inorg. Chem.* **1986**, *25*, 37-41. (c) Inoue, M. B.; Inoue, M.; Fernando, Q.; Nebesny, K.W.; *J. Phys.Chem.* **1987**, *91*, 527-530.

61. Frisch, M. J.; Trucks, G. W. ; Schlegel, H. B. ; Scuseria, G. E.; Robb, M. A.; Cheeseman, J. R.; Scalmani, G. ; Barone, V.; Mennucci, B.; Petersson, G. A.; Nakatsuji, H.; Caricato, M.; Li, X.; Hratchian, H. P.; Izmaylov, A. F.; Bloino, J.; Zheng, G.; Sonnenberg, J. L.; Hada, M.; Ehara, M.; Toyota, K.; Fukuda, R.; Hasegawa, J.; Ishida, M.; Nakajima, T.; Honda, Y.; Kitao, O.; Nakai, H.; Vreven, T.; Montgomery Jr, J. A.; Peralta, J. E.; Ogliaro, F.; Bearpark, M.; Heyd, J. J.; Brothers, E.; Kudin, K. N.; Staroverov, V. N. ; Kobayashi, R.; Normand, J.; Raghavachari, K.; Rendell, A. ; Burant, J. C.; Iyengar, S. S.; Tomasi, J. ; Cossi, M.; Rega, N.; Millam, J. M.; Klene, M. ; Knox, J. E.; Cross, J. B.; Bakken, V.; Adamo, C.; Jaramillo, J.;

Gomperts, R.; Stratmann, R. E.; Yazyev, O.; Austin, A. J.; Cammi, R.; Pomelli, C.; Ochterski, J. W.; Martin, R. L.; Morokuma, K.; Zakrzewski, V. G.; Voth, G. A.; Salvador, P.; Dannenberg, J. J.; Dapprich, S.; Daniels, A. D.; Farkas, O.; Foresman, J. B.; Ortiz, J. V.; Cioslowski, J.; Fox, D. J., Gaussian 09, Revision B.01, Gaussian, Inc.,Wallingford CT, **2009**.

62. Mori, T.; Katsuhara, M.; *J. Phys. Soc. Jpn.,* **2002**, *71*, 826–844.

63. Metzger, R. M.; *Chem. Rev.* **2003**, *103,* 3803-3834.

64. (a) Acker, D. S.; Hertler, W. R.; *J. Am. Chem. Soc.* **1962**, *84*, 3370-3374. (b) Melby, L. R.; Harder, R, J.; Hertler, W. R.; Mahler, W.; Benson, R. E.; Mochel, W. E.; *J. Am. Chem. Soc.* **1962**, *84*, 3374-3387

65. (a) Hoffmann, R.; *J. Chem. Phys*. **1964**, *40*, 2474-2479. (b) Hoffmann, R.; *J. Chem. Phys*. **1964**, *40*, 2480-2488. (c) Hoffmann, R.; *J. Chem. Phys*. **1964**, *40*, 2745.

66. Mori, T.; Kobayashi, A.; Sasaki, Y.; Kobayashi, H.; Saito, G.; Inokuchi, H.; *Bull. Chem. Soc. Jpn*., **1984**, *57*, 627-633.

67. Bengtsson, L. A.; Hoffmann, R.; *J. Am. Chem. Soc*. **1993**, *115*, 2666-2676.

68. Avendano, C.; Zhang, Z.; Ota, A.; Zhao, H.; Dunbar, K. R.; *Angew. Chem. Intl. Ed.* **2011**, *50*, 6543-6547.

69. Akhbari, K.; Morsali, A.; *Coord. Chem. Rev.* **2010**, *254*, 1977-2006.

70. Kato, R.; Aonuma, S.; Sawa, H.; *Synth. Met.* **1995**, *70*, 1071-1074.

71. (a) Hoffmann, R.; *J. Chem. Phys.* **1963**, *39*, 1397-1412. (b) Hoffmann, R.; *J. Am. Chem. Soc.* **1978**, *100*, 6093-6098. (c) Mori, T.; Katsuhara, M.; *J. Phys. Soc. Jpn.* **2002**, *71*, 826-844.

72. McGuire, T.; Potter, R., *IEEE Transactions on Magnetics*, **1975**, *11*, 1018.

73. Smith, C. S., *Phys. Rev.* **1954**, *94*, 42.

74. Law, K. Y., Chem. Rev. **1993**, *93*,449.

75. Auckland, D.W.; Brown, N. E.; Varlow, N. E., *Electrical Insulation and Dielectric Phenomena, IEEE,* **1997**, *1*, 186.

76. Brown, W. D.; Brewer, J.; *Nonvolatile Semiconductor Memory Technology: A Comprehensive* , Wiley-IEEE press, Germany, 1997)

77. Lankhorst, M. H. R.; Ketelaars, B. W.; Wolters, R.A.M., *Nat. Mater*. **2005**, *4*, 347.

78. (a) Dearnaley, G.; Stoneham, A. M.; Morgan, D. V., *Rep. Prog. Phys*.**1970**, *33*, 1129. (b) Pagnia, H.; Sotnik, N., *Phys. Stat. Sol*. *A* **1988**, *108*, 11.

79. Khan, M. A.; Bhansali, U. S.; Alshareef, H. N., *Adv. Mater.* **2012**, *24*, 2165.

80. Tayi, A. S.; Shveyd, A. K.; Sue, C. H.; Szarko, J. M.; Rolczynski, B. S.; Cao, D.; Kennedy, T. J.; Sarjeant, A. A. ; Stern, C. L.; Paxton, W. F.; Wu, W.; Dey, S. K.; Fahrenbach, A. C.; Guest, J. R.; Mohseni, H.; Chen, L. X.; Wang, K. L.; Stoddart, J. F. ; Stupp, S. I., *Nature* **2012**, *488*, 485.

81. Ishiwara, H.; Okuyama, M.; Arimoto, Y.; *Ferroelectric Random Acess Memories: Fundamentals and Applications.* Spinger-Verlag, **2004**.

82. (a) Neufeld, A. K.; Madsen, I.; Bond, A. M.; Hogan, C. F.; *Chem. Mater.* **2003**, *15*, 3573. (b) Wang, D.; Lu, J. G.; Mo, X.; Lou, C.; Yao, Y.; Chen, G., *Third conference on Nanotechnology, IEEE-NANO*, **2003**. (c) Di, C.; Yu, G.; Liu, Y.; Guo, Y.; Wu, W.; Wei, D.; Zhu, D., *Phys. Chem. Chem. Phys.,* **2008**, *10*, 2302. (d) Xiao, K.; Tao, J.; Pan, Z.; Puretzky, A. A.; Ivanov, I. N.; Pennycook, S. J.; Geohegan, D. B., *Angew. Chem. Int. Ed.* **2007**, *46*, 2650. (e) Zhou, X.; Wei, S.; Zhang, S.,

Langmuir **2008**, *24*, 4464.(f) Ren, L.; Fu, L.; Liu, Y. W.; Chen, S.; Liu, Z. F., *Adv.Mater.* **2009**, *21*, 4742.

83. (a) Müller, R.; Naulaerts, R.; Billen, J.; Genoe, J.; Heremans, P.; *Appl. Phys. Lett.* **2007**, *90*, 063503. (b) Kamitsos, E. I.; Tzinis, C. H.; Risen, Jr. W. M., *Solid State Comm.* **1982**, *42*, 561.. (c) Gu, Z.; Wu, H.; Wei, Y.; Liu, J., *J. Phys. Chem.***1993**, *97*, 2543. (d) Flannigan, D. J.; Lobastov, V. A.; Zewail. A. H., *Angew. Chem. Int. Ed.* **2007**, *46*, 9206.(e) Park, S. T.; Flannigan, D. J.; Zewail, A. H., *J. Am. Chem. Soc.*, **2011**, *133*, 1730.

84. Wheland, R. C.; Martin, E. L., *J. Org. Chem.***1975**, *40*, 3101.

85. Ikegami, H.; Chong, C.-H.; Yamochi, H.; Saito, G.; *Mol. Cryst. Liq. Cryst. 2002*, **382**, 21.

86. Sheldrick, G.M., *Acta Cryst*., 2008, **A64**, 112.

87. Zhang, Z.; Zhao, H.; Kojima, H.; Mori, T.; Dunbar, K. R., *Chem. Eur. J.* **2013**, *19*, 3348.